HIGH-PRESSURE SILICATES: CRYSTAL CHEMISTRY AND SYSTEMATICS

© 2021 г. S. V. Krivovichev[1, 2, *]

[1]*Nanomaterials Research Centre, Kola Science Centre RAS, Fersman st., 14, Apatity, 184209 Russia*
[2]*Saint Petersburg State University, University Emb., 7/9, Saint Petersburg, 199034 Russia*
**e-mail: s.krivovichev@ksc.ru*

Received August 3, 2021; Revised August 9, 2021; Accepted August 15, 2021

The crystal chemistry of high-pressure (HP) silicates has been reviewed with special emphasis on their structural topology and Si coordination. The HP silicates are subdivided into eleven major groups according to their chemical compositions: (i) SiO_2 polymorphs; (ii) feldspar polymorphs; (iii) pyroxene and amphibole high-pressure polymorphs; (iv) garnet-type phases with octahedral Si; (v) $MSiO_3$ high-pressure polymorphs (M = Mg, Fe); (vi) M_2SiO_4 high-pressure polymorphs (M = Mg, Fe); (vii) dense hydrous Mg silicates and related structures; (viii) high-pressure silicates in the Al_2O_3–SiO_2 and Al_2O_3–SiO_2–H_2O systems; (ix) Ca, Sr and Ba high-pressure silicates and aluminosilicates; (x) alkali metal high-pressure silicates and aluminosilicates; (xi) miscellaneous high-pressure silicates. In total, more than 160 HP silicates are considered that crystallize in over 115 different structure types. On the basis of the recent advances in the field, the whole crystal chemistry of inorganic silicates can be systematized on the basis of the coordination numbers (CNs) of Si atoms relative to oxygen into seven groups corresponding to the following combinations of CNs(Si): 4; 4 + 5; 4 + 5 + 6; 4 + 6; 5; 5 + 6; 6. Less than half of all known HP silicates are based upon closest packings of anions. The topological properties of linkage between Si coordination polyhedra include corner (for all CNs(Si)), edge (for CN(Si) = 5 and 6) and face (for CN(Si) = 6) sharing. One oxygen atom may be shared between three or less Si coordination polyhedra at the same time.

Keywords: high pressures, silicates, crystal structure, crystal chemistry, hexacoordinated silicon, pentacoordinated silicon, high-pressure mineralogy, phase transitions, structural complexity, structural topology

DOI: 10.31857/S0869605521050038

1. INTRODUCTION

Silicates are the most important constituents of the Earth's crust and mantle and their systematic investigations have long been in the focus of mineralogists and crystallographers (Liebau, 1985; Pushcharovsky, 1986). Special attention had been paid to the behavior of silicates under conditions of high pressures (HP) and high temperatures (HT) that is of primary importance for the understanding of crystalline matter in deep Earth geospheres (Pushcharovsky, Pushcharovsky, 2012; Pushcharovsky, 2012; Wicks, Duffy, 2016). This review is intended to cover the advances achieved in the HP crystal chemistry of silicates since 1960s, when the first experimental reports appear in the literature on the silicate phases with sixfold coordinated Si (Stishov, Popova, 1961). The crystal chemistry of HP silicates was first reviewed by Finger and Hazen in 1991 (Finger, Hazen, 1991), when only twelve structure topologies have been known. Ten years later Finger and Hazen (2000) reviewed two dozen high-pressure structure types containing ^{VI}Si, outlined major trends in HP phase transitions in silicates, and predicted

a series of possible HP structures on the basis of their potential similarities with minerals and inorganic compounds containing ^{VI}Al, ^{VI}Ge and ^{VI}Ti. However, since the beginning of XXIst century, major advances have been achieved in the HP mineralogy and crystal chemistry of silicates, due to the considerable advances in experimental and theoretical techniques, including diamond anvil technologies and synchrotron radiation. Enormous achievements were made in the study of meteorites and terrestrial impactites that allowed to reveal a whole series of natural phases (minerals) produced during shock metamorphism either in space or on the Earth's surface (Tomioka, Miyahara, 2017; Tschauner, 2019). Detailed studies of crystalline inclusions in diamonds led to the discovery of the whole suite of HP minerals originated in the Earth mantle (Kaminsky, 2012, 2017, 2020). According to seismic tomography maps for various depth levels and the new available data on geophysical discontinuities in combination with the most recent experimental results of HP-silicate transformations, the middle mantle can be recognized within the lower mantle in the interval between 840 and 1700 km (Pushcharovsky, Pushcharovsky, 2016; Pushcharovsky, 2020). The experimental advances in HP single-crystal diffraction allowed to describe a range of metastable HP silicates obtained as a result of the cold compression experiments (Finkelstein et al., 2014, 2015a, b; Pakhomova et al., 2017a, b, 2020; Bykova et al., 2018; Gorelova et al., 2018, 2019, 2020a, b, 2021a, b; Lazarz et al., 2019, etc.).

The aim of the present review is to provide crystal chemical description and systematics of known HP silicates, including not only phases with ^{VI}Si (or ^{V}Si), but also some phases with ^{IV}Si that form or exist under HP conditions. The organization of the review is different from that published by Finger and Hazen (2000), who focused on structure types rather than on composition. In contrast, we decided to separate HP crystalline silicate phases according to their compositions into the following major groups: (i) SiO_2 polymorphs; (ii) feldspar polymorphs; (iii) pyroxene and amphibole high-pressure polymorphs; (iv) garnet-type phases with octahedral Si; (v) $MSiO_3$ high-pressure polymorphs (M = Mg, Fe); (vi) M_2SiO_4 high-pressure polymorphs (M = Mg, Fe); (vii) dense hydrous Mg silicates and related structures; (viii) high-pressure silicates in the Al_2O_3–SiO_2 and Al_2O_3–SiO_2–H_2O systems; (ix) Ca, Sr and Ba high-pressure silicates and aluminosilicates; (x) alkali metal high-pressure silicates and aluminosilicates; (xi) miscellaneous high-pressure silicates. After systematic description, we attempt to use the collected information to outline some fundamental trends in the HP silicate crystal chemistry.

2. SiO_2 POLYMORPHS

2.1. Preliminary remarks

The high-pressure crystal chemistry of SiO_2 polymorphs was reviewed by Hemley et al. (1996) and the field developed greatly during last 25 years. Table 1 summarizes crystallographic parameters of HP silica phases with known crystal structures, determined either experimentally or by combination of experimental and theoretical methods (purely theoretical structures are not included). In the following, we group the known HP silica polymorphs according to their structural topologies and transformational sequences into coesite polymorphs, post-quartz phases, cristobalite phases, stishovite and post-stishovite structures.

2.2. Coesite polymorphs

Coesite was first reported by Coes (1953) as a "new dense crystalline silica" prepared at 3.55 GPa at temperatures between 773 and 1073 K. The phase was found in natural impactites of the Meteor crater in Arizona, U.S., and named "coesite" in honor of its first discoverer (Chao et al., 1960). Later coesite was found in kimberlites (Smyth, Hatton, 1977) and ultrahigh-pressure metamorphic rocks of the Western Alps (Chopin, 1984). The crystal structure

Table 1. Crystallographic data for high-pressure SiO_2 polymorphs
Таблица 1. Кристаллографические данные для высокобарических полиморфов кремнезема

Mineral/phase name	Structure type	*P*, GPa	SG	*a* [Å]/α [°]	*b* [Å]/β [°]	*c* [Å]/γ [°]	CN(Si)	Reference
Coesite-I	–	9.2	$C2/c$	6.875/90	12.122/121.0	7.055/90	4	1
Coesite-II	–	27.5	$P2_1/n$	6.559/90	23.228/121.1	6.795	4	1
Coesite-III	–	27.9	$P\bar{1}$	6.571/82.1	17.790/120.8	6.766/87.1	4	2
Coesite-IV	–	40.2	$P\bar{1}$	6.599/69.1	7.000/83.2	8.649/81.8	4, 5, 6	2
Coesite-V	–	56.7	$P\bar{1}$	6.403/72.4	6.768/84.0	8.399/81.6	5, 6	2
Cristobalite-II	–	3.5	$P2_1/c$	8.378/90	4.602/124.9	9.057/90	4	3, 4
Cristobalite-X-1	–	10.7	$P2_1/n$	6.613/90	4.114/98.3	6.912/90	6	5, 6
Stishovite	Rutile	Atm	$P4_2/mnm$	4.177/90	= a/α	2.665	6	7
–	Baddeleyite	Atm	$P2_1/c$ (?)	4.375/90	4.584/100.0	4.708/90	6?	8, 9
"β-stishovite"	$CaCl_2$	108	$Pnnm$	4.097/90	3.795/90	2.559/90	6	10
Seifertite	α-PbO_2	129	$Pbcn$	4.097/90	5.046/90	4.495/90	6	11
–	Pyrite	268	$Pa\bar{3}$	3.933/90	= a/α	= a/α	6 + 2	12, 13
m-silica*	–	35	$P2/c$	3.982/90	4.574/91.2	4.700/90	6	14
IP-phase*	–	50	$C222$	3.637/90	10.067/90	3.698/90	4, 6	14
Post-quartz	–	45	$P2_1/c$	7.66/90	4.10/117.9	5.03/90	6	15
Quartz II*	–	38	$C2$	8.232/90	3.329/110.1	5.104/90	4, 6	16
–	Nickeline or Fe_2N	53	$P6_3/mmc$	2.474/90	= a/α	3.929/120	6	17

* Combined theoretical and experimental data.
References: (1) Černok et al., 2014a; (2) Bykova et al., 2018; (3) Dove et al., 2000; (4) Dera et al., 2011; (5) Černok et al., 2017; (6) Shelton et al., 2018; (7) Sinclair, Ringwood, 1978; (8) El Goresy et al., 2000a; (9) El Goresy et al., 2004; (10) Tsuchida, Yagi, 1989; (11) El Goresy et al., 2008; (12) Kuwayama et al., 2005; (13) Kuwayama et al., 2011; (14) Hu et al., 2017a; (15) Haines et al., 2001; (16) Choudhury, Chaplot, 2006; (17) Prakapenka et al., 2004.

of coesite was first determined by Zoltai and Buerger (1959) and refined by Araki and Zoltai (1969), Gibbs et al. (1977), and Smyth et al. (1987).

The high-pressure behaviour and phase transitions of coesite was the subject of extensive studies (see, e.g.: Angel et al., 2001a, 2003; Černok et al., 2014a, b; Hu et al., 2015a; Liu et al., 2017a; Bykova et al., 2018; Wu et al., 2018), but the most comprehensive results on the crystal chemistry of HP coesite polymorphs were obtained by Dubrovinsky and co-authors (Černok et al., 2014a, b; Bykova et al., 2018).

The crystal structure of coesite-I contains a 3D framework of corner-linked SiO_4 tetrahedra (Fig. 1*a*, *b*). The framework is based upon the double crankshaft chains running parallel to [101] (Fig. 1*c, d*) and similar to those found in the feldspar (**fsp**) and paracelsian (**pcl**) topologies (Krivovichev, 2020). However, the topology of the linkage of the chains is different; in fact, the coesite topology is inflexible in the sense of Smith (1968, 1974), i.e. the chains cannot rotate freely under increasing pressure.

The coesite-I → coesite-II → coesite-III phase transitions are displacive and do not modify the topology of the framework; Si atoms remain in tetrahedral coordination. Along the pathway, the symmetry is decreasing ($C2/c \rightarrow P2_1/n \rightarrow P\bar{1}$), which corresponds to the increasing number of symmetrically independent sites and the increasing structural complexity (in bits per atom (Krivovichev, 2013): see Table 2).

The double crankshaft chains can be considered as formed by edge-sharing four-membered tetrahedral rings oriented alternatively either approximately perpendicular or approximately parallel to the extension of the chains. Figure 2 shows topologies of Si networks in the crystal

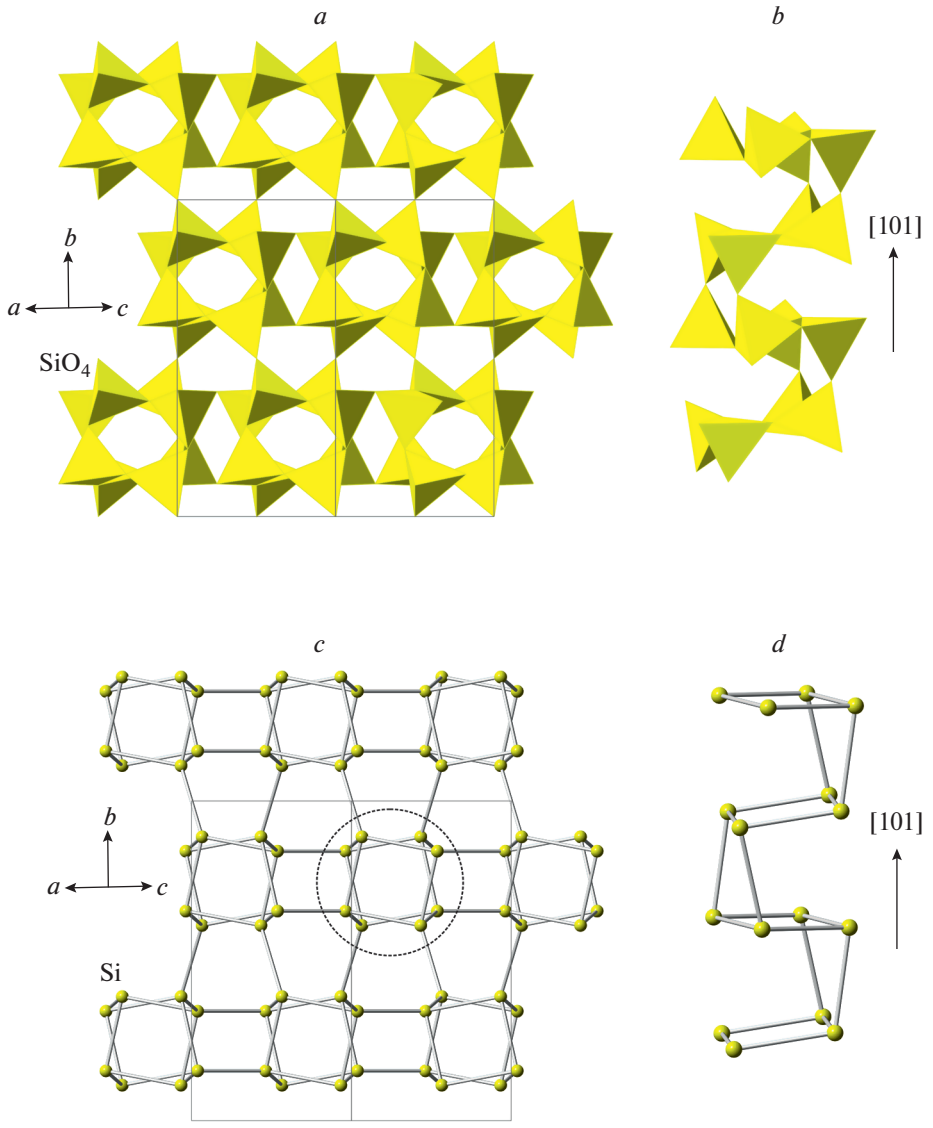

Fig. 1. The crystal structure of coesite-I projected along [101] (*a*), its double crankshaft chain (*b*), topology of Si linkage in coesite-I (*c*) and the topology of the chain (*d*). The dotted line indicates cross-section of the chain.
Рис. 1. Кристаллическая структура коэсита-I в проекции вдоль [101] (*a*), двойная карданновальная цепочка (*b*), топология кремниевого каркаса в коэсите-I (*c*) и топология карданновальной цепочки (*d*). Точечной линией показано сечение цепочки.

structures of coesite-II and coesite-III. In terms of “perpendicular” rings, the crystal structure of coesite-I contains one independent ring, which is splitted into two in coesite-II and four in coesite-III.

At pressures above 30 GPa coesite-III transforms into coesite-IV, the phase that possesses remarkable structural and topological features (Bykova et al., 2018). First, it consists of Si atoms in four-, five- and sixfold coordination environments simultaneously. The other phases

Table 2. Structural complexity parameters for coesite polymorphs
Таблица 2. Параметры структурной сложности для полиморфов коэсита

Mineral/phase name	SG	I_G, bit/atom	$I_{G,\,total}$, bit/cell
Coesite-I	$C2/c$	2.752	66.039
Coesite-II	$P2_1/n$	4.585	440.156
Coesite-III	$P\bar{1}$	5.198	374.235
Coesite-IV	$P\bar{1}$	4.585	220.078
Coesite-V	$P\bar{1}$	4.585	220.078

of this kind are: α-$CaSi_2O_5$ (Angel et al., 1996; Kudoh, Kanzaki, 1998), feldspar polymorphs, and other phases, which will be described in detail below. Second, the crystal structure of coesite-IV contains SiO_6 octahedra that share common faces to form $[Si_2O_9]$ dimers shown in Fig. 3*d*. Bykova et al. (2018) mentioned that "...such a structural element has been neither experimentally observed for any silicon compounds, nor expected for small and high-valence cations like Si^{4+}", which is not exactly the case. The face-sharing between Si-centered octahe-

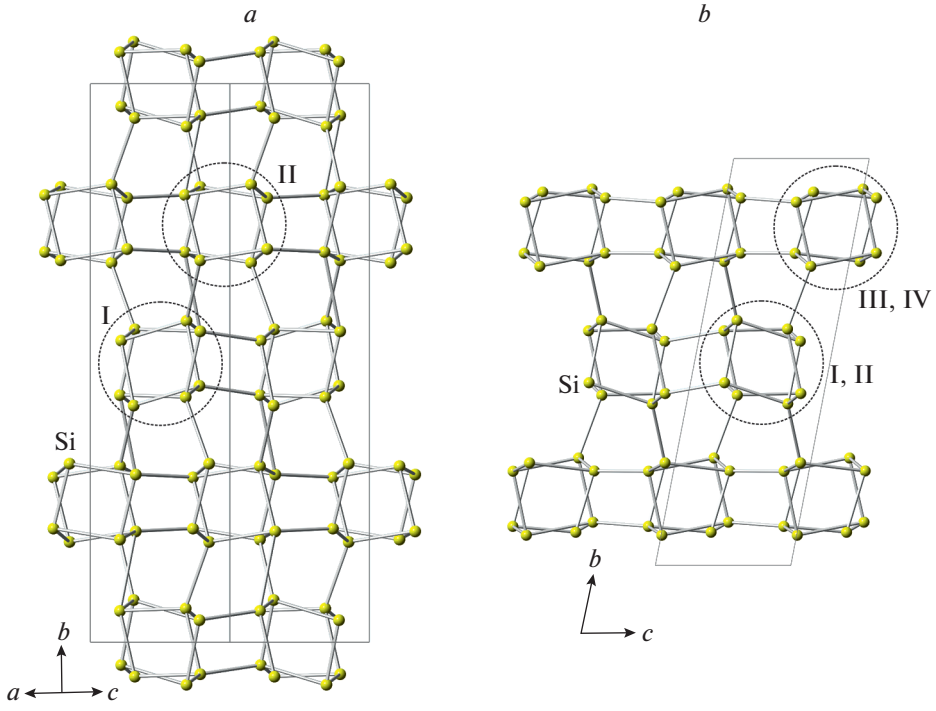

Fig. 2. The topology of the Si network in coesite-II (*a*) and coesite-(III) (*b*). Dotted lines show cross-section of the chain. In coesite-II and -III, there are two and four symmetrically idependent four-membered rings, respectively, oriented approximately perpendicular to the extension of the chains.
Рис. 2. Топология кремнекислородных каркасов в коэсите-II (*a*) и коэсите-III (*b*). Точечная линия указывает сечения двойных карданновальных цепочек. В кристаллических структурах коэсита-II и III имеется два и четыре симметрично независимых четырехчленных кремнекислородных кольца, соответственно, ориентированных приблизительно перпендикулярно направлению цепочек.

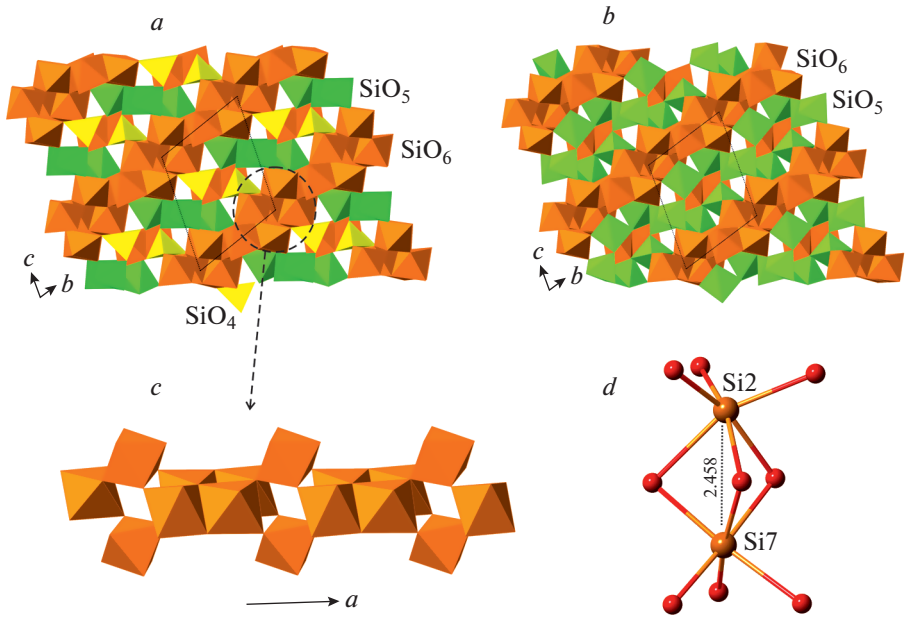

Fig. 3. The crystal structures of coesite-IV (*a*) and coesite-V (*b*), the close-packed hcp-derived 1D unit in coesite-IV (*c*) and the geometry of a face-sharing $[Si_2O_9]$ dimer at 40.2 GPa (*d*).

Рис. 3. Кристаллические структуры коэсита-IV (*a*) и коэсита-V (*b*), плотноупакованный одномерный мотив в коэсите-IV (*c*) и геометрия гранно-связанного димера $[Si_2O_9]$ при 40.2 ГПа (*d*).

dra had been described previously by Yusa et al. (2007) for hexagonal and rhombohedral $BaSiO_3$ perovskites (see below). Face linkage of SiO_6 octahedra was also claimed for the high-pressure polymorph of SiO_2 studied by Luo et al. (2004), but the structure details remain to be confirmed. The crystal structure of coesite-IV is shown in Fig. 3*a*. It may be described as based upon dense slabs of SiO_6 octahedra parallel to (001) and linked via additional SiO_6, SiO_5 and SiO_4 polyhedra. The slabs contain rods of edge- and corner-sharing octahedra that can be viewed as one-dimensional blocks of close-packed O atoms with Si in octahedral interstices (Fig. 3*c*). The packing of O atoms corresponds to the hexagonal AB closest packing (hcp). Thus, the mechanism of densification of the coesite structure corresponds to the appearance, under high pressures, of close-packed hcp blocks, which is frequently observed for HP silicates (e.g., in danburite: Pakhomova et al., 2017a). In terms of coordination of Si and O atoms, the crystal-chemical formula of coesite-IV can be written as $^{VI}Si_5{}^{V}Si_2{}^{IV}Si^{III}O_{12}{}^{II}O_4$. Three fourths of the O atoms in coesite-IV are 3-coordinated, whereas one fourth is 2-coordinated. At ~50 GPa, coesite-IV transforms completely into coesite-V, the phase that differs from its precursor by the transition of all ^{IV}Si into ^{V}Si. As a result, one of 2-coordinated O atoms transforms into 3-coordinated and the crystal-chemical formula of coesite-V can be written as $^{VI}Si_5{}^{V}Si_3{}^{III}O_{13}{}^{II}O_3$. The crystal structure of coesite-V is similar to that of coesite-IV (Fig. 3*b*).

2.3. Cristobalite polymorphs

The high-pressure behavior and phase transitions of cristobalite attracted considerable attention (Tsuneyuki et al., 1989; Yamakata, Yagi, 1997; Prokopenko et al., 2001; Akins, Ahrens, 2002; Dove et al., 2000; Shieh et al., 2005; Dera et al., 2011; Černok et al., 2017; Shelton et al.,

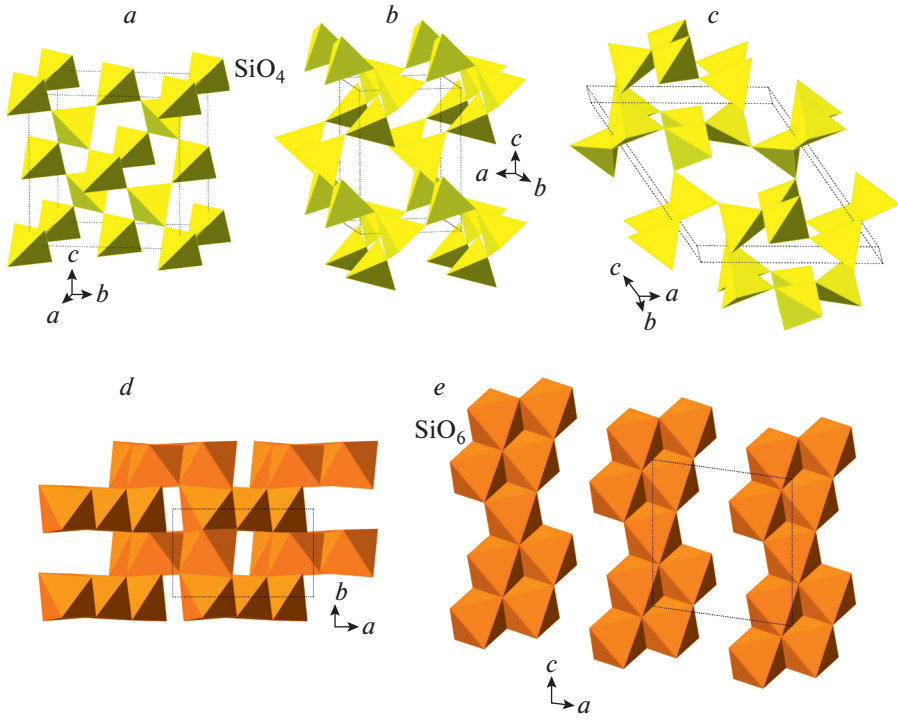

Fig. 4. The crystal structures of β- (*a*) and α- (*b*) cristobalites and cristobalite-II (*c*), and crystal structure of cristobalite-X_1 projected along the *c* axis (*d*), and projection of the layer of chains of edge-sharing SiO_6 octahedra along the *b* axis (*e*).

Рис. 4. Кристаллические структуры β- (*a*) и α- (*b*) кристобалита и кристобалита-II (*c*), кристаллическая структура кристобалита-X_1 в проекции вдоль оси *c* (*d*) и проекция слоя из реберно-связанных октаэдров SiO_6 вдоль оси *b* (*e*).

2018). Under ambient pressure, there are two polymorphs of cristobalite, α- and β-, that are based upon tetrahedral network of the diamond topology, **dia**. The high-temperature β-cristobalite crystallizes in the "diamond" space group $Fd\bar{3}m$ (Fig. 4*a*) and under decreasing temperature transforms into low-temperature tetragonal α-form (Fig. 4*b*; space group $P4_22_12$). Under high pressure, α-cristobalite experiences a displacive phase transition with the formation of monoclinic cristobalite-II with conservation of Si coordination number and the overall **dia** structural topology (Fig. 4*c*). The series of displacive phase transitions β → α → II corresponds to the overall increase of structural complexity [$I_G/I_{G,\text{total}}$, in bits]: 0.918/5.510 → → 0.918/11.012 → 2.585/62.039.

There have been many reports about other cristobalite polymorphs, but the reliable crystal-structure data have been obtained only recently for cristobalite-X_1 (Černok et al., 2017; Shelton et al., 2018). In this polymorph, all Si atoms are in octahedral coordination, whereas all O atoms are 3-coordinated. The crystal structure is based upon hcp with close-packed layers parallel to (010) (Fig. 4*d*). Alternatively, it can be described as consisting of layers formed by ribbons of edge-sharing SiO_6 octahedra (Fig. 4*e*).

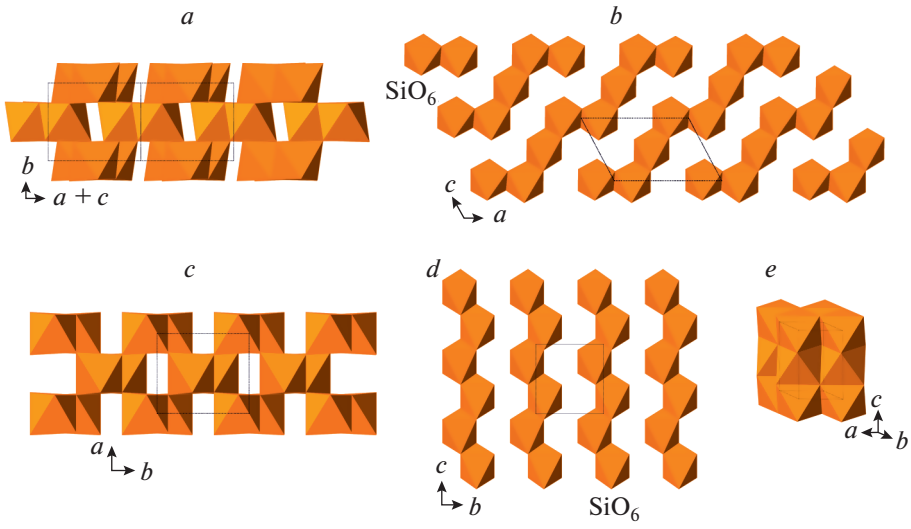

Fig. 5. The crystal structure of post-quartz projected along [101] (*a*) and the layer of octahedral chains (*b*); the crystal structure of *m*-silica projected along the *c* axis (*c*) and the layer of octahedral chains (*d*); the crystal structure of the Fe_2N-type polymorph of SiO_2 (*e*).

Рис. 5. Кристаллическая структура пост-кварца в проекции вдоль [101] (*a*) и слой октаэдрических цепочек (*b*); кристаллическая структура *m*-кремнезема в проекции вдоль оси *c* (*c*) и слой октаэдрических цепочек (*d*); кристаллическая структура Fe_2N-структурированного полиморфа SiO_2 (*e*).

2.4. Post quartz polymorphs and related structures

The compression of quartz was studied in a number of works (McNeil, Grimsditch, 1992; Kingma et al., 1993a, b; Haines et al., 2001; Prakapenka et al., 2004; Choudhury, Chaplot, 2006; Carl et al., 2017), but the reliable experimental crystal-structure information exists for very few polymorphs only. The crystal structure of post-quartz (Haines et al., 2001) is based upon octahedral framework of edge-sharing SiO_6 octahedra (Fig. 5*a*) formed by layers of zigzag octahedral chains (Fig. 5*b*). As the crystal structure of cristobalite-X_1, that of post-quartz can also be viewed as an hcp of O atoms with Si in octahedral interstices; the close-packed layers are parallel to (010). The crystal structure of "*m*-silica" reported by Hu et al. (2017a) is topologically identical to that of seifertite (see below) and can be considered as its monoclinically distorted version. It is again based upon an hcp of O atoms (Fig. 5*c*), but the character of linkage of SiO_6 octahedra differs from those observed in cristobalite-X_1 and post-quartz (Fig. 5*d*). This class of structures was theoretically predicted and analyzed by Teter et al. (1998), who predicted the crystal structure of post-quartz, but not that of cristobalite-X_1. All the octahedral hcp SiO_2 polymorphs can be viewed as ordered versions of the parent nickeline- or disordered Fe_2N-type phase, which was first reported by Liu et al. (1978) in experiments with SiO_2 glass and Sekine et al. (1987) in shock experiments with quartz. The structure of this phase (Prakapenka et al., 2004) is an ideal hcp arrangement of O atoms with Si filling all octahedral interstices with the site occupancies of 50% (Fig. 5*e*).

Several octahedral-tetrahedral structures have been proposed for some SiO_2 polymorphs that are shown in Fig. 6. For instance, the crystal structure of quartz II (Choudhury, Chaplot, 2006) is based upon layer of edge-sharing octahedra interlinked by SiO_4 tetrahedra (Figs. 6*a*, *b*). It can also be viewed as a cubic close packing (ccp) of O atoms with Si in both octahedral and tetrahedral interstices. The crystal structure of the "IP phase" suggested by Hu et al. (2017a)

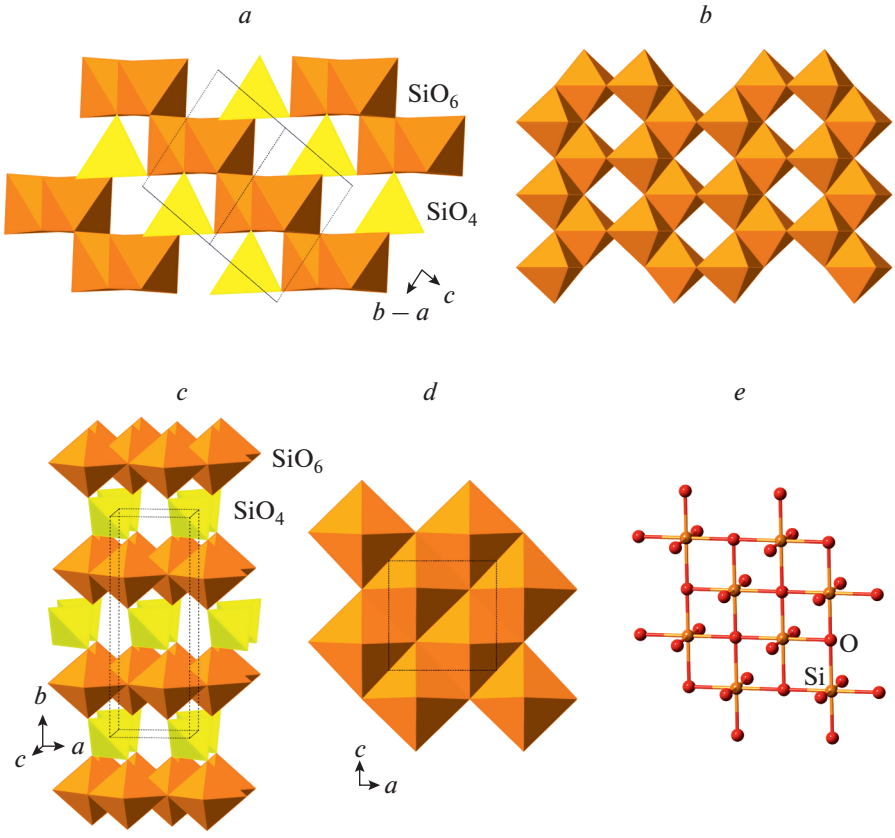

Fig. 6. The crystal structure of quartz II (*a*) and the layer of edge-sharing SiO_6 octahedra (*b*); the crystal structure of the IP phase (*c*), and its octahedral layer in polyhedral (*d*) and ball-and-stick representations (*e*).

Рис. 6. Кристаллическая структура кварца II (*a*) и слой из связанных ребрами октаэдров SiO_6 (*b*); кристаллическая структура IP-фазы (*c*) и ее октаэдрический слой в полиэдрическом (*d*) и шариковом представлениях (*e*).

has similar features and is based upon layers of edge-sharing octahedra linked by SiO_4 tetrahedra (Fig. 6*c, d, e*). Alternatively, it can also be described as a ccp with layers parallel to (111) and Si atoms in octahedral and tetrahedral coordinations. Taking into account the coordination of Si and O atoms, the crystal-chemical formula of quartz II and "IP phase" can be written as $^{VI}Si_2{}^{IV}Si^{III}O_4{}^{II}O_2$ and $^{VI}Si_2{}^{IV}Si^{IV}O_2{}^{II}O_4$, respectively. The presence of 4-coordinated O atoms in the "IP phase" makes the structure model questionable, since it is the only known case of the fourfold coordination of O with respect to Si atoms.

2.5. Stishovite and post-stishovite polymorphs

Since the discovery of stishovite in laboratory (Stishov, Popova, 1961) and nature (Chao et al., 1962), and its first crystal-structure determinations (Stishov, Belov, 1962; Preisinger, 1962; Sinclair, Ringwood, 1978), many studies have been devoted to the understanding of its properties and behavior under high-pressure conditions (Hill et al., 1983; Ross et al., 1990; Li et al., 1996; Zhang et al., 1996; Andrault et al., 2003; Panero et al., 2003, etc.). Tsuchida and Yagi

(1989) observed the transition of stishovite(rutile)-type of SiO_2 into $CaCl_2$-type polymorph ("β-stishovite" (Das et al., 2020)), which was supported by the subsequent experimental and theoretical studies (Cohen, 1991; Kingma et al., 1995; Dubrovinsky, Belonoshko, 1996; Andrault et al., 1998; Ono et al., 2002). Further investigations revealed the existence of other post-stishovite phases, including seifertite (El Goresy et al., 2008), baddeleyite- (Dubrovinsky et al., 1997; El Goresy et al., 2000a, 2004) and pyrite-structured SiO_2 polymorphs (Kuwayama et al., 2005, 2011).

The crystal structure of stishovite is isotypic to rutile, TiO_2, and is based upon octahedral framework of chains of edge-sharing SiO_6 octahedra (Fig. 7*a*, *b*). Each Si is in octahedral coordination, whereas each O has a triangular coordination. It is of interest that the crystal structure of stishovite is not close-packed and its phase transition to the $CaCl_2$-type structure ("β-stishovite") is driven by the tendency of O atoms to adopt a close-packing arrangement through the cooperative rotation of octahedral chains around their axes (adjacent chains rotate in different directions). At higher pressures, "β-stishovite" transforms into seifertite that was first obtained experimentally by German et al. (1973) and later found in meteorites (Sharp et al., 1999; Dera et al., 2002; El Goresy et al., 2008; Miyahara et al., 2013). The crystal structure of seifertite (Zhang et al., 2016a) belongs to the α-PbO_2 structure type, is remarkably similar to *m*-silica (see above) and was observed during the studies of the phase transitions of cristobalite by Dubrovinsky et al. (2001). It is well probable that seifertite or seifertite-structured phases may form metastably under pressures much lower than those of other post-stishovite phases. Its crystal structure (Fig. 7*c*) is based upon an hcp arrangement of O atoms with Si occupying octahedral interstices such that 1 × 1 zigzag chains are formed (Fig. 7*d*).

As it was mentioned above, there were reports about baddeleyite-related SiO_2 polymorphs (Dubrovinsky et al., 1997; El Goresy et al., 2000a, 2004), but no detailed crystal-structure information is known for these phases (it is noteworthy that, in the crystal structure of baddeleyite, ZrO_2, the coordination number of Zr is 7), except for the unit-cell parameters and possible space groups. In contrast, the crystal structure of pyrite-type SiO_2 stable over 270 GPa and theoretically predicted by Park et al. (1988) was synthesized and structurally characterized by Kuwayama et al. (2005, 2011). It can be described as a three-dimensional framework of corner-sharing SiO_6 octahedra with each O sharing between three octahedra (Fig. 7*e*). The coordination of Si can be described as [6 + 2], since, in addition to six short Si–O distances (~1.61 Å), each Si atom has two additional Si–O contacts of ~2.37 Å (Fig. 7*f*).

The example of pyrite-structured SiO_2 shows that, even at higher pressure, the coordination number of Si may increase above six (Lyle et al., 2015; Prescher et al., 2017; Kono et al., 2020; Liu et al., 2021). For instance, the Fe_2P structure was proposed as a possible model of an ultra-HP silicate (Tsuchiya, Tsuchiya, 2011; Wu et al., 2011), whereas the earlier proposals of fluorite (CaF_2) structure type (Al'tshuler et al., 1973; Simakov et al., 1973) were later shown to be unreliable.

3. FELDSPAR POLYMORPHS

The polymorphism of felspars, including high-pressure polymorphs, was considered in detail in our recent review (Krivovichev, 2020) and therefore is described here only briefly. Table 3 contains crystallographic information on HP feldspar polymorphs. The field experienced dramatic advances within recent five years, due to the discovery of a number of new modifications obtained via cold compression of natural crystals of feldspar-group minerals (Pakhomova et al., 2017a, 2020; Gorelova et al., 2019, 2020a, 2021a, b).

The high-pressure behavior of the silicate members of the feldspar group strongly depends upon their framework topologies. There are two basic topologies, **pcl** (paracelsian-type) and **fsp** (feldspar-type sensu stricto). Both topologies are based upon double crankshaft chains of tetrahedra linked in different modes such that eight-membered rings are formed in the planes

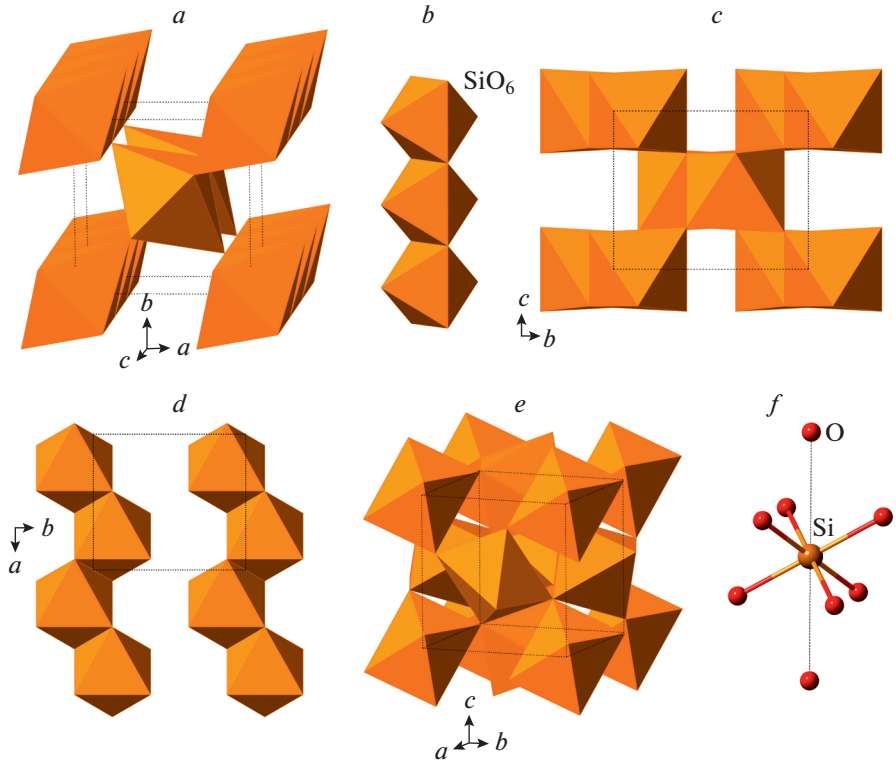

Fig. 7. The crystal structure of stishovite (*a*) and its octahedral chain (*b*); the crystal structure of seifertite (*c*) and the layer of octahedral chains (*d*); the crystal structure of pyrite-structured SiO_2 (*e*) and the [6 + 2] coordination of the Si atom (*f*).

Рис. 7. Кристаллическая структура стишовита (*a*) и ее октаэдрическая цепочка (*b*); кристаллическая структура зайфертита (*c*) и слой из октаэдрических цепочек (*d*); кристаллическая структура пиритоподобного SiO_2 (*e*) [6 + 2]-координация атомов Si (*f*).

perpendicular to the chain extension. The **pcl** topology is *flexible*, which means that it allows for the cooperative rotation of the crankshaft chains around their vertical axes with opening and closing of channels outlined by the eight-membered rings. In contrast, the **fsp** topology does not allow for such rotations, i.e. is *inflexible* (Smith, 1968, 1974).

Under increasing pressure, the crystal structures of minerals with the **pcl** topologies experience rich and interesting phase transitions associated with the formation of penta- and hexacoordinated Si atoms (Pakhomova et al., 2017a; Gorelova et al., 2019, 2020a, 2021a). For instance, danburite-II was the first inorganic silicate possessing Si in exclusively fivefold (triangular bipyramidal) coordination (Pakhomova et al., 2017a). The densification of the crystal structures with the **pcl** topologies proceeds through the formation of architectures with local closely-packed atomic arrangements and ends up with the formation of closest packings formed by O atoms and large cations such as Ca, Sr and Ba. For example, the high-pressure modifications of paracelsian, $BaAl_2Si_2O_8$, paracelsian III and IV, are based upon 9-layer closest packings with the "rhombohedral" layer sequence ABACACBCB (Gorelova et al., 2019).

The high-pressure behavior of the structures with the **fsp** topology (all common feldspars belong to this group) is of great interest due to the high abundance of feldspars in the Earth's

Table 3. Crystallographic data on high-pressure feldspar polymorphs in comparison with ambient pressure structures
Таблица 3. Кристаллографические данные для высокобарических полиморфов полевых шпатов в сравнении с низкобарическими структурами

Chemical formula	Mineral name/conditions	Top.	CN(Si)	Sp. gr.	*a* [Å]/α [°]	*b* [Å]/β [°]	*c* [Å]/γ [°]	*V*, Å^3	Ref.
				Aluminosilicates					
$NaAlSi_3O_8$	Albite	**fsp**	4	$C\bar{1}$	8.161/93.5	12.875/116.5	7.110/90.2	669.8	1
	“Albite-II” (13.5 GPa)	–	4	$P\bar{1}$	6.585/63.6	6.885/64.2	7.022/75.6	256.1	2
	“Albite-III” (17.5 GPa)	–	4, 5	$P\bar{1}$	6.983/113.7	6.906/92.7	11.729/71.1	487.9	2
	Lingunite	**hol**	6	$I4/m$	9.263/90	= *a*/α	2.706/90	232.2	3
$KAlSi_3O_8$	Microcline	**fsp**	4	$C\bar{1}$	8.592/90.62	12.963/116.0	7.222/87.67	722.7	4
	“Microcline-II”	–	4	$P\bar{1}$	6.308/74.1	6.765/85.0	7.029/64.8	260.9	2
	Liebermannite	**hol**	6	$I4/m$	9.15/90	= *a*/α	2.74/90	229	5
	“Liebermannite-II” (25.1 GPa)	**hol**	6	$I112/m$	9.147/90	8.783/90	2.651/91.2	213	6
$CaAl_2Si_2O_8$	Anorthite	**fsp**	4	$P\bar{1}$	8.173/93.1	12.869/115.9	14.165/91.3	1336.4	7
	“Anorthite-II” (2.5 GPa)	–	4	$I\bar{1}$	8.082/92.8	12.767/115.8	14.032/91.7	1300.3	8
	“Anorthite-III” (11.1 GPa)	–	4	$P\bar{1}$	7.645/96.7	11.944/109.6	12.906/80.2	1091.9	2
	Stöfflerite	**hol**	6	$I4/m$	9.255/90	= *a*/α	2.745/90	235.1	9
$Pb_{0.8}Al_{1.6}Si_{2.4}O_8$	–	**hol**	6	$I4$	9.414/90	= *a*/α	2.750/90	243.7	10
$BaAl_2Si_2O_8$	Paracelsian	**pcl**	4	$P2_1/c$	8.576/90	9.573/90.2	9.068/90	744.4	11
	“Paracelsian-II” (14.2 GPa)	–	4, 5	$P2_1/c$	8.897/90	8.837/90.1	6.904/90	542.9	11
	“Paracelsian-III” (28.5 GPa)	–	6	$Pna2_1$	5.434/90	8.743/90	9.685/90	460.1	11
	“Paracelsian-IV” (32.4 GPa)	–	6	Pn	8.742/90	5.387/91.4	9.634/90	453.5	11
$SrAl_2Si_2O_8$	Slawsonite	**pcl**	4	$P2_1/c$	8.348/90	9.369/90.3	8.907/90	696.6	12
	“Slawsonite-IIa” (11.0 GPa)	–	4	$P2_1/c$	8.827/90	8.735/90.2	6.831/90	526.7	12
	“Slawsonite-IIb” (14.5 GPa)	–	4, 5	$P2_1/c$	8.856/90	8.672/90.3	6.650/90	510.7	12

Table 3. (Contd.)

Chemical formula	Mineral name/conditions	Top.	CN(Si)	Sp. gr.	*a* [Å]/α [°]	*b* [Å]/β [°]	*c* [Å]/γ [°]	*V*, Å^3	Ref.
				Borosilicates					
$NaBSi_3O_8$	Reedmergnerite	**fsp**	4	$P\bar{1}$	6.802/115.3	7.196/100.8	7.435/106.9	293.6	13
	"Reedmergnerite-II" (16.2 GPa)	–	4	$P\bar{1}$	6.757/97.6	7.109/90.9	11.921/118.3	498.0	13
	"Reedmergnerite-III" (24.8 GPa)	–	4	$P\bar{1}$	6.378/103.8	6.408/115.7	6.632/102.1	221.6	13
$CaB_2Si_2O_8$	Danburite	**pcl**	4	*Pnam*	8.038/90	8.752/90	7.730/90	543.8	14
	"Danburite-II" (25.4 GPa)	–	5	*Pnam*	6.354/90	7.952/90	8.011/90	404.8	15
	"Danburite-III" (25.4 GPa)	–	6	$P\bar{1}$	5.479/91.7	5.532/104.6	6.681/95.6	194.7	15
	"Danburite-IV" (32.0 GPa)	–	6	$P2_1/c$	7.999/90	7.870/89.8	6.249/90	393.4	15
$SrB_2Si_2O_8$	Pekovite	**pcl**	4	*Pnma*	8.155/90	7.919/90	8.921/90	576.1	16
	"Pekovite-II" (29.4 GPa)	–	4, 5	*Pnma*	6.697/90	7.869/90	8.159/90	430.0	17
	"Pekovite-III" (33.3 GPa)	–	6	$P\bar{1}$	5.44/93.3	5.60/104.2	6.72/93.4	198	17
$BaB_2Si_2O_8$	Maleevite	**pcl**	4	*Pnma*	8.141/90	8.176/90	9.038/90	601.6	16
	"Maleevite-II" (38.3 GPa)	–	4, 5	$P\bar{1}$	5.630/92.1	5.538/104.0	6.746/95.0	203.0	17

References: (1) Winter et al., 1979; (2) Pakhomova et al., 2020; (3) Gillet et al., 2000; (4) Kroll, Ribbe, 1987; (5) Ma et al., 2018; (6) Ferroir et al., 2006; (7) Wainwright, Starkey, 1971; (8) Angel, 1988; (9) Tschauner et al., 2021; (10) Downs et al., 1995; (11) Gorelova et al., 2019; (12) Gorelova et al., 2021a; (13) Gorelova et al., 2021b; (14) Phillips et al., 1974; (15) Pakhomova et al., 2017a; (16) Pautov et al., 2004; (17) Gorelova et al., 2020a.

crust. The **fsp** tolopogy is inflexible and does not allow for the rotation of crankshaft chains. As a result, the HP phase transitions in these structures involve either structural reconstruction with the formation of penta- and hexacoordinated Si (for the minerals with Al : Si = 1 : 1, e.g. for anorthite, $CaAl_2Si_2O_8$ (Pakhomova et al., 2020)) or conservation of the tetrahedral silicate substructures in minerals with T : Si = 1 : 3 (T = Al or B) with "exsolution" of Al (in the HP polymorphs of microcline and albite (Pakhomova et al., 2020)) or B (in reedmergnerite (Gorelova et al., 2021b) into separate regions. Gorelova et al. (2021b) recently noticed that the ordered $[TSi_3O_8]$ **fsp**-frameworks can be considered as based upon okenite-type silicate ribbons linked by (TO_4) tetrahedra. During the phase transition, the topology of the silicate chains is conserved and the main reconstruction events involve formation of five- and sixfold coordinated Al (in aluminosilicates) or edge-sharing BO_4 tetrahedra (in borosilicate reedmergnerite). More details about the HP phase transitions in feldspar-group minerals based upon tetrahedral frameworks can be found in (Krivovichev, 2020) and recent publications by Gorelova et al. (2020a, 2021a, b).

The hollandite-type feldspar polymorphs with Si in octahedral coordination were first reported by Ringwood et al. (1967). Their crystal structures (Yamada et al., 1984; Zhang et al., 1993) are based upon double chains of edge-sharing octahedra occupied by Al and Si (no ordering in octahedral sites was observed so far) with channels occupied by large cations such as K^+, Na^+ or Ca^{2+}. The natural Na-dominant member, $Na[AlSi_3O_8]$, was described as lingunite, first observed by Mori (1990, 1994) in the Yamato-790729 L6 chondrite followed by its other findings in meteorites with the X-ray diffraction data and Raman spectrum first provided by Gillet et al. (2000) (see also: Liu, El Goresy, 2007). The K-dominant member was found in the Zagami Martian meteorite and named liebermannite (Ma et al., 2018). It was reported to form *via* solid-state transformation of primary K-feldspar during an impact event that achieved pressures of ~20 GPa or higher. The natural Ca-dominant member is known as stöfflerite that, prior to its establishment as a separate mineral species (Tschauner et al., 2021), was reported by El Goresy et al. (2000b), Langenhorst and Poirier (2000) and Beck et al. (2004) from the Zagami and NWA-856 meteorites.

4. PYROXENE AND AMPHIBOLE HIGH-PRESSURE POLYMORPHS

The high-pressure and high-temperature polymorphism of pyroxenes and amphiboles was reviewed in detail by Yang and Prewitt (2000) and Welch et al. (2007). A number of recent investigations revealed several new pressure-induced polymorphic transitions, most of which do not involve changes in Si coordination and correspond to the deformation of silicate chains achieved through the rotation of tetrahedra (Zhang et al., 2012; Dera et al., 2013; Hu et al., 2015b; Yong et al., 2019a, b; Xu et al., 2020). The character of these transitions strongly depends upon chemical composition and symmetry of the respective compounds. Herein we shall concentrate only on the pyroxene polymorphs with hexacoordinated Si and those phase transitions that are accompanied by the changes in Si coordination number. The crystallographic data for HP polymorphs of pyroxenes and amphiboles are given in Table 4.

The first Si-rich pyroxene with hexacoordinated Si was reported by Angel et al. (1988) as a synthetic phase with the composition $Na(Mg_{0.5}Si_{0.5})Si_2O_6$. In its crystal structure, Si occupies a separate crystallographic sites M(1)1, so the crystal-chemical formula of the phase can be written as $Na_2Mg^{VI}Si[^{IV}Si_2O_6]_2$. In the crystal structure (Fig. 8*a*), one may subdivide a silicate substructure consisting of $[Si_2O_6]$ chains of corner-sharing SiO_4 tetrahedra interlinked by SiO_6 octahedra into a layer parallel to (010) (Fig. 8*b, c*). Yang and Konzett (2005) reported the crystal structure of synthetic pyroxene $(Ca_{0.36}Na_{0.56}Mg_{0.08})(Mg_{0.73}Si_{0.27})Si_2O_6$ that crystallizes in the *C*2/*c* space group with no ordering of Si, whereas Posner et al. (2012) refined the structure of $(Na_{0.97}Mg_{0.03})(Mg_{0.43}Fe^{3+}_{0.17}Si_{0.40})Si_2O_6$ in the *P*2/*n* space group with Si incorporated, along

Table 4. Crystallographic data for high-pressure pyroxene polymorphs with coordination number of Si greater than 4
Таблица 4. Кристаллографические параметры для высокобарических полиморфов пироксенов с координационным числом кремния выше 4

Mineral/phase name	Chemical formula	SG	*a* [Å]/α [°]	*b* [Å]/β []	*c* [Å]/γ [°]	*V*, Å^3	CN(Si)	Ref.
–	$NaMg_{0.5}Si_{0.5}Si_2O_6$	*P*2/*n*	9.418/90	8.647/108.1	5.274/90	408.2	4, 6	1
–	$(Ca_{0.36}Na_{0.56}Mg_{0.08})(Mg_{0.73}Si_{0.27})Si_2O_6$	*C*2/*c*	9.579/90	8.759/107.2	5.261/90	421.7	4, 6	2
–	$(Na_{0.97}Mg_{0.03})(Mg_{0.43}Fe^{3+}_{0.17}Si_{0.40})Si_2O_6$	*P*2/*n*	9.443/90	8.646/108.0	5.254/90	408.0	4, 6	3
“β-diopside” (48.4 GPa)	$CaMgSi_2O_6$	$P2_1/c$	9.053/90	7.677/96.3	4.751/90	328.2	4, 6	4
“γ-diopside” (55.1 GPa)	$CaMgSi_2O_6$	$P2_1/c$	9.279/90	7.566/98.5	4.628/90	321.5	5, 6	5
HPCEN2*	$Mg_2Si_2O_6$	$P2_1/c$	8.760/90	7.919/100.2	4.610/90	314.7	4, 6	6
“Clinoferrosilite-HP-$P2_1/c$” (35.9 GPa)	$Fe_2Si_2O_6$	$P2_1/c$	9.180/90	8.110/100.3	4.602/90	337.1	4, 6	7
“α-popx”** (34.0 GPa)	$Mg_{2.8}Fe_{0.2}Si_2O_6$	$Pca2_1$	4.568/90	8.278/90	17.492/90	674.5	4, 5	8
“β-popx”** (48.5 GPa)	$Mg_{2.8}Fe_{0.2}Si_2O_6$	$Pca2_1$	4.527/90	7.847/90	17.377/90	617.3	4, 5, 6	8

* HPCEN2 = high-pressure clinoenstatite-2.
** popx = post-orthopyroxene.
References: (1) Angel et al., 1988; (2) Yang, Konzett, 2005; (3) Posner et al., 2012; (4) Plonka et al., 2012; (5) Hu et al., 2017b; (6) Lazarz et al., 2019; (7) Pakhomova et al., 2017b; (8) Finkelstein et al., 2015a.

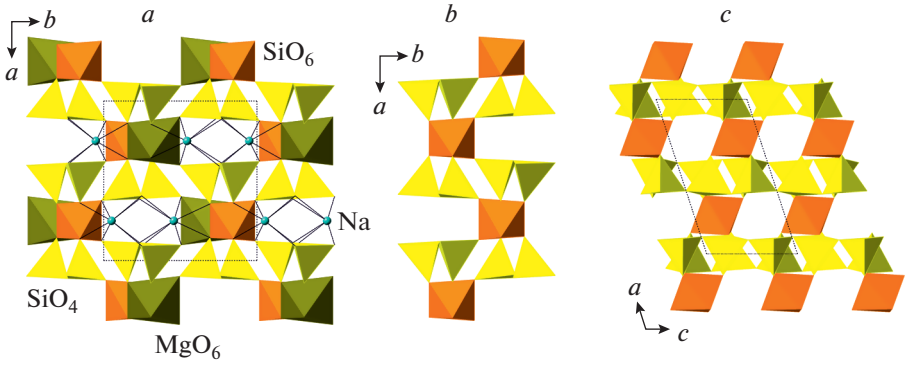

Fig. 8. The crystal structure of $Na(Mg_{0.5}Si_{0.5})Si_2O_6$ ($=Na_2Mg^{VI}Si[^{IV}Si_2O_6]_2$) projected along the *c* axis (*a*), and the silicate sublayer $\{^{VI}Si[^{IV}Si_2O_6]_2\}$ projected along the *c* (*b*) and *b* (*c*) axes.

Рис. 8. Кристаллическая структура $Na(Mg_{0.5}Si_{0.5})Si_2O_6$ ($=Na_2Mg^{VI}Si[^{IV}Si_2O_6]_2$) в проекции вдоль оси *c* (*a*) и силикатный слой $\{^{VI}Si[^{IV}Si_2O_6]_2\}$ в проекциях вдоль осей *c* (*b*) и *b* (*c*).

with Mg and Fe^{3+}, into the M(1)1 site. Yang et al. (2009a) investigated the crystal chemistry of clinopyroxene phases in the $Na(Mg_{0.5}Si_{0.5})Si_2O_6$–$NaAlSi_2O_6$ system and demonstrated that the ordering of Si and the formation of the *P*2/*n* arrangement is favorable when the amount of ^{VI}Si is greater than 0.35 atoms per formula unit (*apfu*).

The first observation of a pyroxene with ^{IV}Si transforming into ^{VI}Si under compression was reported by Plonka et al. (2012) for diopside, $CaMgSi_2O_6$. The crystal structure of its HP-polymorph β-diopside is shown in Fig. 9*a*. In ordinary clinopyroxenes, the $[Si_2O_6]$ chains are arranged into layers parallel to (100) (see, e.g., Fig. 8*a*). In β-diopside, every second of such layers is replaced by the continuous dioctahedral layer of edge-sharing SiO_6 octahedra (Fig. 9*c*). Hu et al. (2017b) reported the crystal structure of even higher-pressure polymorph, γ-diopside, that contains no ^{IV}Si, but, instead, is based upon alternating dioctahedral layers and layers of corner-sharing dimers of edge-linked SiO_5 triangular bipyramids. Pakhomova et al. (2017b) observed the high-pressure transition of clinoferrosilite, $Fe_2Si_2O_6$, into its HP-$P2_1/c$ modification isotypic to β-diopside, whereas Lazarz et al. (2019) discovered the same phase transition for clinoenstatite, $Mg_2Si_2O_6$.

The similar phase transitions accompanied by the change in Si coordination number and replacement of layers of tetrahedral chains by the layers of Si polyhedra in higher coordinations were reported for orthopyroxenes by Finkelstein et al. (2015a). These authors investigated phase transitions for the orthorhombic $Mg_{2.8}Fe_{0.2}Si_2O_6$ and found two phase transitions to the phases identified as α-post-orthopyroxene (α-popx) and β-post-orthopyroxene (β-popx) (Fig. 10). In the crystal structure of α-popx, every second layer of tetrahedral chains ($\mathbf{L_1}$: Fig. 10*c*) is replaced by the layer of SiO_4 tetrahedra and SiO_5 tetragonal pyramids ($\mathbf{L_2}$: Fig. 10*d*). In the higher-pressure polymorph, β-popx, the $\mathbf{L_2}$ layers alternate with the $\mathbf{L_3}$ dioctahedral layers of edge-sharing SiO_6 octahedra (Fig. 10*e*), i.e. the crystal structure contains Si in four-, five- and sixfold coordinations.

In contrast to pyroxenes, as to our knowledge, there are no reports on the occurrence of non-tetrahedral Si in the crystal structure of amphiboles (Yang, Prewitt, 2000; Welch et al., 2007).

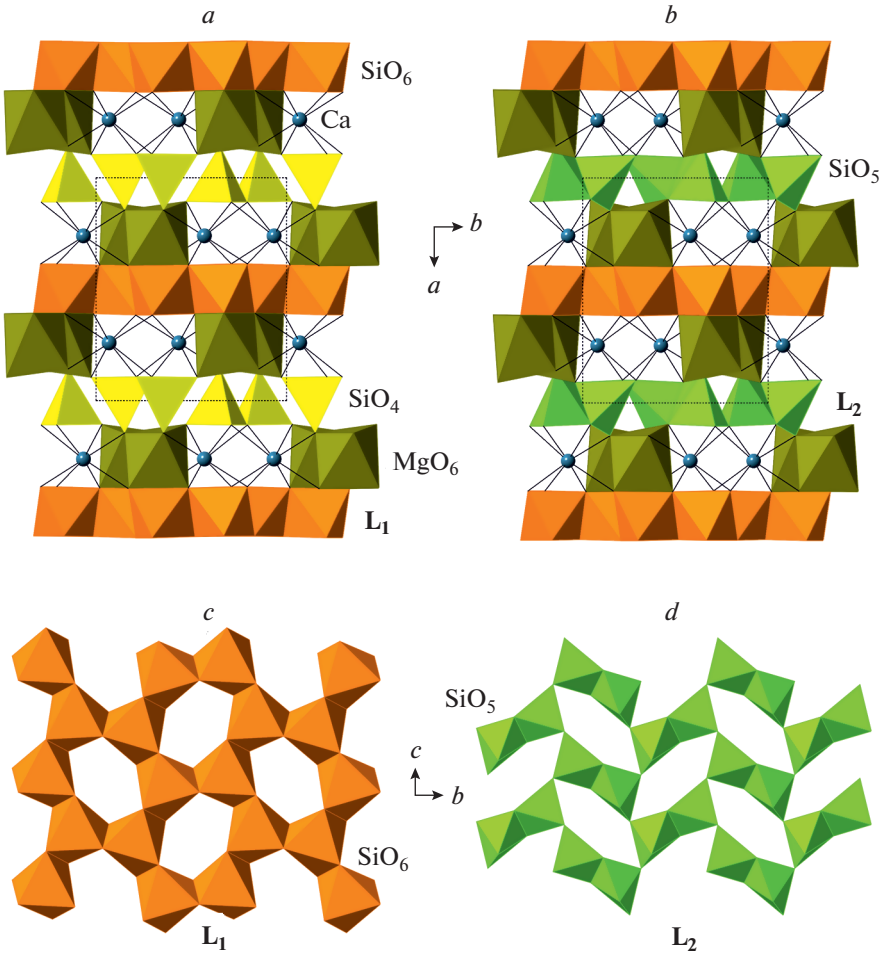

Fig. 9. The crystal structures of β- (*a*) and γ- (*b*) diopside in projections along the *c* axes and the structures of the $\mathbf{L_1}$ (*c*) and $\mathbf{L_2}$ (*d*) layers based upon SiO_6 and SiO_5 polyhedra, respectively.

Рис. 9. Кристаллические структуры β-диопсида (*a*) и γ-диопсида (*b*) в проекциях вдоль осей *c* и структура слоев $\mathbf{L_1}$ (*c*) и $\mathbf{L_2}$ (*d*), состоящих из полиэдров SiO_6 и SiO_5, соответственно.

5. OCTAHEDRAL Si IN GARNETS

Silicate garnets with Si in octahedral coordination were first synthesized by Ringwood and Major (1967a). Three years later, Smith and Mason (1970) reported the occurrence of the garnet-structured $MgSiO_3$ [$4MgSiO_3 = Mg_3(MgSi)(SiO_4)_3$] in the Coorara meteorite and named it majorite in honor of Alan Major, a collaborator of A.E. Ringwood. Majorite was subsequently reported in various natural environments associated with high-pressure conditions (Tomioka et al., 2016; Tschauner, 2019). As to our knowledge, no full crystal-structure determinations have been done on natural crystals and all the crystal-structure data originate from the studies of synthetic materials (Table 5). Fujino et al. (1986) determined the crystal structure of $Mn_3(MnSi)(SiO_4)_3$ in the tetragonal space group $I4_1/a$. The group-subgroup reduction of symmetry from the ideal $Ia\bar{3}d$ garnet structure type to $I4_1/a$ is due to the complete ordering

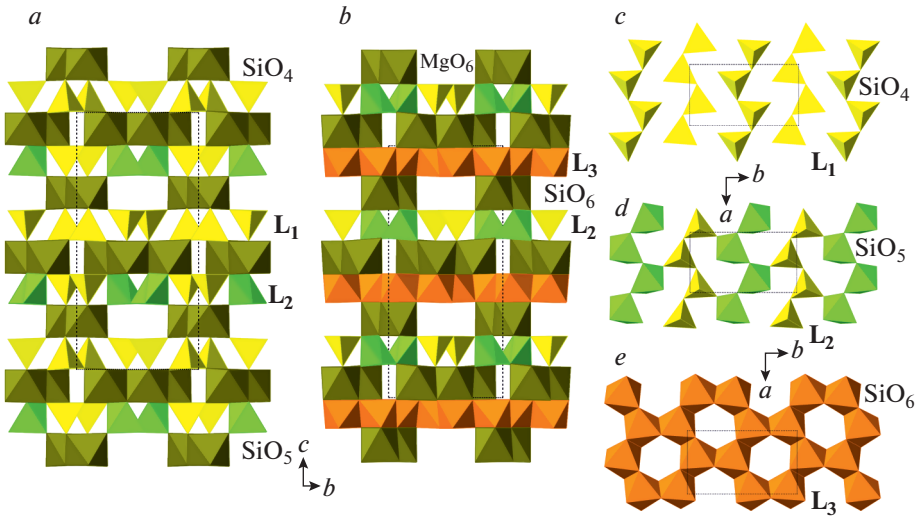

Fig. 10. The crystal structures of α-popx (*a*) and β-popx (*b*), and the diagrams of the silicate layers in their structures (*c*–*e*).
Рис. 10. Кристаллические структуры α-пост-ортопироксена (*a*) и β-пост-ортопироксена (*b*) и диаграммы силикатных слоев в их структурах (*c*–*e*).

of Mn and Si into two separate octahedral sites (Fig. 11*a*). The same kind of ordering, but with slight disorder, was observed by Angel et al. (1989) for synthetic majorite, $Mg_3(MgSi)(SiO_4)_3$. Considering the silicate substructure only, the crystal structure is based upon the heteropolyhedral $[^{VI}Si(^{IV}SiO_4)_2]$ framework of corner-sharing SiO_6 octahedra and SiO_4 tetrahedra with Mg atoms and additional SiO_4 groups in the cavities (Fig. 11*b*).

The symmetry of majorite-bearing garnets had been a subject of extensive investigations (Parise et al., 1996; Heinemann et al., 1997; Nakatsuka et al., 1999a, b; Hofmeister et al., 2004; Liu et al., 2017b): by analogy with pyroxenes, the symmetry depends upon the amount of excessive ^{VI}Si in the chemical formula. Bindi et al. (2011) reported the crystal structure of

Table 5. Crystallographic data for synthetic majorite and related phases
Таблица 5. Кристаллографические данные для синтетических аналогов мэйджорита и близких фаз

Chemical formula	SG	*a*, Å	*c*, Å	*V*, Å^3	CN(Si)	Ref.
$Mn_3(MnSi)(SiO_4)_3$	$I4_1/a$	11.774	11.636	1613.1	4, 6	1
$Mg_3(MgSi)(SiO_4)_3$	$I4_1/a$	11.501	11.480	1518.5	4, 6	2
$Mg_{2.51}Ca_{0.49}(MgSi)(SiO_4)_3$	$I4_1/a$	11.582	11.529	1546.4	4, 6	3
$Mg_3(Mg_{0.34}Si_{0.34}Al_{0.18}Cr_{0.14})_2(SiO_4)_3$	$I4_1/a$	11.512	11.515	1526.0	4, 6	4
$Mg_3(Cr_{1.58}Mg_{0.21}Si_{0.21})(SiO_4)_3$	Ia-3d	11.572	= a	1549.5	4, 6	5
$(Na_2Mg)Si_2(SiO_4)_3$	$I4_1/acd$	11.397	11.337	1472.5	4, 6	6
$Fe_3^{2+}(Fe_{1.532}^{3+}Fe_{0.234}^{2+}Si_{0.234})(SiO_4)_3$	$Ia\bar{3}d$	11.751	= a	1622.7	4, 6	7
$(Na_2Mg)Si_2(SiO_4)_3$	$Ia\bar{3}d$	11.266	= a	1429.9	4, 6	8

References: (1) Fujino et al., 1986; (2) Angel et al., 1989; (3) Hazen et al., 1994b; (4) Nakatsuka et al., 1999b; (5) Bykova et al., 2014; (6) Bindi et al., 2011; (7) Ismailova et al., 2015; (8) Yang et al., 2009b.

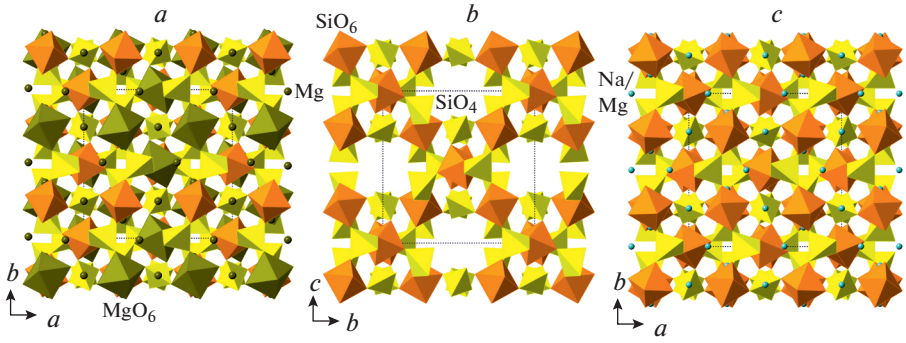

Fig. 11. The crystal structure of majoritic garnet $Mg_3(MgSi)(SiO_4)_3$ (*a*) and its silicate substructure $\{^{VI}Si(^{IV}SiO_4)_2\}$ projected along the *a* axis (*b*); the crystal structure of $Na_2MgSi_2(SiO_4)_3$ (*c*).

Рис. 11. Кристаллическая структура мэйджоритового граната $Mg_3(MgSi)(SiO_4)_3$ (*a*) и его каркасная силикатная подструктура $\{^{VI}Si(^{IV}SiO_4)_2\}$ в проекции вдоль оси *a* (b); кристаллическая структура $Na_2MgSi_2(SiO_4)_3$ (*c*).

$(Na_2Mg)^{VI}Si_2(^{IV}SiO_4)_3$ with both octahedral sites in the garnet structure occupied by ^{IV}Si. The structure has the $I4_1/acd$ space group and represents a fully connected $[^{VI}Si_2(^{IV}SiO_4)_3]$ octahedral-tetrahedral framework with Mg^{2+} and Na^+ ions in the cavities (Fig. 11*c*). It is of interest that Hazen et al. (1994a) determined for $(Na_2Mg)^{VI}Si_2(^{IV}SiO_4)_3$ a cubic symmetry, but the structure details have never been published in full (see also: Finger, Hazen, 2000). Yang et al. (2009b) reported the crystal structure of $(Li_2Mg)^{VI}Si_2(^{IV}SiO_4)_3$ in the $Ia\bar{3}d$ space group with single octahedral site occupied by Si.

6. $MSiO_3$ HP POLYMORPHS (M = Mg, Fe)

The $MSiO_3$ polymorphs (M = Mg, Fe) with pyroxene and garnet crystal structure and their HP transformations into phases with non-tetrahedral Si under pressure were considered in sections 4 and 5. According to the current knowledge (see, e.g., Gasparik, 1990; Tomioka, Miyahara, 2017), at ~15–16 GPa $MgSiO_3$ pyroxene transforms (depending upon temperature) into either majoritic garnet (at >1800 K) or a mixture of Mg_2SiO_4 (ringwoodite or wadsleyite) and stishovite, SiO_2 (however, recent findings of Kim et al. (2021) challenge these observations and present a more complicated picture). Under increasing pressure, the Mg_2SiO_4 + SiO_2 mixture transforms into akimotoite, the $MgSiO_3$ polymorph with the ilmenite structure (see below) and, above 25 GPa, into bridgmanite, a $MgSiO_3$ perovskite. The last phase stable under Earth mantle conditions is post-perovskite $MgSiO_3$, which exists above 120 GPa and 2500 K. It is believed that bridgmanite is the most abundant mineral in the Earth (constituting about 38% of its volume) and the major mineral phase in the lower mantle (Pushcharovsky D., Pushcharovsky Yu., 2012; Wicks, Duffy, 2016; Tschauner, 2019). Below we provide brief structural and mineralogical descriptions on the HP polymorphs of $MgSiO_3$ and their Fe analogues. The crystallographic information on these phases is provided in Table 6.

Akimotoite, a $MgSiO_3$ polymorph crystallizing in the ilmenite structure type, was first synthesized by Kawai et al. (1974) and identified by Liu (1976) as an analogue of ilmenite, $FeTiO_3$. Its single-crystal structure study was done by Horiuchi et al. (1982). Sharp et al. (1997)

Table 6. Crystallographic data for high-pressure $MSiO_3$ phases (M = Mg, Fe)
Таблица 6. Кристаллографические данные для высокобарических фаз $MSiO_3$ (M = Mg, Fe)

Mineral/phase name	Chemical formula	SG	*a* [Å]/α [°]	*b* [Å]/β [°]	*c* [Å]/γ [°]	*V*, Å^3	CN(Si)	Ref.
Akimotoite	$MgSiO_3$	$R\bar{3}$	4.780/90	4.780/90	13.600/120	269.0	6	1
Synthetic akimotoite	$MgSiO_3$	$R\bar{3}$	4.728/90	4.728/90	13.559/120	262.5	6	2
Hemleyite	$FeSiO_3$	$R\bar{3}$	4.748/90	4.748/90	13.665/120	266.8	6	3
Bridgmanite	$MgSiO_3$	*Pbnm*	4.81/90	5.02/90	6.90/90	167.0	6	4
Synthetic bridgmanite	$MgSiO_3$	*Pbnm*	4.778/90	4.930/90	6.899/90	162.5	6	5
Hiroseite	$FeSiO_3$	*Pbnm*	5.002/90	7.003/90	4.846/90	169.7	6	6
–	$(Mg_{0.5}Fe^{3+}_{0.5})(Si_{0.5}Al^{3+}_{0.5})O_3$	*R*3*c*	4.872/90	4.872/90	12.898/120	265.1	6	7
“H-phase”	$FeSiO_3$	*hex*	5.096/90	5.096/90	2.862/120	64.4	6?	8
Mg-“H-phase”	$Mg_{0.6}Fe_{0.4}SiO_3$	*hex*	5.136/90	5.136/90	2.883/120	65.9	6?	8
“Post-perovskite” (121 GPa)	$MgSiO_3$	*Cmcm*	2.456/90	8.042/90	6.093/90	120.3	6	9

References: (1) Tomioka, Fujino, 1999; (2) Horiuchi et al., 1982; (3) Bindi et al., 2017b; (4) Tschauner et al., 2014; (5) Dobson, Jacobsen, 2004; (6) Bindi et al., 2020b; (7) Liu et al., 2019; (8) Zhang et al., 2014; (9) Murakami et al., 2004.

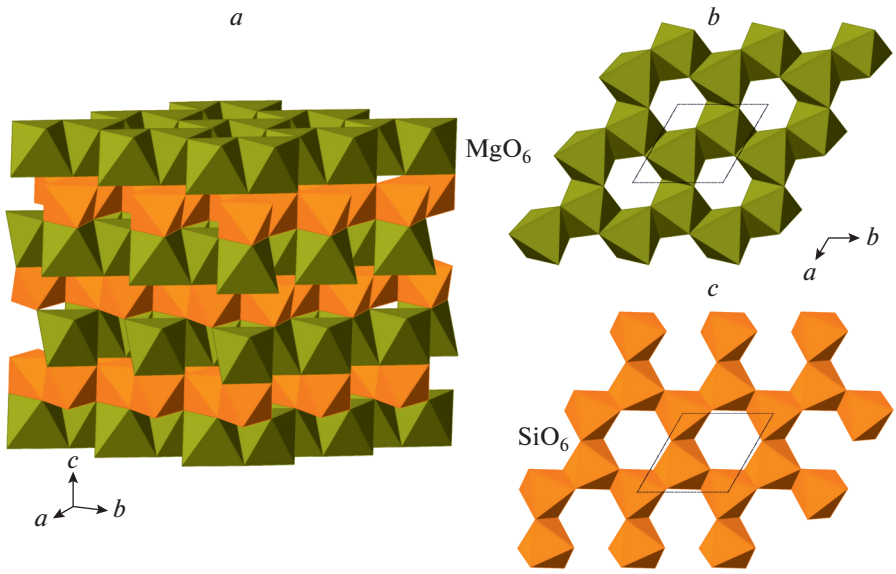

Fig. 12. The crystal structure of akimotoite (*a*) as consisting of alternating layers of MgO_6 (*b*) and SiO_6 (*c*) octahedra.
Рис. 12. Кристаллическая структура акимотоита (*a*) как состоящая из чередующихся слоев октаэдров MgO_6 (*b*) и SiO_6 (*c*).

and Tomioka and Fujino (1997) reported the occurrence of natural $MgSiO_3$ ilmenite in shocked meteorites and the mineral was described as a single species and named "akimotoite" by Tomioka and Fujino (1999). Later studies by Ferroir et al. (2008) and Tschauner et al. (2018) contributed to the understanding of its properties and formation mechanisms. Bindi et al. (2017b) described the Fe-analogue of akimotoite in the shocked Suizhou L6 chondrite and named it "hemleyite" in honor of Russell J. Hemley. It is worthy to note that the empirical chemical formula, $(Fe^{2+}_{0.48}Mg_{0.37}Ca_{0.04}Na_{0.04}Mn^{2+}_{0.03}Al_{0.03}Cr^{3+}_{0.01})_{\Sigma\,=\,1.00}Si_{1.00}O_3$, has only slight prevalence of Fe over Mg and the Fe amount does not exceed 0.5 *apfu*. The crystal structure of akimotoite (Fig. 12*a*) is based upon octahedral framework consisting of two alternating types of dioctahedral sheets (Fig. 12*b, c*) formed by edge-sharing SiO_6 and MgO_6 octahedra. The sheets are linked together by face sharing of SiO_6 and MgO_6 octahedra from the adjacent sheets. The dioctahedral silicate sheet in akimotoite is identical to the $\mathbf{L_3}$ sheet in β-popx (Fig. 10*e*) and the $\mathbf{L_1}$ sheet in β- and γ-diopsides and HP-$P2_1/c$ polymorph of clinoferrosilite described by Pakhomova et al. (2017b). The face-sharing between MO_6 and SiO_6 octahedra (M = Fe, Mg) exists in all the mentioned structures as well, which allows to suggest the direct transformation pathways between the structures of $MSiO_3$ pyroxenes to that of $MSiO_3$ ilmenite through the transitional polymorphs with five- and sixfold coordinated Si. The alternative way to describe the crystal structure of akimotoite is to consider it as a hexagonal close packing with 6-layer sequence ABABAB = $[AB]^3$, where the superstructure is formed due to the different occupancies of octahedral sites in similar layers oriented parallel to (001) and stacked along the *c* axis.

Bridgmanite, a perovskite-structured $MgSiO_3$ polymorph, was predicted by Ringwood (1962) and first discovered as a synthetic phase by Liu (1974, 1975). Its structural features and variations with temperature and pressure have been under extensive investigations (Yagi et al., 1978; Ito, Matsui, 1978; O'Keeffe et al., 1979; Kudoh et al., 1987; Horiuchi et al., 1987; Ross,

Hazen, 1989, 1990; Sugahara et al., 2006; Vanpeteghem et al., 2006; Hummer, Fei, 2012). The natural occurrence of bridgmanite in shocked meteorites was described by Sharp et al. (1997) and Tomioka and Fujino (1997), but the full mineral description of the IMA-approved mineral species was reported only recently by Tschauner et al. (2014). The crystal structure of bridgmanite (Fig. 13) is based upon distorted perovskite-type framework of corner-sharing SiO_6 octahedra with Mg atoms in cavities. The coordination of Mg is very irregular and is far from the ideal twelve-fold coordination in closed-packed structures, as can be expected for an ideal perovskite. At ambient pressure, Mg is coordinated by eight short (2.0–2.5 Å), two longer (2.8–3.0 Å) and two long (>3.1 Å) Mg–O bonds, and the coordination evolves toward eightfold under increasing pressure (O'Keeffe et al., 1979; Kudoh et al., 1987; Ross, Hazen, 1990; Sugahara et al., 2006). Thus, under compression the structure of bridgmanite becomes more distorted towards orthorhombic rather than cubic symmetry and it is rather surprising that the most abundant Earth's mineral demonstrates such a strong deviation from any aristotype structure with an ideal closest packing of ions. The Fe analogue of bridgmanite, hiroseite, was recently described by Bindi et al. (2020b) for the mineral with the empirical formula $(Fe_{0.54}Mg_{0.37}Al_{0.15}Na_{0.03}Ca_{0.02}Si_{0.89})O_3$ found in a shock vein of the Suizhou meteorite. Zhang et al. (2014) investigated the $Mg_{0.90}Fe_{0.10}SiO_3$ perovskite and observed that, at 95–101 GPa and 2200–2400 K, this phase is unstable and disproportionates into pure $MgSiO_3$ and hexagonal $FeSiO_3$ "H-phase" with unknown structural details. On the basis of theoretical calculations, Cohen and Lin (2014) proposed that the structure of this phase is in fact orthorhombic (space group *Cmmm*), but this hypothesis still awaits experimental confirmation. Liu et al. (2019) recently reported synthesis and crystal structure of $(Mg_{0.5}Fe^{3+}_{0.5})(Si_{0.5}Al^{3+}_{0.5})O_3$ that belongs to the $LiNbO_3$ structure type. In contrast to bridgmanite and hiroseite, this structure is close-packed: the arrangement of anions corresponds to the distorted threefold hcp superstructure with the layer sequence ABABAB = $[AB]^3$ (i.e. is analogous to the one observed in akimotoite). The cations reside in octahedral cavities. The connectivity of the $(Si_{0.5}Al^{3+}_{0.5})O_6$ octahedra corresponds to the perovskite topology.

The "post-perovskite" $MgSiO_3$ phase was discovered independently by two research groups (Murakami et al., 2004; Oganov, Ono, 2004) and studied extensively as reviewed in (Hirose et al., 2013, 2017; Hirose, 2014). The structure belongs to the $CaIrO_3$ structure type and is based upon layers of SiO_6 octahedra parallel to (010) with Mg atoms in capped square antiprismatic coordination (Fig. 14). The layers are formed by chains of edge-sharing SiO_6 octahedra parallel to [100]. The octahedra of the adjacent chains share corners to produce a two-dimensional layer. Though the natural "post-perovskite" had not yet been found, its discovery allowed to interpret the seismology and geodynamics of the D" layer in the lower mantle (Hirose et al., 2017).

7. M_2SiO_4 HP POLYMORPHS (M = Mg, Fe)

The M_2SiO_4 polymorphs (M = Mg, Fe) are believed to be important phases in the upper mantle and the mantle transition zone (Frost, 2008). Olivine, the general name for the members of the forsterite Mg_2SiO_4 – fayalite Fe_2SiO_4 series, is stable up to 14 GPa (~440 km depth), when its transformation to wadsleyite, β-$(Mg,Fe)_2SiO_4$, marks the beginning of the mantle transition zone. Within the mantle transition zones, wadsleyite transforms into ringwoodite, γ-$(Mg,Fe)_2SiO_4$, at 17.5 GPa (~520 km depth). The $Mg_2SiO_4 \rightarrow MgSiO_3 + MgO$ disproportionation of ringwoodite into bridgmanite and periclase corresponds to the beginning of the lower mantle. The transition from the crystal structure of olivine to the crystal structure of ringwoodite that belongs to the spinel structure type goes through the intermedi-

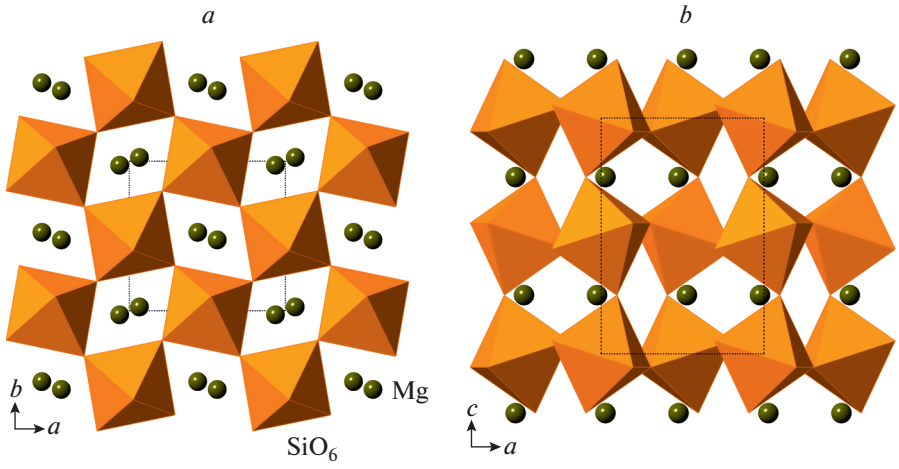

Fig. 13. The crystal structure of bridgmanite projected along the *c* (*a*) and *b* (*b*) axes.
Рис. 13. Кристаллическая структура бриджманита в проекциях вдоль осей *c* (*a*) и *b* (*b*).

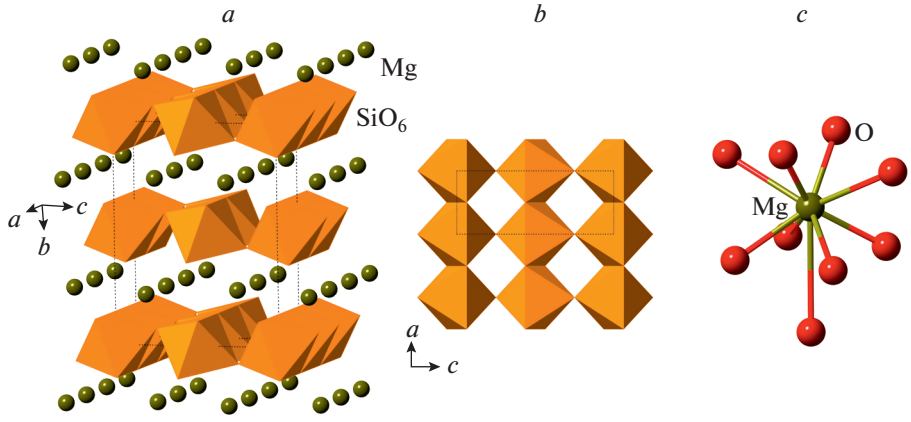

Fig. 14. The crystal structure of "post-perovskite" (*a*), its octahedral layer (*b*) and coordination of Mg atom (*c*).
Рис. 14. Кристаллическая структура «пост-перовскита» (*a*), ее октаэдрический слой (*b*) и координация атома Mg (*c*).

ate spinelloid structures explained and classified by Hyde et al. (1982) and Horiuchi et al. (1980).

The ideal crystal structure of spinel, M_2TO_4, is based upon ccp with M and T in octahedral and tetrahedral interstices, respectively. Fig. 15*a* shows the crystal structure of spinel projected along [110]. It can be considered as built up by spinel modules shown in Fig. 15*b* (in Fig. 15*a*, the borders of the modules are indicated by dashed lines). In ideal spinel, the modules with "up" (↑) and "down" (↓) orientations alternate. The border between two modules with opposite orientations is identified as **S**, whereas the border between two modules with the same orientation (↑↑ or ↓↓) is identified as **T**. In fact, the **T**-plane can be considered as a local chemical twinning plane. Figure 16 shows the crystal structure of "wadsleyite-II", Mg_2SiO_4, that

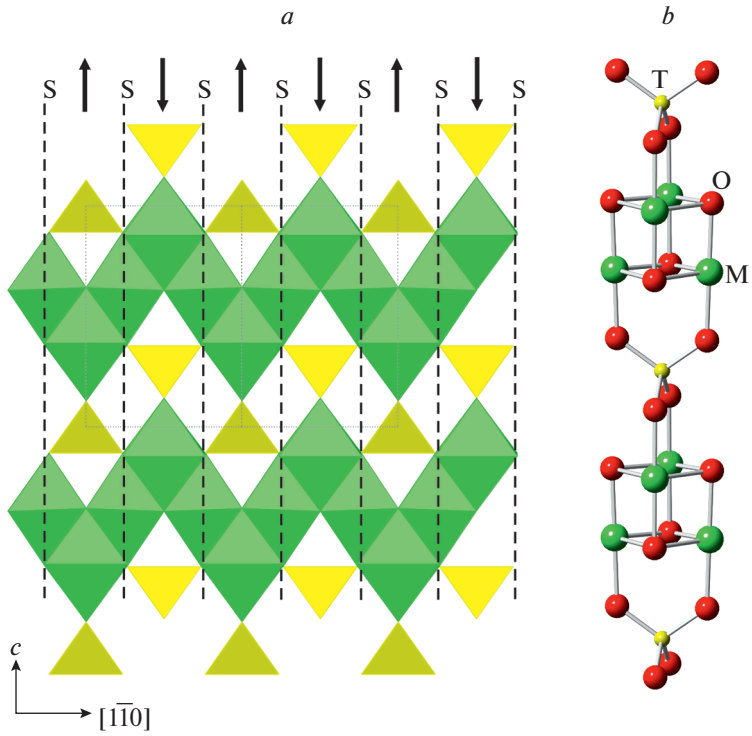

Fig. 15. The crystal structure of spinel projected along [110] (*a*) and the ball-and-stick representation of a spinel module (*b*). The dashed lines outline the contours of the modules, whereas the arrows indicate their orientation. The T- and M-centered polyhedra in (*a*) are shown in yellow and green, respectively.
Рис. 15. Кристаллическая структура шпинели в проекции вдоль [110] (*a*) и шариковое представление шпинелевого модуля (*b*). Штриховые линии указывают контуры шпинелевых модулей, а стрелки – их ориентацию. Т- и М-центрированные полиэдры в части (*a*) показаны желтым и зеленым цветами, соответственно.

has the sequence of modules ... ↓[↑↑↓↑↑↓↓↑↓↓]↑..., where square brackets indicate the unit-cell content along the direction of module stacking. Thus, the sequence of borders (or Hyde symbol) is **[STSSTSTSST]** or $[\mathbf{TS^2TS}]^2$. The number of spinel modules in between the two **T** planes is given as *n* or *m*. These numbers correspond to the widths of the spinel-like blocks (inside which only **S**-borders are allowed) along the direction of the module stacking. For instance, in "wadsleyite-II", the (*n*, *m*) numbers are (3, 2, 3, 2) or simply (3, 2). Table 7 provides the full classification of spinelloid structures known today, including those observed in HP mineral and synthetic phases. The structural complexity parameters indicate that only the simplest structures have been observed in nature so far. Below we concentrate on HP minerals as the most relevant for our review.

The crystal structure of forsterite, Mg_2SiO_4, is based upon hcp packing of O atoms with Mg and Si in octahedral and tetrahedral interstices, respectively. Since spinel and all spinelloid structures are based upon ccp arrangement, the transition from olivine structure to that of spinel requires shear mechanisms as predicted by Hyde et al. (1982) and first observed by Madon and Poirier (1983). The first phase that forms as a result of the shear transformations is the (1,1) spinelloid with the module sequence [↑] (or equivalent [↓]) and the sequence of borders [**T**]. Despite its high simplicity, in silicates, this phase with the formula $M_2(SiO_3)O$ contains one-

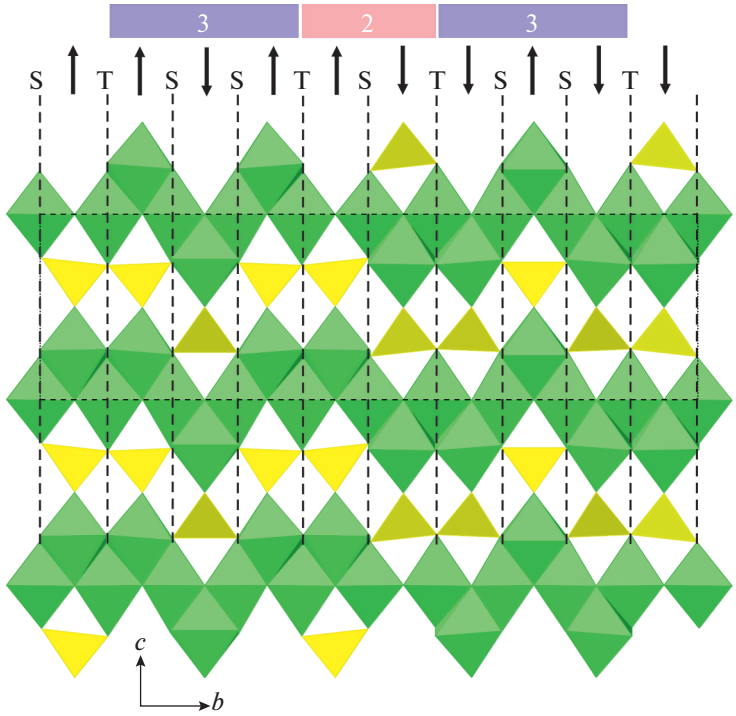

Fig. 16. The crystal structure of "wadsleyite-II" featuring borders and orientations of spinel modules. The numbers above provide the widths of spinel blocks in terms of the numbers of modules between the two **T**-planes.
Рис. 16. Кристаллическая структура "вадслеита-II" с обозначением границ и ориентации шпинелевых модулей. Цифры вверху показывают ширину шпинелевых блоков, заключенных между плоскостями **T**, в терминах числа шпинелевых модулей.

periodic (or *einer* in the Liebau's (1985) notation) chains of corner-sharing SiO_4 tetrahedra that is quite untypical for silicate crystal chemistry (though it has been known for germanates (Pushcharovsky, 1986)). Nevertheless, this phase with the ideal chemical composition Mg_2SiO_4 was observed by Tomioka and Okuchi (2017) as nanometer-scale lamellae in ringwoodite crystals from shocked meteorites and recently described as a separate mineral species, poirierite, ε-Mg_2SiO_4 (Tomioka et al., 2021).

Wadsleyite or β-Mg_2SiO_4 was first synthesized by Ringwood and Major (1966) and the phase was indentified as a transitional form in the transformation of olivine into spinel by Akimoto and Sato (1968). Its crystal structure (Moore, Smith, 1970; Hazen et al., 2000a, b; Zhang et al., 2016b; Sirotkina et al., 2018, etc.) is the (2,2) member of the spinelloid group (Table 7) with the module sequence [↑↑↓↓] and the Hyde symbol (**TS**)^2. Its chemical formula can be written as $Mg_4(Si_2O_7)O$, featuring the "additional" O atom prone to protonation. The possibility and the existence of "hydrous wadsleyite" prompted its consideration as a significant reservoir of H_2O in the Earth" interior (its stability outlines the mantle hydrous transition zone) (Kudoh et al., 1996; Smyth et al., 1997; Kudoh, 2001; Holl et al., 2008; Ye et al., 2010, 2011; Sano-Furukawa et al., 2011). The natural occurrences of wadsleyite are associated with shocked meteorites (Price et al., 1983). The Fe-analogue of wadsleyite, ideally β-Fe_2SiO_4, was recently described as a separate mineral species asimowite (Bindi et al., 2019).

Table 7. Crystallographic data and structural complexity parameters for spinelloid structure types
Таблица 7. Кристаллографические данные и параметры сложности для структурных типов шпинеллоидов

Phase	OS	HS	n, m	SG	a, Å	b, Å	c, Å	I_G, bit/atom	$I_{G,total}$, bit/cell	Formula	Example	Ref.
ε	(↑)	(**T**)	(1, 1)	*Pmma*	5.802	2.905	8.411	2.522	35.303	$M_2(TO_3)O$	ε-Mg_2SiO_4 poirierite	1
I	(↑↑↑↓)	(**T**^{2}**S**^{2})	(3, 1)	*Pmma*	5.666	11.496	8.098	3.807	213.212	$M_8(T_3O_{10})(TO_4)O_2$	$(Ni_{10.3}Al_{7.7})(Al_{3.6}Si_{2.4})O_{32}$	2
II	(↑↑↑↓↓↓)	(**T**^{2}**S**)^2	(2, 1)	*Imma*	5.660	17.298	8.110	3.345	140.477	$M_6(T_3O_{10})O_2$	$(Ni_{17}Al_7)(Al_{6.9}Si_{5.1})O_{48}$	3
III	(↑↑↓↓)	(**TS**)^2	(2, 2)	*Imma*	5.696	11.444	8.248	2.807	78.606	$M_4(T_2O_7)O$	β-Mg_2SiO_4 wadsleyite	4
				Imma	5.749	11.576	8.363	2.807	78.606	$M_4(T_2O_7)O$	β-Fe_2SiO_4 asimowite	5
IV	(↑↑↓↑↑↓↓↑↓↓)	(**TS**^{2}**TS**)^2	(3, 2)	*Imma*	5.665	28.646	8.091	3.986	279.050	$M_{10}(T_2O_7)_2(TO_4)O_2$	$Ni_3Al_2SiO_8$	6
				Imma	5.688	28.924	8.238	3.986	279.050	$M_{10}(T_2O_7)_2(TO_4)O_2$	Mg_2SiO_4 “wadsleyite II”	7
V	(↑↑↓)	(**TS**^{2})	(3, 3)	*Pmma*	5.661	8.590	8.097	3.440	144.477	$M_6(T_2O_7)(TO_4)O$	$Ni_3Al_2SiO_8$	8
Spinel	(↑↓)	(**S**)	–	*Fd*$\bar{3}$*m*	8.065	= *a*	= *a*	1.379	19.303	$M_2(TO_4)$	γ-Mg_2SiO_4 ringwoodite	9
				Fd$\bar{3}$*m*	8.163	= *a*	= *a*	1.379	19.303	$M_2(TO_4)$	γ-Fe_2SiO_4 ahrensite	10
				R$\bar{3}$*m*	5.393	= *a*	13.891	–	–		γ-Fe_2SiO_4	11
				$I4_1/amd$	5.896	= *a*	8.416	1.379	19.303	$M_2(TO_4)$	$(Mg,Fe,Si)_2(Si,\square)O_4$	12
Olivine	–	–	–	*Pbnm*	4.756	10.207	5.980	2.522	70.606	$M_2(TO_4)$	α-Mg_2SiO_4	13

OS = orientation sequence of spinel modules; HS = Hyde symbol; SG = space group.
References: (1) Tomioka et al., 2021; (2) Ma et al., 1975; (3) Ma, Tillmanns, 1975; (4) Moore, Smith, 1970; (5) Bindi et al., 2019; (6) Horioka et al., 1981a; (7) Smyth, Kawamoto, 1997; (8) Horioka et al., 1981b; (9) Sasaki et al., 1982; (10) Ma et al., 2016; (11) Greenberg et al., 2011; (12) Ma et al., 2019a; (13) Smyth, Hazen, 1973.

Along with wadsleyite, ringwoodite or γ-Mg_2SiO_4 was first prepared experimentally (Ringwood, Major, 1966) and later found in shocked meteorites (Binns et al., 1969) and recently in mineral inclusions in diamonds (Pearson et al., 2014). Ringwoodite has a *sensu stricto* spinel $Fd\bar{3}m$ structure with the crystal-chemical formula $Mg_2(SiO_4)$ with isolated SiO_4 tetrahedra. Thus the transition forsterite → poirierite → wadsleyite → ringwoodite involves polymerization of isolated SiO_4 tetrahedra (in forsterite) into infinite chains (in poirierite), depolymerization of chains into SiO_4 and Si_2O_7 groups (in wadsleyite) and final depolymerization of Si_2O_7 groups into SiO_4 tetrahedra (in ringwoodite). The Fe analogue of ringwoodite is ahrensite, γ-Fe_2SiO_4 (Ma et al., 2016). Greenberg et al. (2011) reported on the rhombohedral distortion of the γ-Fe_2SiO_4 spinel structure type above 30GPa, whereas Ma et al. (2019a) recently described a spinel-structured phase with the chemical composition $(Mg,Fe,Si)_2(Si,\square)O_4$ that has the overall ringwoodite topology, but the reduced symmetry $I4_1/amd$, associated with splitting of the Mg site into two inequivalent sites with different occupancies. It is of interest that the authors assign 0.10 Si apfu to the octahedral site, thus suggesting the existence in the structure of Si in octahedral coordination. Van de Moortèle et al. (2007) described another $(Mg,Fe)_2SiO_4$ polymorph with the crystal structure close to that of olivine and based upon hcp of O atoms with Si tetrahedra in tetrahedral cavities and M atoms possibly disordered in octahedral interstices. However, the details of the structure remain unclear.

As for other HP silicates, cold compression may lead to novel metastable polymorphs with the M_2SiO_4 composition. Finkelstein et al. (2014) described two new HP modifications of forsterite, forsterite-II and forsterite-III, stable in the range of pressure of 50–58 and 58–90 GPa, respectively, at ambient temperature. The crystal structure of forsterite-II (Fig. 17*a*) determined by the combination of experimental and theoretical techniques is based upon ccp of O atoms with Mg in octahedral interstices and Si in both octahedral and tetrahedral interstices. The structure can also be described as based upon alternating layers of two types shown in Figs. 17*b* and *c*. The first layer $\mathbf{L_1}$ contains infinite 2 × 2 zigzag chains of MgO_6 octahedra ("seifertite chains") interlinked by dimers of edge-sharing SiO_6 octahedra (Fig. 17*b*). In contrast, the $\mathbf{L_2}$ layer (Fig. 17*c*) consists of triples of edge-sharing MgO_6 octahedra linked by isolated SiO_4 tetrahedra. Considering the connectivity of Si-centered polyhedra, the crystal structure contains dimers of edge-sharing SiO_6 octahedra sharing corners with two adjacent SiO_4 tetrahedra (Fig. 17*d*). In contrast to forsterite-II, the crystal structure of forsterite-III contains Si in octahedral coordination only (Fig. 18). Mg has two different coordination polyhedra. Mg1 is in octahedral coordination, whereas Mg2 has a tricapped trigonal prismatic coordination (Fig. 18*c*). The Mg–O bonds directed towards the vertices of the trigonal prism are rather short (<2.1 Å), whereas three additional Mg–O bonds are longer than 2.3 Å. The crystal structure is based upon ladder-like layers of edge-sharing $Mg1O_6$ and SiO_6 octahedra (Fig. 18*b*) parallel to (001) and linked by sharing corners to form channels with triangular cross-sections occupied by the Mg2 atoms (Fig. 18*a*). The silicate substructure is a "stishovite-type" chain of edge-sharing SiO_6 octahedra running parallel to the *a* axis. The crystal structure of forsterite-III belongs to the $CaTi_2O_4$ structure type, which had also been observed for another HP silicate, $Mg(Cr_{0.8}Mg_{0.2})(Si_{0.6}Mg_{0.4})O_4$ (Bindi et al., 2015a). The crystal structures of this phase and forsterite-III are very similar and differ in the predominant occupation of the M1 site by Cr, whereas the Mg2 site is occupied by Mg in both structures. The formation of forsterite-III was recently observed by Kim et al. (2021) in the experiments on laser-shock compression of olivine studied by femtosecond X-ray diffraction.

Yamanaka et al. (2015) investigated the high-pressure polymorphism of Fe_2SiO_4 at ambient temperature. They found the transformation of the Fe_2SiO_4 cubic spinel structure into the *I*-Fe_2SiO_4 polymorph crystallizing in the orthorhombic *Imma* space group. In the course of transition, the connectivity of the FeO_6 octahedra do not change, whereas Si changes its co-

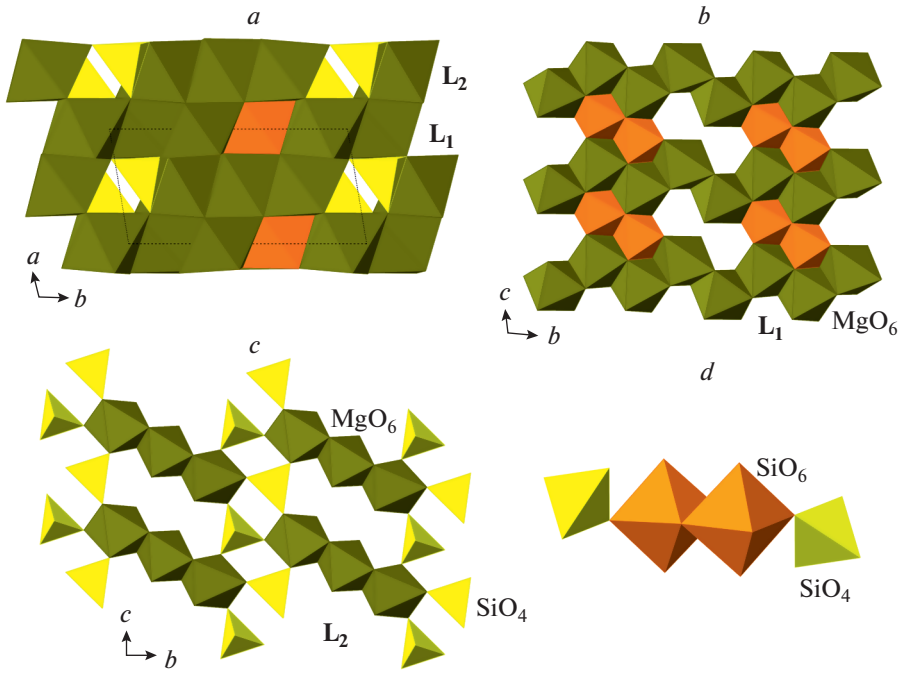

Fig. 17. The crystal structure of forsterite-II in projection along the *c* axis (*a*), the structures of the $\mathbf{L_1}$ (*b*) and $\mathbf{L_2}$ (*c*) layers, and the finite silicate anion consisting of two edge-sharing SiO_6 octahedra and two corner-sharing SiO_4 tetrahedra (*d*).

Рис. 17. Кристаллическая структура форстерита-II в проекции вдоль оси *c* (*a*), структура слоев $\mathbf{L_1}$ (*b*) и $\mathbf{L_2}$ (*c*) и островной силикатный анион, состоящий из двух связанных ребрами октаэдров SiO_6 и двух тетраэдров SiO_4 (*d*).

ordination from tetrahedral to octahedral. As a result, the SiO_4 tetrahedra transform into $[SiO_4]$ chains of edge-sharing SiO_6 octahedra running parallel to the *b* axis (Fig. 19). As a result, the symmetry reduces from cubic (that does not allow for a single orientation of chains) to orthorhombic with one orientation of chains. The crystallographic information on metastable M_2SiO_4 polymorphs (M = Mg, Fe) is given in Table 8.

8. DENSE HYDROUS MAGNESIUM SILICATES AND RELATED STRUCTURES

Dense hydrous magnesium silicates (DHMS) are high-pressure Mg silicates that are expected to be major hosts of H_2O under mantle conditions above 10 GPa. They were first synthesized by Ringwood and Major (1967b), who distinguished three new phases by X-ray diffraction analysis and identified them as A, B, and C phases, thus giving start to the investigations of the so-called "aphabet phases". The field was reviewed in (Frost, 1999; Ohtani et al., 2000, 2001; Angel et al., 2001b), where more details about the stability and identity of these phases can be found. Herein we concentrate on the crystal chemistry of DHMSs and related phases. The relevant crystallographic information is provided in Table 9.

The phase A, $Mg_7(SiO_4)_2(OH)_6$, is considered as a product of transformation of serpentine at depths greater than 180 km in cold subducting slabs (Ohtani et al., 2004). Its crystal structure was solved by Horiuchi et al. (1979) and further studied in (Kagi et al., 2000; Kuribayashi et al., 2003;

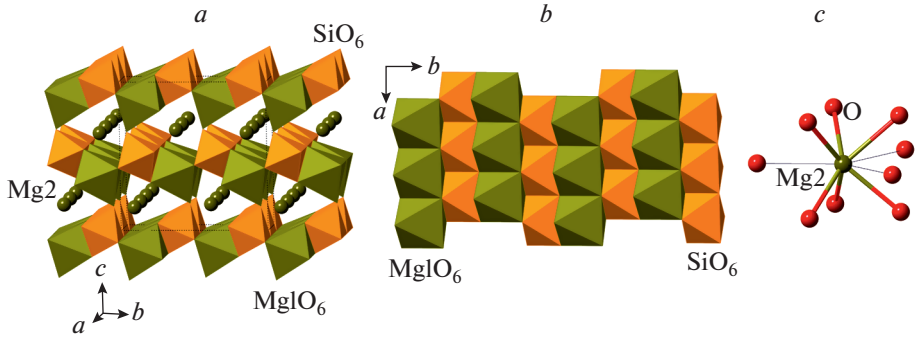

Fig. 18. The crystal structure of forsterite-III (*a*), its layer of edge-sharing SiO_6 and MgO_6 octahedra (*b*), and the coordination of the Mg2 atom (*c*).
Рис. 18. Кристаллическая структура форстерита-III (*a*), слой из связанных ребрами октаэдров SiO_6 и MgO_6 (*b*) и координация позиции Mg2 (*c*).

Holl et al., 2006). The structure (Fig. 20*a*) can be described as based upon two types of layers, $\mathbf{L_1}$ and $\mathbf{L_2}$, shown in Figs. 20*b* and *c*, respectively. The $\mathbf{L_1}$ layer consists of edge-sharing MgO_6 octahedra with triangular cavities occupied by SiO_4 tetrahedra, whereas the $\mathbf{L_2}$ layer is formed by condensation of edge-sharing trimers of Mg-centered octahedra interlinked by SiO_4 tetrahedra. The arrangement of anions corresponds to the ABCB 4-layer closest sphere packing with Mg and Si in octahedral and tetrahedral interstices, respectively.

The phase B exists in at least three topological varieties, phase B, anhydrous phase B (AnhB), and superhydrous phase B (ShyB) that correspond to different connectivities of Mg and Si coordination polyhedra. The anion packings in the three varieties are the same and are of the 6-layer ABACBC sequence. However, the occupancies of octahedral and tetrahedral interstices are different, which results in three different structure topologies (Fig. 21*a, d, g*). For all three phases, the crystal structures can be represented as built up by stacking of two different layers, $\mathbf{L_1}$ and $\mathbf{L_2}$, taken in the sequence ...$\mathbf{L_1L_2L_2L_1L_2L_2}$... The $\mathbf{L_1}$ layers in the three structures consist of SiO_6 and MgO_6 octahedra that share edges to form continuous layers with single octahedral vacancies (Fig. 21*b, e, h*). However, the patterns of arrangements of SiO_6 units and vacancies are topologically different in the three varieties. The $\mathbf{L_2}$ layers contains chains of edge-sharing MgO_6 octahedra interlinked by single SiO_4 tetrahedra, but again the topologies of the chains and their linkages differ in the three phases (Fig. 21*c, f, i*). The topological differences are dictated by different chemical compositions: the Mg : Si ratios are equal to 3 : 1, 14 : 5 and 10 : 3 for B, AhnB and ShyB, respectively. The crystal structure of superfluous phase, $Mg_{10}Si_3O_{14}F_4$ (Hazen et al., 1997), is isotypic to the high-temperature modification of ShyB (Pacalo, Parise, 1992), except for the presence of H atoms in the latter. Taking into account the coordination of Si in all three phases, their crystal-chemical formulae can be written as $Mg_{12}(^{VI}SiO_6)(^{IV}SiO_4)_3O(OH)_2$, $Mg_{14}(^{VI}SiO_6)(^{IV}SiO_4)_4O_2$, and $Mg_{10}(^{VI}SiO_6)(^{IV}SiO_4)_2(OH)_4$ for the phases B, AhnB and ShyB, respectively. It is worthy to note that the crystal structures of B and AhnB contain "additional" O atoms that are not bonded to ^{VI}Si or ^{IV}Si. These atoms are coordinated octahedrally by Mg atoms as in the crystal structure of periclase and thus represent fragments of periclase structure.

The phase D, $MgSi_2O_4(OH)_2$, was prepared by Liu (1987) as a dissociation product of serpentine above ~20 GPa and, prior to the discovery of phase H (Nishi et al., 2014), was thought to be the densest DHMS phase stable under deep lower mantle pressures. Its crystal structure

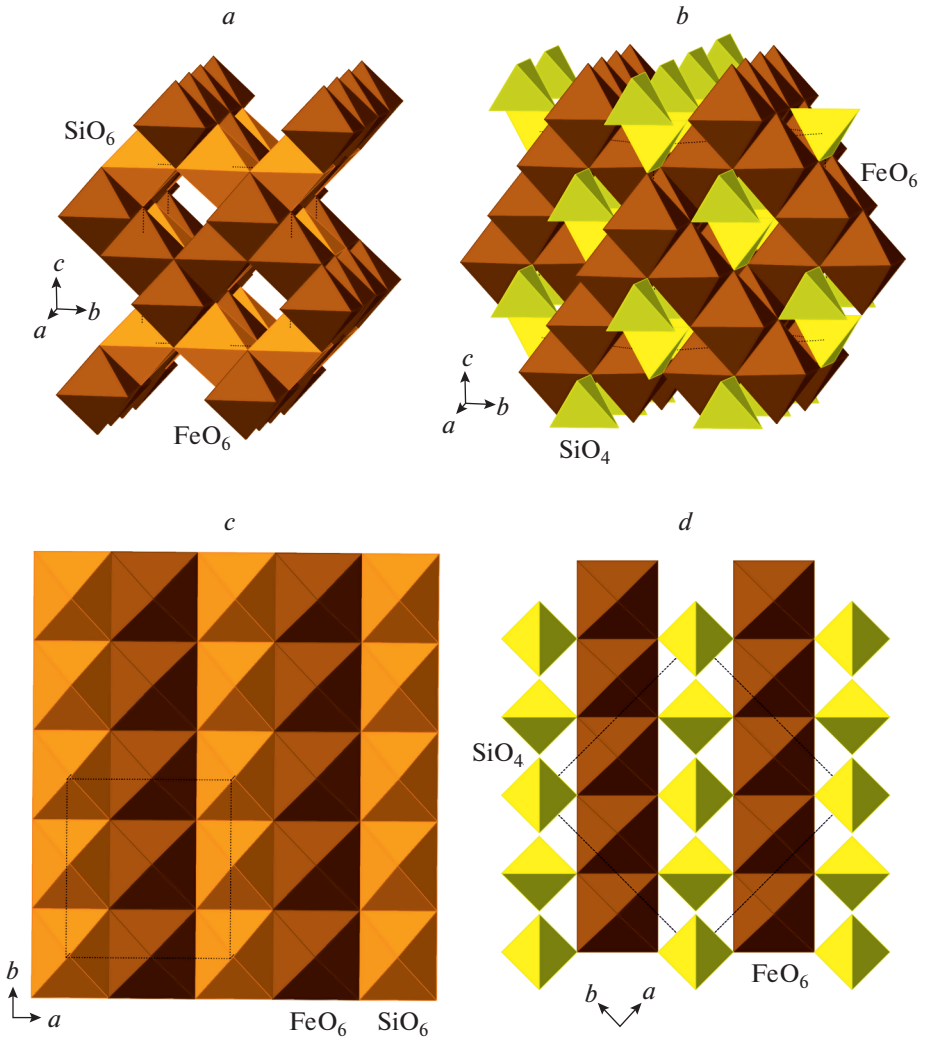

Fig. 19. The crystal structure of *I*-Fe_2SiO_4 (*a*) in comparison with the crystal structure of γ-Fe_2SiO_4 (*b*) and the layers of Fe- and Si-centered polyhedra in *I*-Fe_2SiO_4 (*c*) and γ-Fe_2SiO_4 (*d*).

Рис. 19. Кристаллическая структура *I*-Fe_2SiO_4 (*a*) в сравнении с кристаллической структурой γ-Fe_2SiO_4 (*b*) и слои Fe- и Si-центрированных полиэдров в структурах *I*-Fe_2SiO_4 (*c*) и γ-Fe_2SiO_4 (*d*).

(Yang et al., 1997; Kudoh et al., 1997; Ballaran et al., 2010; Bindi et al., 2015b) is rather simple and is based upon dioctahedral layers of SiO_6 octahedra linked into a 3D framework by interlayer MgO_6 octahedra (Fig. 22*a, b*). The anion packing corresponds to the hexagonal AB sequence.

The crystal structure of phase E (Fig. 22*c*) is strongly disordered (Kudoh et al., 1993; Yang et al., 2002) and can be described as 6-layer ccp arrangement of O atoms with the sequence ABCABC = $[ABC]^2$. The Mg and Si atoms are disordered over octahedral and tetrahedral interstices.

Table 8. Crystallographic data for metastable M_2SiO_4 polymorphs (M = Mg, Fe) obtained by cold compression and related structures
Таблица 8. Кристаллографические данные для метастабильных полиморфов M_2SiO_4 (M = Mg, Fe), полученных методом холодной компрессии, и родственных структур

Phase	Chemical formula	SG	*a* [Å]/α [°]	*b* [Å]/β [°]	*c* [Å]/γ [°]	*V*, Å^3	CN(Si)	Ref.
Forsterite-II (52.4 GPa)	Mg_2SiO_4	*P*1	4.695/93.1	9.201/107.3	5.311/98.1	215.8	4, 6	1
Forsterite-III (58.2 GPa)	Mg_2SiO_4	$Cmc2_1$	2.591/90	8.726/90	8.794/90	198.8	6	1
I-Fe_2SiO_4 (54.6 GPa)	Fe_2SiO_4	*Imma*	5.543/90	6.032/90	7.201/90	240.8	6	2
–	$Mg(Cr_{0.8}Mg_{0.2})(Si_{0.6}Mg_{0.4})O_4$	$Cmc2_1$	2.848/90	9.459/90	9.635/90	259.6	6	3

References: (1) Finkelstein et al., 2014; (2) Yamanaka et al., 2015; (3) Bindi et al., 2015a.

Table 9. Crystallographic data on dense hydrous magnesium silicates (DHMS) and related phases
Таблица 9. Кристаллографические данные по плотным водным магнезиальным силикатам и родственным фазам

Phase	Chemical formula	Sp. gr.	a, Å	b, Å	c, Å	β, °	V, Å^3	CN(Si)	Reference
A	$Mg_7(SiO_4)_2(OH)_6$	$P6_3$	7.860	= a	9.573	90	512.2	4	1
B (= C)	$Mg_{12}Si_4O_{19}(OH)_2$	$P2_1/c$	10.588	14.097	10.073	104.1	1458.2	4, 6	2
AnhB	$Mg_{14}Si_5O_{24}$	$Pmcb$	5.868	14.178	10.048	90	836.0	4, 6	2
ShyB-HT	$Mg_{10}Si_3O_{14}(OH)_4$	$Pnnm$	5.089	13.968	8.696	90	618.2	4, 6	3
ShyB-LT	$Mg_{10}Si_3O_{14}(OH)_4$	$Pnn2$	14.024	5.109	8.733	90	625.7	4, 6	4
SflB	$Mg_{10}Si_3O_{14}F_4$	$Pnnm$	5.050	13.969	8.640	90	609.5	4, 6	5
D (= F = G)	$MgSi_2O_4(OH)_2$	$P\bar{3}1m$	4.745	= a	4.345	90	84.7	6	6
E	$Mg_2SiO_2(OH)_6$	$R\bar{3}m$	2.970	= a	13.882	90	106.1	4	7
H	$MgSiO_2(OH)_2$	$Pnnm$	4.733	4.325	2.842	90	58.2	6	8
10-Å phase	$Mg_3Si_4O_{10}(OH)_2{\cdot}H_2O$	$C2/m$	5.323	9.203	10.216	99.98	492.9	4	9
3.65-Å phase	$MgSi(OH)_6$	$P2_1/n$	5.117	5.193	7.336	90.02	195.0	6	10
"HySo"	$Mg_3Al(OH)_3(Si_2O_7)$	$C2/m$	9.150	14.740	5.071	98.3	676.8	4	11
11.5-Å phase	$Mg_6Al(OH)_7(SiO_4)_2$	$C2/c$	9.012	5.201	23.202	97.8	1077.4	4	11
"Mg-sursassite"	$Mg_4Al_5(OH)_5Si_7O_{23}$	$P2_1/m$	8.422	5.581	9.406	106.8	423.3	4, 6	12
X, hydrous K	$K_{2-x}Mg_2Si_2O_7H_x$	$P6_3/mcm$	5.065	= a	13.238	90	294.1	4	13
X, anhydrous K	$K_2Mg_2Si_2O_7$	$P\bar{3}1m$	5.076	= a	6.597	90	147.2	4	14
X, anhydrous Na	$Na_2Mg_2Si_2O_7$	$P\bar{3}1m$	4.893	= a	6.435	90	138.4	4	15

Legend: AnhB = anhydrous B phase; ShyB = syperhydrous B phase; SflB = superfluous phase B; LT = low-temperature; HT = high-temperature.
References: (1) Horiuchi et al., 1979; (2) Finger et al., 1989, 1991; (3) Pacalo, Parise, 1992; (4) Koch-Müller et al., 2005; (5) Hazen et al., 1997; (6) Yang et al., 1997; (7) Kudoh et al., 1993; (8) Bindi et al., 2014; (9) Comodi et al., 2005; (10) Welch, Wunder, 2012; (11) Gemmi et al., 2016; (12) Bindi et al., 2020b; (13) Welch et al., 2012; (14) Matsuzaki et al., 2010; (15) Yang et al., 2001.

The crystal structure of phase H, $MgSiO_2(OH)_2$ (Bindi et al., 2014, 2015b), has a rutile-type topology consisting of chains of edge-sharing octahedra occupied equally by Mg and Si atoms (therefore, all Si is in octahedral coordination) (Fig. 22*d*). Topologically the structure is similar to that of stishovite (see above), but the chains are rotated in such a way that the anions form a hexagonal AB close packing. The structure of the phase can be obtained from that of stishovite by the $Si^{4+} \leftrightarrow Mg^{2+} + 2H^+$ substitution and the tetragonal-to-orthorhombic distortion resulting in a closest packing of anions.

The 10 Å phase, $Mg_3Si_4O_{10}(OH)_2 \cdot H_2O$, was obtained by Yamamoto and Akimoto (1977) from talc at 3–5 GPa. The phase is suggested to be stable under upper mantle pressures and controls recycling of H_2O in subduction zone environments (Fumagalli et al., 2001; Khisina, Wirth, 2008). Its crystal structure (Fig. 23) belongs to the mica-type and contains 2 : 1 layers consisting of the central trioctahedral layers of MgO_6 octahedra sandwiched between two $[Si_2O_5]$ layers of corner-sharing SiO_4 tetrahedra (Comodi et al., 2005).

The formation of the 3.65 Å phase, $MgSi(OH)_6$, was reported by Wunder et al. (2011), who suggested that it belongs to the hydroxide perovskite group. The structure model was revised by Welch and Wunder (2012), who confirmed this suggestion and demonstrated that the crystal structure of the phase is based upon the framework of alternating corner-sharing $Mg(OH)_6$ and $Si(OH)_6$ octahedra (Fig. 24).

The incorporation of Al into DHMS is a subject of continuing interest, since the admixture of Al changes the stability diagram and phase relations. In many cases, Al have no separate

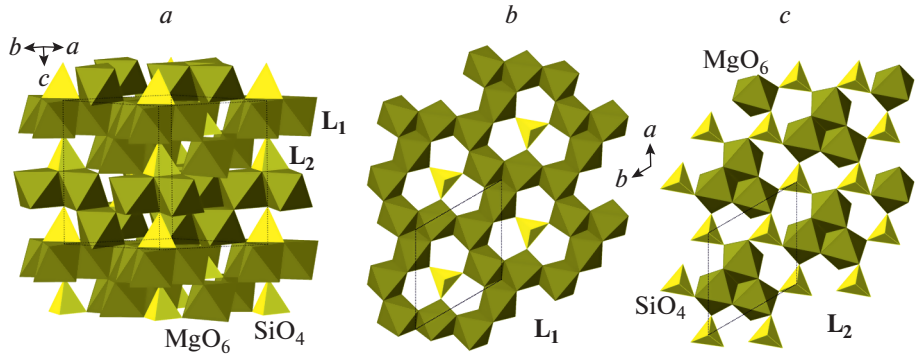

Fig. 20. The crystal structure of phase A (*a*) as consisting of two types of octahedral-tetrahedral layers (*b*, *c*).

Рис. 20. Кристаллическая структура фазы A (*a*) как состоящая из двух типов окта-тетраэдрических слоев (*b*, *c*).

sites in the crystal structure (see, e.g., Ballaran et al., 2010), but, in some Mg-Al hydrous silicates, the Al–Mg ordering has been observed. For instance, Gemmi et al. (2011) reported the synthesis and crystal structure of hydrous Al-bearing pyroxene (HAPY phase) with the composition $Mg_{2.1}Al_{0.9}(OH)_2[Al_{0.9}Si_{1.1}O_6]$ and Al occurring in both octahedral and tetrahedral sites. Gemmi et al. (2016) prepared and structurally characterized the HySo phase with the composition $Mg_3Al(OH)_3(Si_2O_7)$. Its crystal structure (Fig. 25) contains layers of Mg- and Al-centered octahedra linked by sorosilicate groups $[Si_2O_7]$; the interlayer contains also low-occupied Mg positions. The arrangement of anions corresponds to the distorted ABC closest packing. The 11.5 Å phase was discovered by Fumagalli et al. (2014). Its crystal structure was solved by Gemmi et al. (2016) using electron diffraction techniques. As can be seen from Fig. 26, it is based upon two types of layers, $\mathbf{L_1}$ and $\mathbf{L_2}$. The $\mathbf{L_1}$ layer is of the hydrotalcite- (or quintinite-) type and consists of Mg- and Al-centered octahedra taken in the 2 : 1 ratio. The $\mathbf{L_2}$ layer is dioctahedral with vacancies covered on both sides by SiO_4 tetrahedra. The packing of anions is remarkable by its relative complexity. It corresponds to the distorted 10-layer sequence ABCABCBACBA (Fig. 26*d*). This sequence may be represented as obtained from the pure cubic ABC sequence by inserting chemical twinning plane m_{tw} into every fifth layer. At the place of twinning, the sequence transforms into the hexagonal one. The Pauling symbol of the packing is [*hccchcccc*] or $[hcccc]^2$. Gemmi et al. (2016) pointed out that the 11.5 Å phase is probably identical or closely related to the 23 Å phase with the stoichiometry $Mg_{11}Al_2Si_4O_{16}(OH)_{12}$ reported by Cai et al. (2015).

Bindi et al. (2020c) reported the crystal structure of Si-rich "Mg-sursassite", $[Mg_4Al_5(OH)_5Si_7O_{23}]$. In contrast to the previous reports on similar materials (e.g., Gottshalk et al., 2000), the new phase contains Si in an octahedral coordination (Fig. 27), though the Si site has the half-half occupancy with Al. The silicate substructure (Fig. 27*b*) may be viewed as a chain of edge-sharing SiO_6 octahedra incrustated on two sides by SiO_4 tetrahedra and (Si_2O_7) groups.

The phase X denotes the whole family of Mg silicates that incorporate alkali metals into their structures (Luth, 1997; Gasparik, Litvin, 1997). The general formula of phases X is $(K,Na)_{2-x}Mg_2Si_2O_7H_x$ $(0 \le x \le 1)$. Their crystal chemical studies revealed the presence of two polymorphic forms, which differ from each other in their space groups and *c* unit-cell parameters (Yang et al., 2001; Mancini et al., 2001, 2002; Bindi et al., 2007; Mtsuzaki et al., 2010; Welch et al., 2012). Both crystal structures are based upon dioctahedral layers of Mg-centered polyhedra linked by sorosilicate (Si_2O_7) groups in such a way that triangular bases of silicate

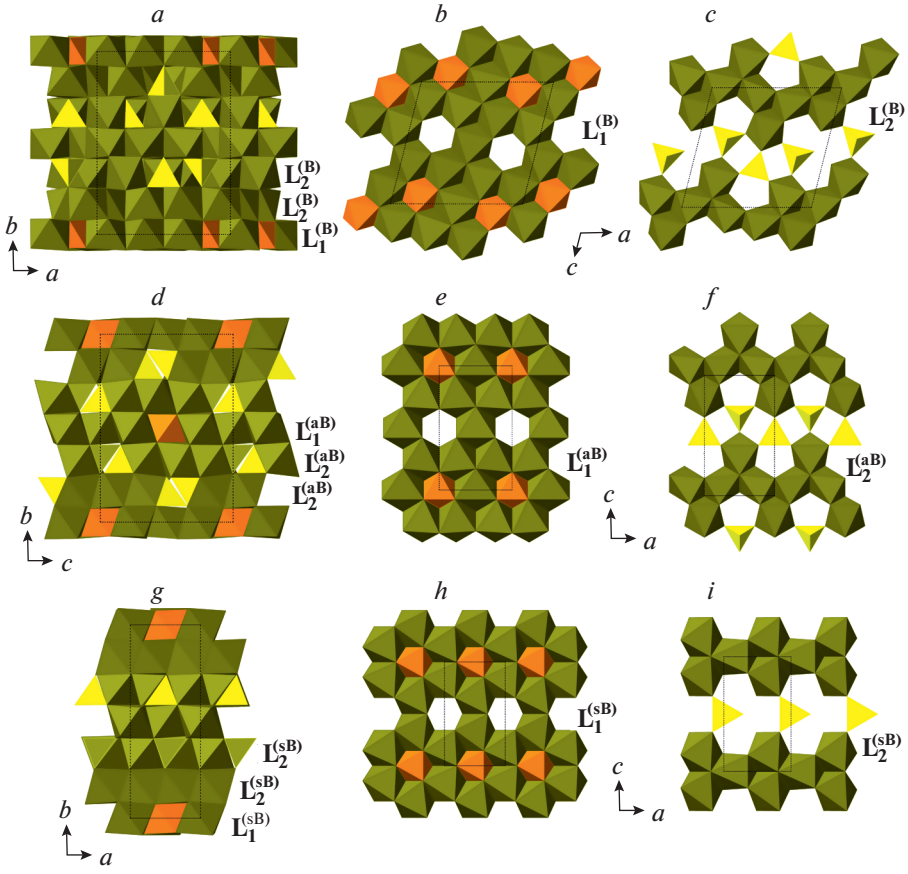

Fig. 21. The crystal structures of the phases B (*a*), AnhB (*d*) and ShyB (*g*) and their subdivision into layers (*b*, *c*, *e*, *f*, *h*, *i*). Legend: aB = AnhB; sB = ShyB; SiO_6 octahedra and SiO_4 tetrahedra are shown in orange and yellow colors, respectively; Mg octahedra are shown in green.

Рис. 21. Кристаллические структуры фаз B (*a*), AnhB (*d*) и ShyB (*g*) и их разделение на слои (*b*, *c*, *e*, *f*, *h*, *i*). Условные обозначения: aB = AnhB; sB = ShyB; октаэдры SiO_6 и тетраэдры SiO_4 показаны оранжевым и желтым цветами, соответственно; октаэдры MgO_6 закрашены зеленым.

tetrahedra are located above the vacancies in the octahedral layers (Fig. 28*c*). In the crystal structure with the $P\bar{3}1m$ space group, the *c* parameter is equal to ~6.4–6.6 Å, adjacent octahedral layers are translationally equivalent, and the structure is non-centrosymmetric (Fig. 28*b*). In the $P6_3/mcm$ structure type, the adjacent octahedral layers are rotated relative to each other by 180°, the *c* parameter is doubled (~13 Å) and the structure is centrosymmetric. It is unclear whether polymorphism is induced by the presence of H or is a consequence of the kinetics of crystal growth.

9. HP SILICATES IN THE Al_2O_3–SiO_2 AND Al_2O_3–SiO_2–H_2O SYSTEMS

The crystallographic information about the HP-phases in the Al_2O_3–SiO_2 and Al_2O_3–SiO_2–H_2O systems is given in Table 10.

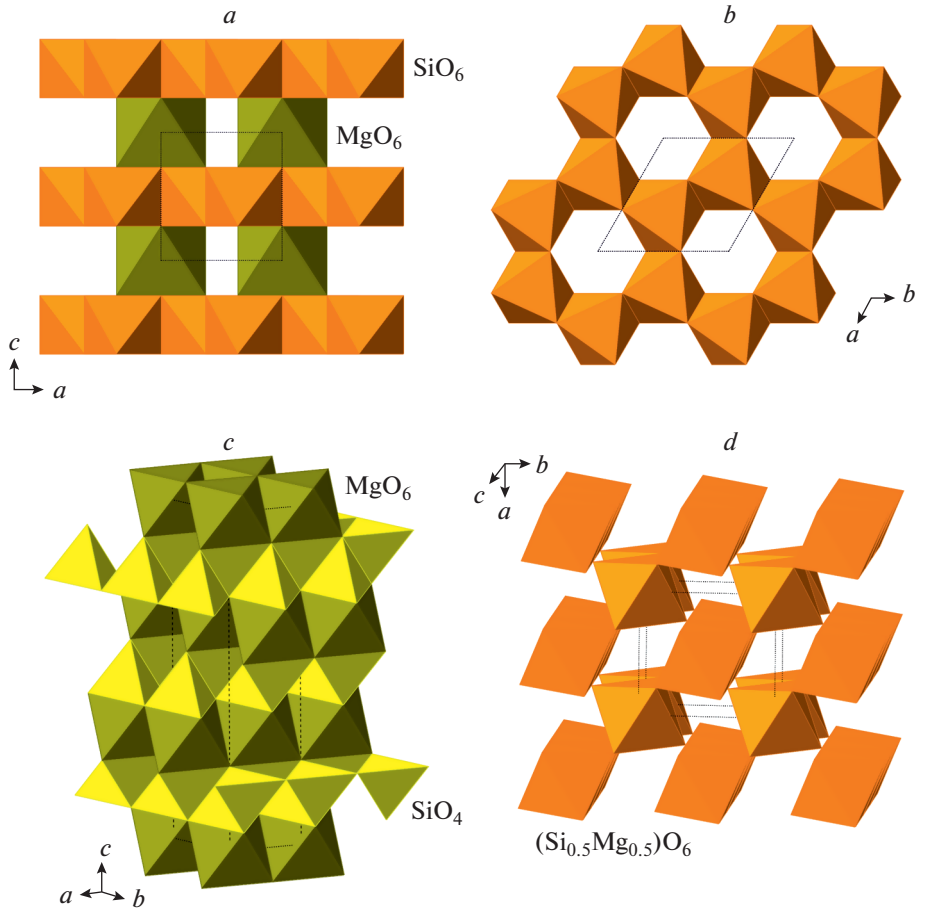

Fig. 22. The crystal structure of phase D (*a*) and the dioctahedral layer of SiO_6 octahedra (b), the crystal structures of phases E (*c*) and H (*d*).

Рис. 22. Кристаллическая структура фазы D (*a*) и диоктаэдрический слой из октаэдров SiO_6 (*b*); кристаллические структуры фаз E (*c*) и H (*d*).

Among three Al_2SiO_5 polymorphs (kyanite, sillimanite, andalusite), kyanite is the high-pressure phase that has the highest physical density. Its crystal structure was first determined by Náray-Szabó et al. (1929) as a cubic close packing of O atoms with Al and Si filling the octahedral and tetrahedral interstices, respectively. According to the results of the high-pressure experiments in diamond-anvil cells at 40–70 GPa and 2500 K, Ahmed-Zaïd and Madon (1991, 1995) reported the existence of the Al_2SiO_5 HP-polymorph with a V_3O_5-type structure. This phase was studied using computational methods by Urusov et al. (1998) and Oganov and Brodholt (2000). Recently, Zhou et al. (2018) reported the formation of two new high-pressure forms of Al_2SiO_5, kyanite-II and kyanite-III, at temperatures higher 2300–2500 K in the pressure range of 14–23 GPa. The transition from kyanite-I to kyanite-II occurs near 14 GPa, whereas the transition to kyanite-III occurs near 17 GPa. The full structural data for both new kyanite polymorphs have not been reported in details. However, Zhou et al. (2018) pointed out that both kyanite-II and kyanite-III are based upon hexagonal closest packing of O atoms with

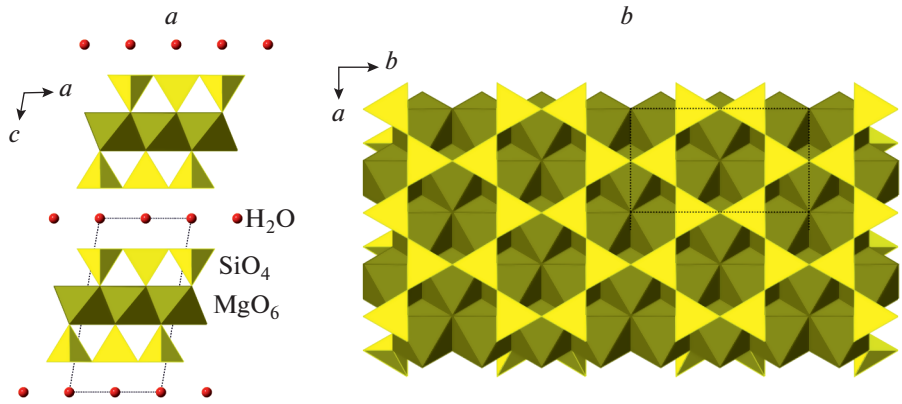

Fig. 23. The crystal structure of the 10 Å phase in projection along the *b* axis (*a*) and its 2 : 1 octahedral-tetrahedral layer (*b*).
Рис. 23. Кристаллическая структура 10-Å фазы в проекции вдоль оси *b* (*a*) и 2 : 1 окта-тетраэдрический слой (*b*).

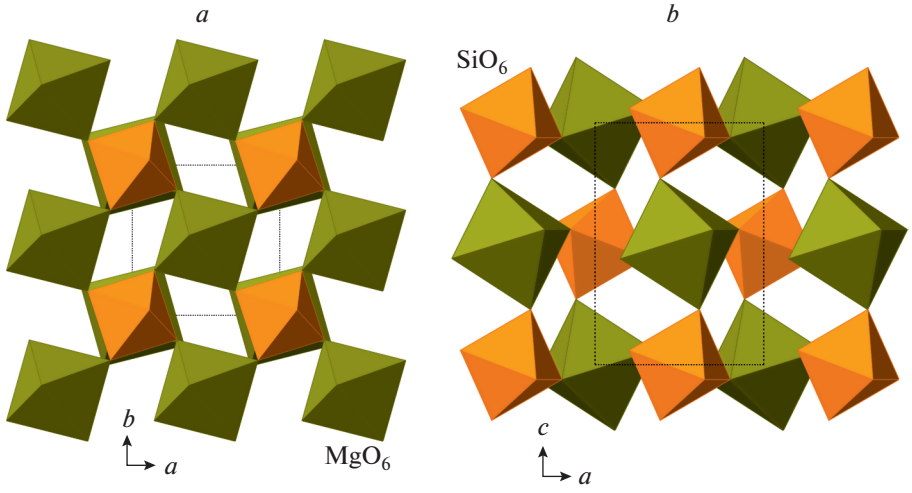

Fig. 24. The crystal structure of the 3.65 Å phase projected along the *c* (*a*) and *b* (*b*) axes.
Рис. 24. Кристаллическая структура 3.65-Å фазы в проекциях вдоль осей *c* (*a*) и *b* (*b*).

Al and Si in interstices. In agreement with the previous reports, kyanite-III adopts a V_3O_5-type structure that is based upon hexagonal packing of O atoms with Al and Si in octahedral interstices. In contrast, the crystal structure of kyanite-II contains Si in tetrahedral cavities as well, though, according to Zhou et al. (2018), in a rather disordered arrangement. These findings indicate that the kyanite-I → kyanite-II phase transition is associated with the reconstructive changes from cubic to hexagonal close packing, whereas the kyanite-II → kyanite-III transition is associated with the re-arrangement of Al and Si atoms over interstices in the hexagonal closest packing.

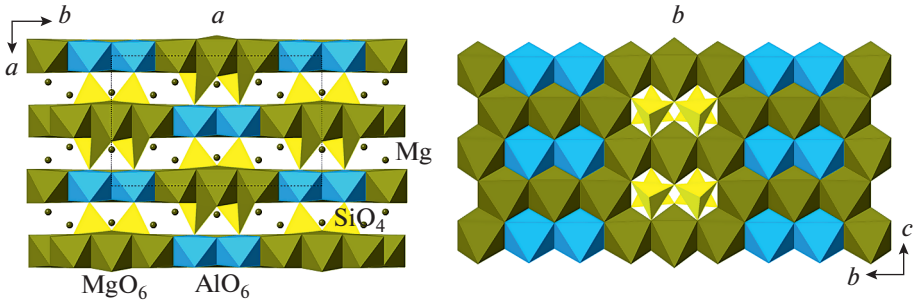

Fig. 25. The crystal structure of the HySo phase projected along the *c* axis (*a*) and projection of the octahedral-tetrahedral layer along the *a* axis (*b*).
Рис. 25. Кристаллическая структура фазы HySo в проекции вдоль оси *c* (*a*) и проекция окта-тетраэдрического слоя вдоль оси *a* (*b*).

The crystal structure of $Al_2Si_2O_7$ (or 227 phase) recently reported by Zhou et al. (2021) is based upon hexagonal closest packing of O atoms as well. All Al and two thirds of Si atoms are in octahedral coordination, whereas one third of Si atoms is in tetrahedral coordination. The structure (Fig. 29*a*) can be described as formed by alternating layers of octahedral chains of Si_2O_{10} and Al_2O_{10} edge-sharing octahedral dimers (**A**: Fig. 29*b*) and layers formed by double zigzag chains (**B**) of SiO_6 and AlO_6 octahedra interlinked by Si_2O_7 tetrahedral dimers (Fig. 29*c, d*). Taking into account the coordination of cations, the crystal-chemical formula of the 227 phase can be written as $^{VI}Al_6{}^{VI}Si_4O_{14}(^{IV}Si_2O_7)$.

The high-pressure silicate phases in the Al_2O_3–SiO_2–H_2O system attracted considerable attention. The most recent research in this area was focused on the phase Egg, $AlSiO_3OH$, which was first discovered by Eggleton et al. (1978) and structurally characterized by Schmidt et al. (1998). This phase is considered as one of the possible H_2O reservoirs in the mantle transition zone (Fukuyama et al., 2017). Its high-pressure structural behavior was investigated by

Table 10. Crystallographic data for high-pressure phases in the Al_2O_3–SiO_2 and Al_2O_3–SiO_2–H_2O systems
Таблица 10. Кристаллографические данные для высокобарических фаз в системах Al_2O_3–SiO_2 и Al_2O_3–SiO_2–H_2O

Mineral/ phase name	Chemical formula	SG	*a* [Å]/α [°]	*b* [Å]/β [°]	*c* [Å]/γ [°]	*V*, Å^3	CN(Si)	Reference
Al_2O_3–SiO_2 system								
Kyanite-I	Al_2SiO_5	$P\bar{1}$	7.126/90.0	7.852/101.1	5.572/106.0	293.6	4	1
Kyanite-II	Al_2SiO_5	$P\bar{1}$	7.056/96.8	9.437/99.2	6.776/108.1	416.5	4, 6(?)	2
Kyanite-III	Al_2SiO_5	$C2/c$	9.296/90	4.708/111.3	6.629/90	270.3	6	2
"227 phase"	$Al_2Si_2O_7$	$P\bar{1}$	7.024/103.5	7.100/99.1	6.673/60.5	281.4	4, 6	3
Al_2O_3–SiO_2–H_2O system								
"Phase Egg"	$AlSiO_3OH$	$P2_1/n$	7.144/90	4.335/98.4	6.953/90	213.0	6	4
Topaz-OH-I	$Al_2SiO_4(OH)_2$	*Pbnm*	4.724/90	8.947/90	8.390/90	354.6	4	5
Topaz-OH-II	$Al_2SiO_4(OH)_2$	*Pbnm*	4.723/90	8.915/90	2.773/90	116.8	4, 6	6
"Phase Pi"	$Al_3Si_2O_7(OH)_3$	*P*1	6.089/115.7	7.283/88.9	7.723/92.9	308.2	4	7

References: (1) Winter, Ghose, 1979; (2) Zhou et al., 2018; (3) Zhou et al., 2021; (4) Schmidt et al., 1998; (5) Wunder et al., 1993a; (6) Kanzaki et al., 2010; (7) Daniels, Wunder, 1996.

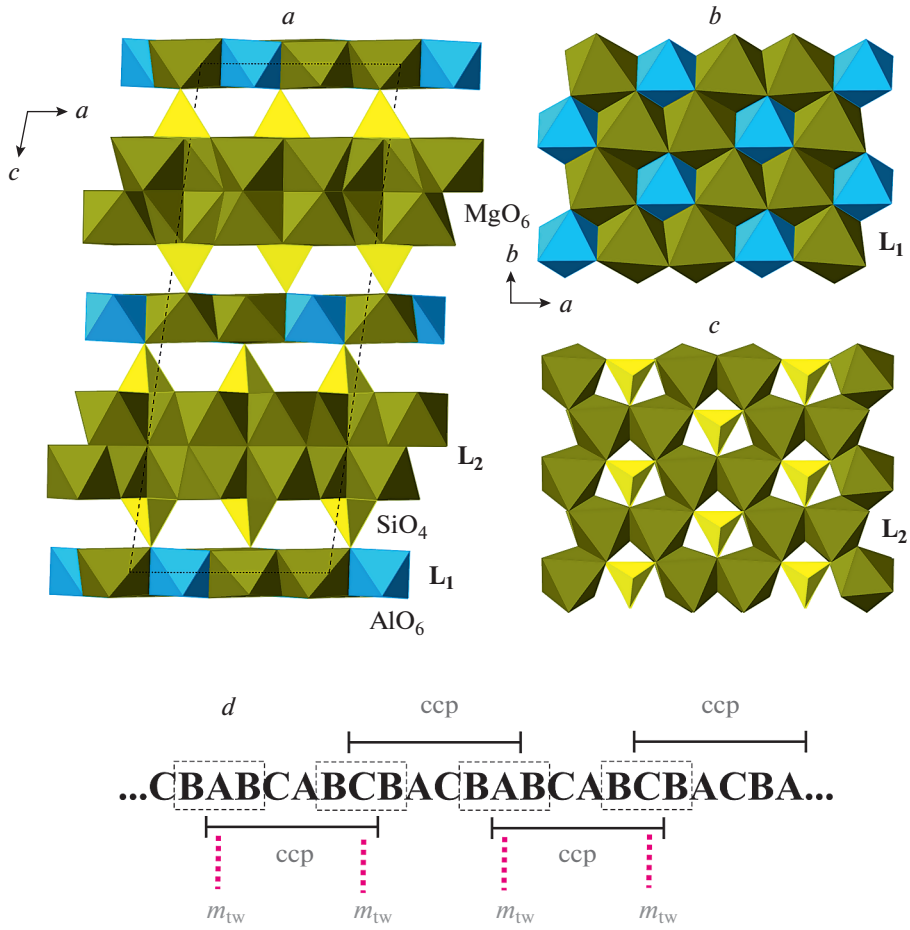

Fig. 26. The crystal structure of the 11.5 Å phase (*a*), projections of its two layers (*b, c*), and the sequence of the close-packed layers with indication of ccp regions and chemical twinning planes (m_{tw}) (dashed boxes indicate the hcp regions on the border between ccp regions).

Рис. 26. Кристаллическая структура фазы 11.5 Å (*a*), проекции составляющих ее слоев (*b*, *c*) и последовательность упаковки плотных анионных слоев с указанием областей кубической плотнейшей упаковки и плоскостей химического двойникования (m_{tw}) (штрихами выделены зоны гексагональной упаковки на границе между зонами кубической упаковки).

Schulze et al. (2018), whereas Bindi et al. (2020a) studied the incorporation of Mg into its structure. The crystal structure of phase Egg is shown in Fig. 30*a* as based upon distorted hexagonal closest packing of O atoms with Si and Al atoms in octahedral interstices. The structure can be viewed as built by linkage of the octahedral chains shown in Fig. 30*b*, which are topologically identical to the chains of the type **A** observed in the 227 phase (Fig. 29*b*).

Topaz-OH, $Al_2SiO_4(OH)_2$, the hydroxyl end-member of the topaz solid solution was prepared by Wunder et al. (1993a) at 5.5–10 GPa and 1000–1200 K and was shown to be stable up to 13 GPa and 1800 K. Its crystal structure was refined in the *Pbnm* space group, which implies hydrogen disorder over two inequivalent sites (Mookherjee et al., 2016). Though there were hypotheses about the existence of the proton-ordered $Pbn2_1$ configurations (Churakov, Wun-

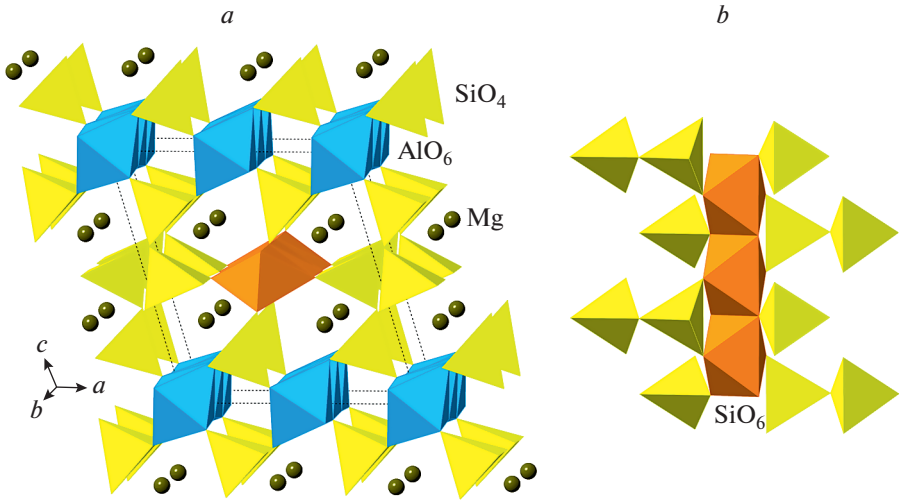

Fig. 27. The crystal structure of Si-rich "Mg-sursassite" (*a*) and its silicate substructure (*b*).
Рис. 27. Кристаллическая структура высококремниевого "Mg-сурсассита" (*a*) и составляющая его силикатная субструктура (*b*).

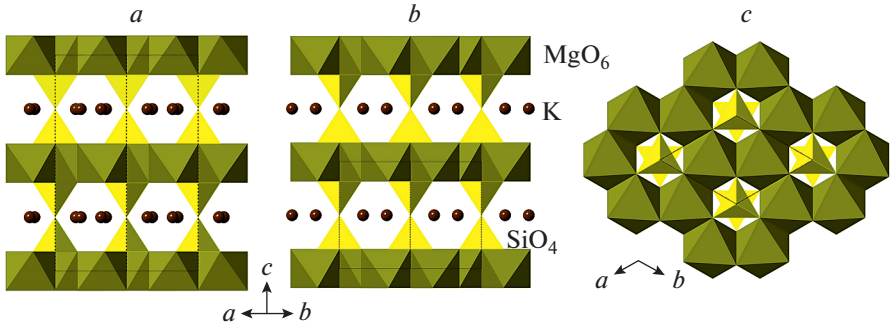

Fig. 28. The crystal structures of two polymorphs of the phase X: the $P\bar{3}1m$ (*a*) and $P6_3/mcm$ (*b*) structures, and the octahedral layer with superpositions of SiO_4 tetrahedra (*c*).
Рис. 28. Кристаллические структуры двух полиморфов фазы X с группами $P\bar{3}1m$ (*a*) и $P6_3/mcm$ (*b*) и проекция октаэдрического слоя с суперпозицией тетраэдров SiO_4 (*c*).

der, 2004), they were not confirmed experimentally. The crystal structure shown in Fig. 31*a* is based upon 4-layered closest-packing arrangement of O atoms with the stacking sequence ABAC. The close-packed layers are parallel to (010). The Al and Si atoms are in octahedral and tetrahedral interstices, respectively. The AlO_6 chains share edges to form chains running parallel to [001] (Fig. 31*b*). Kanzaki (2010) reported the existence of the high-pressure topaz-OH polymorph, topaz-OH-II, which is stable at 13–14 GPa and 1600–1800 K. Its crystal structure is based upon the same ABAC close packing of O atoms with disordered arrangement of Al and Si over tetrahedral and octahedral interstices; at least some Si atoms adopt an octahedral coordination. The crystal chemistry of two polymorphs of topaz was studied using spec-

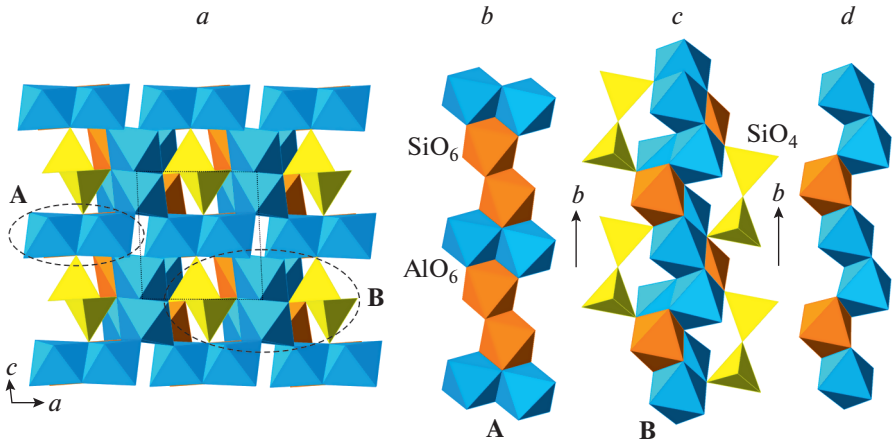

Fig. 29. The crystal structure of $Al_2Si_2O_7$ (or 227 phase) in projection along the *b* axis (*a*) as based upon the chains of the type **A** (*b*) and the double chains of the type **B** (*c*); (*d*) shows a single chain as a constituent of the chain **B**.
Рис. 29. Кристаллическая структура $Al_2Si_2O_7$ (фаза 227) в проекции вдоль оси *b* (*a*) как основанная на цепочках типа **A** (*b*) и двойных цепочках типа B (*c*); (*d*) изображает одинарную цепочку, лежащую в основе цепочек типа **B**.

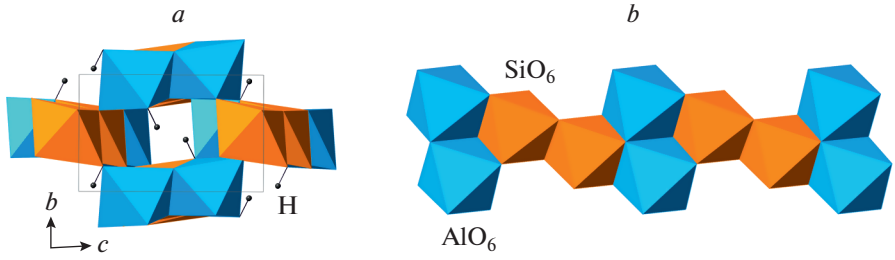

Fig. 30. The crystal structure of phase Egg in projection along the *a* axis (*a*) and its constituent chain of edge-sharing AlO_6 and SiO_6 octahedra running parallel to [100] (*b*).
Рис. 30. Кристаллическая структура фазы Egg в проекции вдоль оси *a* (*a*) и ее базовая цепочка из связанных ребрами октаэдров AlO_6 и SiO_6, вытянутая вдоль направления [100] (*b*).

troscopic methods by Xue et al. (2010). The OH-dominant topaz was reported in nature from HP rocks (Zhang et al., 2002), but had never been approved as a separate mineral species.

Wunder et al. (1993b) synthesized the HP phase with the composition $Al_3Si_2O_7(OH)_3$ ("phase Pi"), first discovered by Coes (1962), who called it "piezotite" and assigned to it the incorrect formula $Al_2O_3 \cdot 3SiO_2$. Daniels and Wunder (1996) determined the crystal structure of the phase as based upon a distorted cubic close packing of O atoms with Al and Si in octahedral and tetrahedral interstices, respectively. The crystal structure shown in Fig. 32*a* can also be described as consisting of Al-deficient brucite-like layers of AlO_6 tetrahedra with cavities covered by SiO_4 tetrahedra (Fig. 32*b*) that provide the layer linkage into 3-dimensional framework. The layers are oriented parallel to the (110) plane. The H atoms are located in the interlayer space.

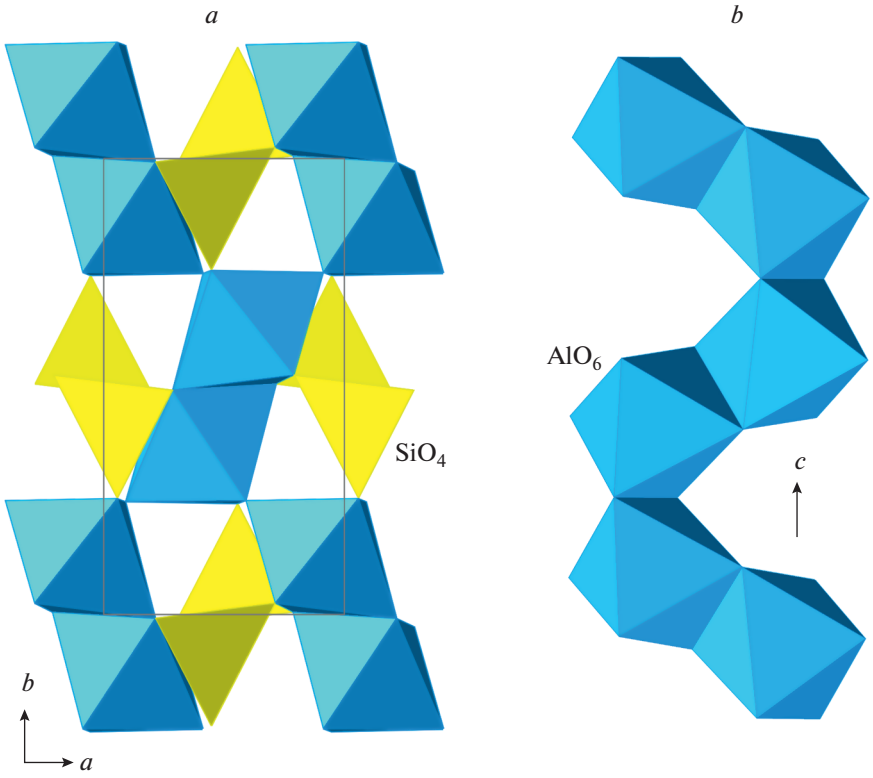

Fig. 31. The crystal structure of topaz-OH projected along the *c* axis (*a*) and the linkage of AlO_6 octahedra along [001] (*b*).

Рис. 31. Кристаллическая структура топаза-OH в проекции вдоль оси *c* (*a*) и связь октаэдров AlO_6 в цепочку вдоль направления [001] (*b*).

10. Ca, Sr AND Ba HP SILICATES AND ALUMINOSILICATES

The crystallographic data on known HP silicates of Ca, Sr and Ba and related phases are given in Table 11. The Ca–Si–O system is of special interest, since the $CaSiO_3$ perovskite (Ca–Pv) is thought to be one of the most important Earth's minerals. According to the current estimates, it may constitute about 7% of the peridotitic mantle and 23% of the mid-oceanic ridge basalts in subducting slabs at lower-mantle pressures (Hirose et al., 2005). The Ca–Pv phase was first reported by Liu and Ringwood (1975) and was the subject of extensive experimental and theoretical studies (Swamy, Dubrovinsky, 1997; Akber-Knutson et al., 2002; Caracas et al., 2005; Jung, Oganov, 2005; Adams, Oganov, 2006; Caracas, Wentzcovitch, 2006, etc.). Initially, it was proposed that Ca–Pv has the only possible cubic symmetry (Mao et al., 1989), until Stixrude et al. (1996) predicted the instability of the cubic phase and its possible transformation into a lower-symmetry polymorph. The existence of tetragonal and orthorhombic Ca–Pv phases was confirmed experimentally (Shim et al., 2002; Kurashina et al., 2004; Komabayashi et al., 2007; Uchida et al., 2009; Chen et al., 2018), but there are no full crystal-structure data for any of them and even space groups cannot be determined reliably. The only natural occurrence of Ca–Pv was reported by Nestola et al. (2018), who found the orthorhombic phase in inclusions in a diamond from South African Cullinan kimberlite. It is believed that, under the release of

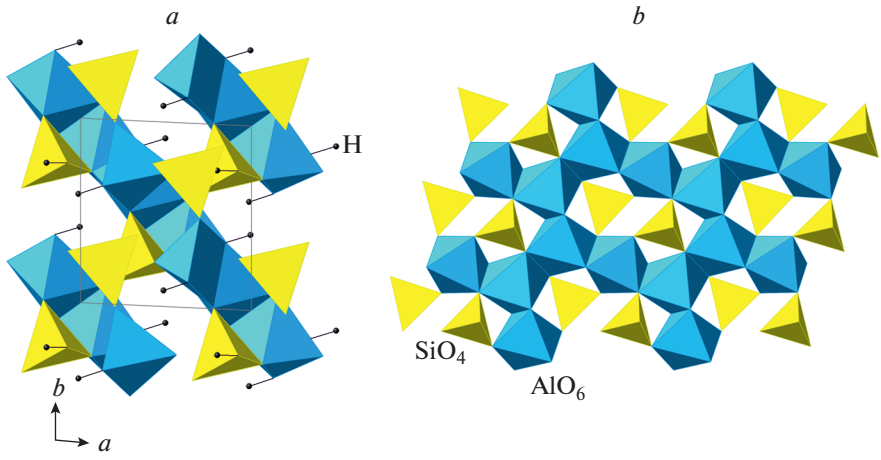

Fig. 32. The crystal structure of the phase Pi in projection along the *c* axis (*a*) and the octahedral-tetrahedral layer parallel to (110) (*b*).
Рис. 32. Кристаллическая структура фазы Pi в проекции вдоль оси *c* (*a*) и окта-тетраэдрический слой, параллельный плоскости (110) (*b*).

high pressure, Ca–Pv transforms into breyite, a walstromite-structured $CaSiO_3$ HP polymorph with tetrahedral Si (Joswig et al., 2003; Anzolini et al., 2016; Brenker et al., 2021). Woodland et al. (2020) pointed out that the formation of breyite as retrogressed Ca–Pv does not preclude its direct crystallization under upper-mantle conditions.

The pressure-induced polymorphism of $CaSiO_3$ was the focus of the recent study by Milani et al. (2021). The low-pressure $CaSiO_3$ polymorphs are wollastonite and pseudowollastonite that may exist in several polytypes each. Milani et al. (2021) reported the cold compression study of wollastonite and breyite (Table 11) and the occurrence of two new phase transitions for both minerals. The crystal structure of wollastonite is based upon $[SiO_3]$ chains of SiO_4 tetrahedra, whereas that of breyite consists of $[Si_3O_9]$ three-membered rings. The wollastonite-I → wollastonite-II → wollastonite-III and breyite-I → breyite-II → breyite-III phase transitions involve rotation of tetrahedra with no changes in the overall structural topologies. During the wollastonite series of phases, the structural complexity is increasing continuously [$I_G/I_{G,\text{total}}$, in bits]: 3.907/117.207 → 4.907/294.413 → 5.907/708.827. In contrast, in the breyite series, breyite-II is simpler than breyite-I, but breyite-III is the most structurally complex phase: 3.907/117.207 → 3.374/101.207 → 3.907/234.413.

The crystal structure of Ca_2SiO_4 (Liu et al., 1978a) differs drastically from the structures of the M_2SiO_4 (M = Mg, Fe) compounds described above. It can be considered as a cubic perovskite structure broken into slices that are shifted relative to each other by the (**a** + **b**)/2 vector (Fig. 33*a*). The slices are one octahedron thick (Fig. 33*b*).

The existence of the $CaSi_2O_5$ phase with a titanite-related structure was first mentioned by Kanzaki et al. (1991). Later it was recognized that there are two $CaSi_2O_5$ polymorphs, triclinic low-pressure and monoclinic high-pressure, denoted as α- and β-phases, respectively (Angel et al., 1996; Angel, 1997; Kudoh, Kanzaki, 1998). The crystal structure of α-$CaSi_2O_5$ (Fig. 34*a*) is remarkable in that it contains four-, five- and six-coordinated Si atoms. The crystal structure of β-$CaSi_2O_5$ (Fig. 34*b*) belongs to the titanite structure type and is based upon a three-dimensional framework consisting of chains of corner-sharing SiO_6 octahedra interlinked by SiO_4 tetrahedra. In α-$CaSi_2O_5$, every second SiO_6 octahedron within the chain is replaced by SiO_5

Table 11. Crystallographic data for high-pressure Ca, Sr and Ba silicates
Таблица 11. Кристаллографические данные для высокобарических силикатов Ca, Sr и Ba

Mineral/phase name	Chemical formula	SG	*a* [Å]/α [°]	*b* [Å]/β [°]	*c* [Å]/γ [°]	*V*, Å^3	CN(Si)	Reference
			Ca silicates					
Ca–Pv	$CaSiO_3$	?	5.397/90	5.404/90	7.646/90	223.0	6	1
Wollastonite-I	$CaSiO_3$	$P\bar{1}$	7.079/103.4	7.331/95.3	7.938/90.1	398.9	4	2
Wollastonite-II	$CaSiO_3$	$P\bar{1}$	6.693/76.0	7.256/87.0	14.297/90.0	702.5	4	2
Wollastonite-III	$CaSiO_3$	$P\bar{1}$	6.571/75.5	14.142/90.0	14.311/91.2	1287.1	4	2
Breyite-I	$CaSiO_3$	$P\bar{1}$	6.644/69.7	6.689/83.7	9.282/76.2	375.6	4	2
Breyite-II	$CaSiO_3$	$C2/m$	10.221/90	7.937/105.2	8.621/90	674.8	4	2
Breyite-III	$CaSiO_3$	$P2_1/c$	8.511/90	7.854/104.9	10.096/90	652.3	4	2
–	Ca_2SiO_4	$I4/mmm$	3.564/90	3.564/90	11.660/90	148.1	6	3
α-$CaSi_2O_5$	$CaSi_2O_5$	$P\bar{1}$	7.243/81.4	7.546/84.8	6.501/69.6	329.0	4, 5, 6	4
β-$CaSi_2O_5$	$CaSi_2O_5$	$A2/a$	6.543/90	8.392/113.2	6.342/90	320.1	4, 6	5
“Post-hatrurite”	$Ca_3O(SiO_4)$	$P\bar{4}/ncc$	6.820/90	6.820/90	10.243/90	476.4	4	6
“Hydrous larnite”	$Ca_2Si_{0.9}O_{3.6}(OH)_{0.4}$	$P2_1/n$	5.461/90	6.712/90	9.276/90	340.0	4	6
			Sr silicates					
$SrSiO_3$ I (α)	$SrSiO_3$	$C2/c$	12.323/90	7.139/11.6	10.873/90	889.5	4	7, 8
$SrSiO_3$ II (δ)	$SrSiO_3$	$P\bar{1}$	6.874/85.0	6.894/110.6	9.717/104.0	418.3	4	7
$SrSiO_3$ III (δ’)	$SrSiO_3$	$P2_1/c$	7.452/90	6.066/117.1	13.479/90	537.1	4	7
$SrSiO_3$-3C	$SrSiO_3$	$Pm\bar{3}m$	3.503/90	3.503/90	3.503/90	43.0	6	9
$SrSiO_3$-6H	$SrSiO_3$	$P6_3/mmc$	5.069/90	5.069/90	12.418/120	276.3	6	10
–	$SrSi_2O_5$	$Cmca$	5.239/90	9.280/90	13.441/90	653.5	4, 6	11
			Ba silicates					
$BaSiO_3$-6H	$BaSiO_3$	$P6_3/mmc$	5.113/90	5.113/90	12.387/120	280.4	6	12
$BaSiO_3$-9R	$BaSiO_3$	$R\bar{3}m$	5.300/90	5.300/90	19.235/120	468.0	6	12
–	$BaSi_4O_9$	$P\bar{6}c2$	6.495/90	6.495/90	9.347/120	341.5	4, 6	13
–	$BaSi_4O_9$	$P3$	11.247/90	11.247/90	4.485/120	491.3	4, 6	14
			Ca aluminosilicates and related phases					
Donwilhelmsite	$CaAl_4Si_2O_{11}$	$P6_3/mmc$	5.42/90	5.42/90	12.70/120	323.0	6	15
Zagamiite	$CaAl_2Si_{3.5}O_{11}$	$P6_3/mmc$	5.403/90	5.403/90	12.77/120	322.9	4, 6	16
–	$CaAl_{12}Si_4O_{27}$	$P\bar{3}$	7.223/90	7.223/90	8.614/120	389.2	4, 6	17
“$CaAl_{0.5}Si_{0.5}O_{2.75}$”	$Ca_4Al_2Si_2O_{11}$	$C2$	9.137/90	5.224/110.0	17.512/90	823.2	4	18
“$CaAl_{0.4}Si_{0.6}O_{2.8}$”	$Ca_5Al_2Si_3O_{14}$	$C2/c$	9.036/90	5.188/98.0	21.629/90	1004.1	4, 6	18
“$CaFe_{0.4}Si_{0.6}O_{2.8}$”	$Ca_5Fe_2Si_3O_{14}$	$C2/c$	9.273/90	5.273/97.9	21.936/90	1062.3	4, 6	19

References: (1) Nestola et al., 2018; (2) Milani et al., 2021; (3) Liu, 1978a; (4) Kudo, Kanzaki, 1998; (5) Angel, 1997; (6) Németh et al., 2017; (7) Machida et al., 1982a; (8) Marsh, Herbstein, 1983; (9) Xiao et al., 2013; (10) Yusa et al., 2005; (11) Kojitani et al., 2005; (12) Yusa et al., 2007; (13) Finger et al., 1995; (14) Hazen et al., 1999; (15) Fritz et al., 2020; (16) Ma et al., 2019b; (17) Grey et al., 2000; (18) Kanzaki et al., 2017; (19) Kanzaki, 2020.

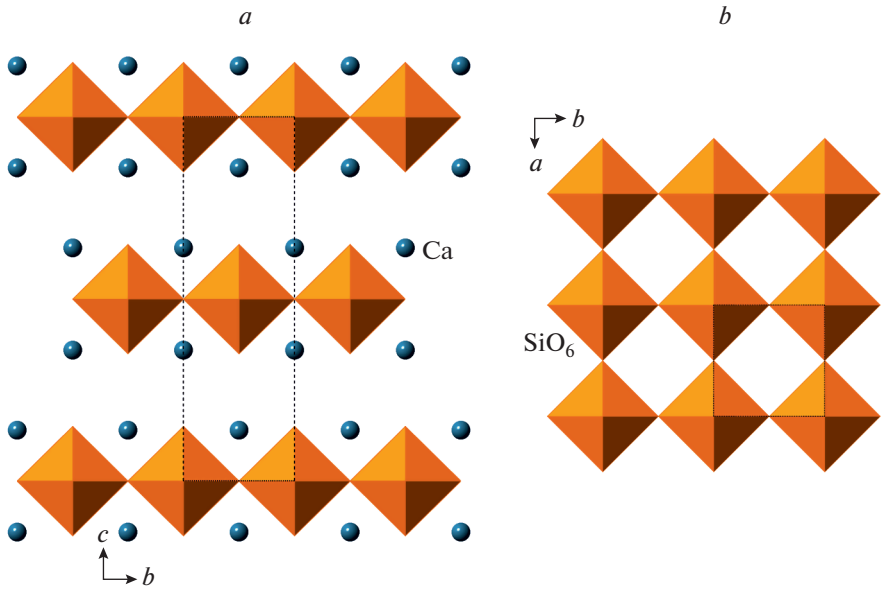

Fig. 33. The crystal structure of Ca_2SiO_4 projected along the *a* axis (*a*) and projection of the layer of corner-sharing SiO_6 octahedra (*b*).

Рис. 33. Кристаллическая структура Ca_2SiO_4 в проекции вдоль оси *a* (*a*) и проекция слоя вершинно-связанных октаэдров SiO_6 (*b*).

tetragonal pyramid (Fig. 34*c*, *d*), which was at the time the first example of five-coordinated silicon in a crystalline state (Angel et al., 1996). Under increasing pressure, α-$CaSi_2O_5$ transforms into β-$CaSi_2O_5$, which corresponds to the transformation of SiO_5 pyramid into SiO_6 octahedron and the formation of the structure with higher symmetry and lower complexity. It is worthy to note that β-$CaSi_2O_5$ had been found in nature in inclusions in natural diamonds (Joswig et al., 1999; Brenker et al., 2005) and therefore may potentially be established as a separate mineral species. Arlt et al. (1998) reported the synthesis and crystal structure of $MnSi_2O_5$, which is isotypic to β-$CaSi_2O_5$ and belongs to the titanite structure type.

The high-pressure Ca_3SiO_5 = $Ca_3O(SiO_4)$ phase ("post-hartrurite") was reported by Németh et al. (2017) as a phase isotypic to Sr_3SiO_5. In contrast to rhombohedral hatrurite, post-hatrurite has a tetragonal symmetry and belongs to the antiperovskite-type family of structures (Krivovichev, 2008). It is based upon perovskite-type framework consisting of corner-sharing OCa_6 octahedra (Fig. 35). Along with post-hatrurite, Németh et al. (2017) also described the formation and structure of "hydrous larnite" that has a threefold superstructure compared to the ambient-pressure anhydrous larnite.

The Sr–Si–O system is of interest because of its similarity with the Ca–Si–O system. The high-pressure polymorphism of $SrSiO_3$ was investigated by Machida et al. (1982*a*, *b*). Under compression, the ambient-pressure α-$SrSiO_3$ transforms into δ-$SrSiO_3$ and then to δ'-$SrSiO_3$ (all structures contain $[Si_3O_9]^{6-}$ three-membered tetrahedral rings). The α → δ → δ' sequence of phases corresponds to the increasing total structural complexity, 93.207 → 117.207 → → 132.877 bit/cell, though the information per atom changes irregularly, 3.107 → 3.907 → → 3.322 bit/atom. The existence of perovskite-related $SrSiO_3$ phases with octahedral coordi-

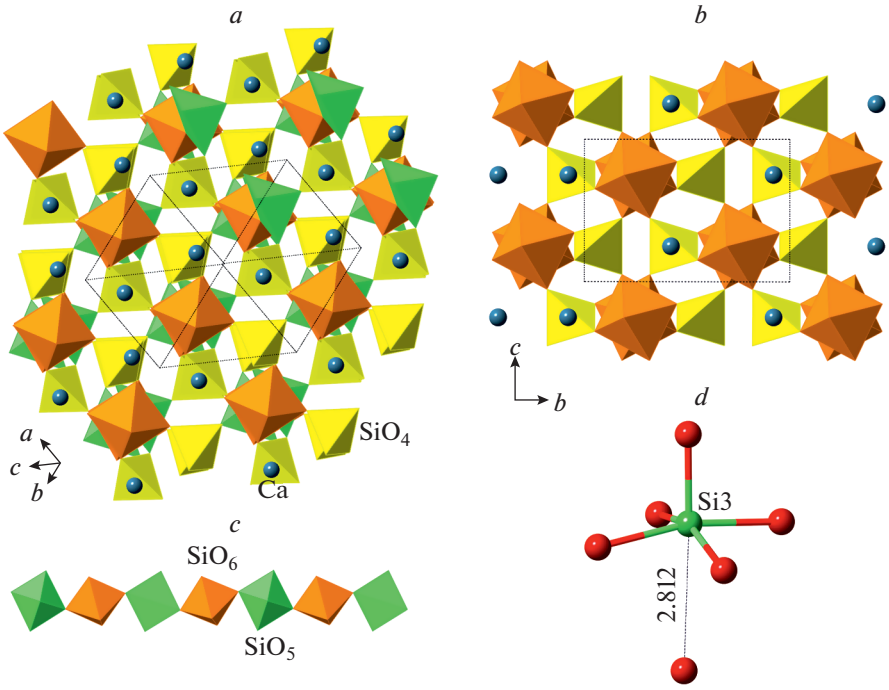

Fig. 34. The crystal structures of α- (*a*) and β- (*b*) polymorphs of $CaSi_2O_5$, the chain of SiO_6 octahedra and SiO_5 square pyramids in α-$CaSi_2O_5$ (*c*) and coordination of Si3 site in α-$CaSi_2O_5$ (*d*) as having additional O atom at the Si–O distance of 2.812 Å.

Рис. 34. Кристаллические структуры α- (*a*) и β- (*b*) полиморфов $CaSi_2O_5$, цепочка из октаэдров SiO_6 и тетрагональных пирамид SiO_5 в структуре α-$CaSi_2O_5$ (*c*) и координация позиции Si3 в α-$CaSi_2O_5$ (*d*), имеющая дополнительный атом O на расстоянии Si–O = 2.812 Å.

nation of Si was discovered by Yusa et al. (2005) and Xiao et al. (2013), who reported the occurrence of hexagonal (6H) and cubic (3C) $SrSiO_3$ perovskites, respectively. The crystal structure of the cubic phase has the highest possible symmetry $Pm\bar{3}m$, whereas the crystal structure of the hexagonal phase was not reported in details.

The crystal structure of $SrSi_2O_5$ (Kojitani et al., 2005) differs from those observed for the $CaSi_2O_5$ polymorphs (see above). It consists of $[^{VI}SiO(^{IV}SiO_4)]$ sheets based upon chains of corner-sharing SiO_6 octahedra running parallel to the *a* axis and interlinked via SiO_4 tetrahedra (Fig. 36). Alternatively, the crystal structure may be described as a 6-layer ABACBC closest packing of Sr and O atoms with Si atoms distributed equally between octahedral and tetrahedral interstices. The octahedral-tetrahedral layers and the layers of close-packed Sr and O atoms are parallel to (001).

The HP polymorphism of $BaSiO_3$ was studied by Yusa et al. (2007), who reported the crystal structures of two perovskite polytypes, 6H and 9R, both of which contain units of face-sharing SiO_6 octahedra (Fig. 37). The only other HP silicate structures with such a remarkable feature are coesite-IV and -V (see above). As in the coesite polymorphs, the linkage of two octahedra by sharing a common face results in the significant distortion of octahedral geometry. In $BaSiO_3$-9R, there are triples of face-sharing octahedra, whereas $BaSiO_3$-6H features di-

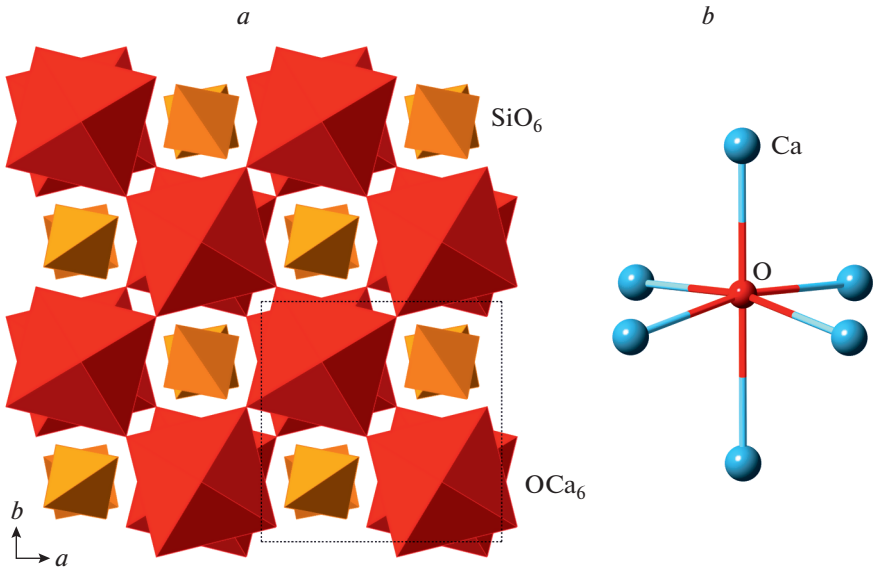

Fig. 35. The crystal structure of "post-hatrurite", Ca_3SiO_5 (*a*), consisting of an antiperovskite framework formed by corner-sharing OCa_6 octahedra (*b*) with SiO_4 tetrahedra in interstices.

Рис. 35. Кристаллическая структура "постхатрурита" Ca_3SiO_5 (*a*), содержащая антиперовсктовый каркас из оксоцентрированных октаэдров OCa_6 (*b*) с полостями, занятыми тетраэдрами SiO_4.

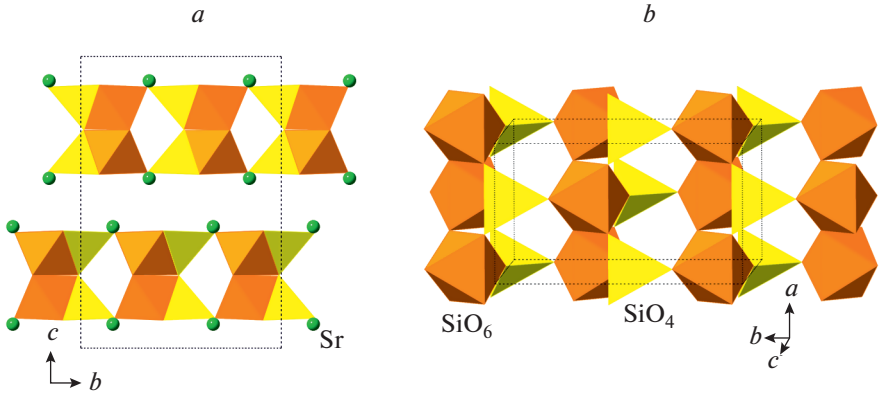

Fig. 36. The crystal structure of $SrSi_2O_5$ projected along the *a* axis (*a*) and projection of the heteropolyhedral silicate layer (*b*).

Рис. 36. Кристаллическая структура $SrSi_2O_5$ в проекции вдоль оси *a* (*a*) и проекция гетерополиэдрического силикатного слоя (*b*).

mers of face-sharing octahedra (Fig. 37*b, d*). In both HP $BaSiO_3$ polymorphs, Ba and O atoms form close packing with layers parallel to (001). The stacking sequences are ABACBC and ABABCBCAC for the 6H and 9R polytypes, respectively.

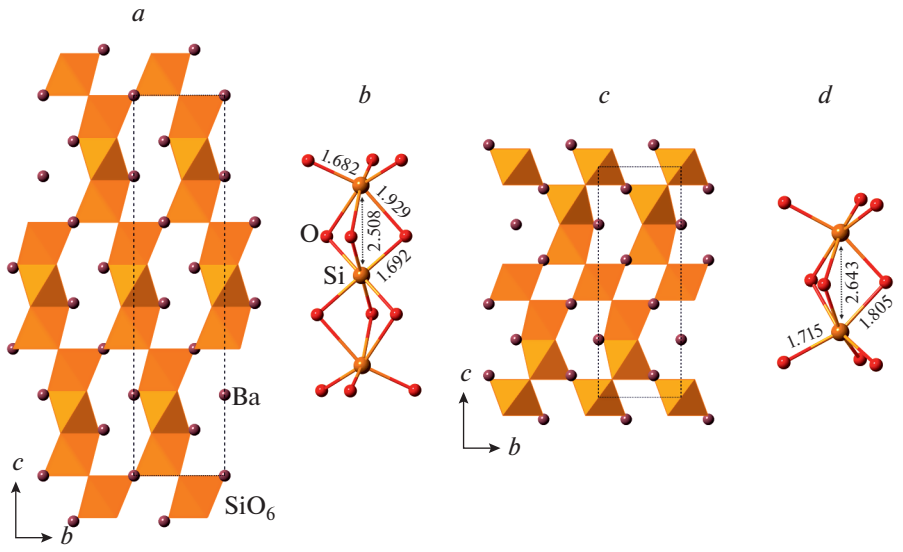

Fig. 37. The crystal structures of $BaSiO_3$-9R (*a*) and $BaSiO_3$-6H (*c*) and configurations of trimers (*b*) and dimers (*d*) of face-sharing SiO_6 octahedra in 9R- and 6H-polymorphs, respectively.

Рис. 37. Кристаллические структуры $BaSiO_3$-9R (*a*) и $BaSiO_3$-6H (*c*) и конфигурации тримеров (*b*) и димеров (*d*) из связанных общими гранями октаэдров SiO_6 в 9R- и 6H-полиморфах, соответственно.

There are two polymorphs of $BaSi_4O_9$ based upon octahedral-tetrahedral silicate frameworks of the same topology. The hexagonal polymorph crystallizes in the $P\bar{6}c2$ space group and belongs to the benitoite structure type (Finger et al., 1995) (Fig. 38*a*). In contrast, the trigonal polymorph has the *P*3 space group and is isotypic to $BaGe_4O_9$ (Hazen et al., 1999) (Fig. 38*b*). Both crystal structures are based upon topologically identical heteropolyhedral frameworks consisting of SiO_6 octahedra interlinked by $[Si_3O_9]$ triple tetrahedral rings. The frameworks have large channels occupied by Ba^{2+} cations. Despite the topological similarities, the *P*3 polymorph is 4.2% denser than the benitoite form, which indicates that the former corresponds to the higher pressure modification. The phase transition between the two forms had not been experimentally observed, but most probably is displacive in character. The structural complexity of the denser polymorph (3.921 bit/atom and 164.664 bit/cell) is higher than that for the benitoite form (2.020 bit/atom and 56.567 bit/cell), which is in agreement with similar observations for displacive phase transitions.

The HP Ca aluminosilicates attracted attention due to the discovery of the $CaAl_4Si_2O_{11}$ phase (CAS) during the experiments on the densification of terrigenous and pelagic sediments in the mantle transition zone (Irifune et al., 1994). This phase was later found as inclusions in shocked basaltic Martian meteorites (shergottites: Beck et al., 2004; El Goresy et al., 2013; Tomioka, Miyahara, 2017) and lunar meteorites and was recently established as a separate mineral species, donwilhelmsite (Fritz et al., 2020). The phase forms a solid solution with its Na analogue, $NaAl_3Si_3O_{11}$ (NAS) (Akaogi et al., 2010; Zhou, Irifune, 2020). The crystal structure of synthetic CAS was investigated using different diffraction and spectroscopic techniques (Gautron et al., 1999; Grey et al., 1999; Ono et al., 2005; Xue et al., 2009). It is based upon close packing of Ca and O atoms that follow the hexagonal ABABAB = $[AB]^3$ sequence (six layers per unit cell), but with different occupancies of the close-packed layers by Ca, which

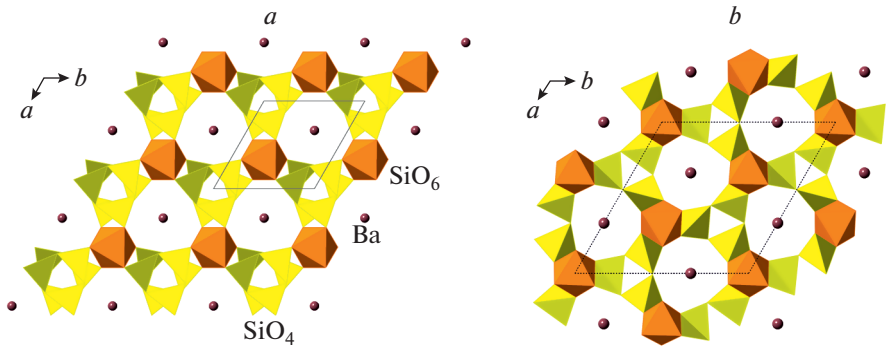

Fig. 38. The crystal structures of the hexagonal (*a*) and trigonal (*b*) polymorphs of $BaSi_4O_9$, both based upon 3D framework of SiO_6 octahedra and SiO_4 tetrahedra.

Рис. 38. Кристаллическая структура гексагонального (*a*) и тригонального (*b*) полиморфов $BaSi_4O_9$, содержащих трехмерные каркасы из октаэдров SiO_6 и тетраэдров SiO_4.

generates a threefold superstructure along the *c* axis. The structure can also be described as consisting of two types of layers, $\mathbf{L_1}$ and $\mathbf{L_2}$ (Fig. 39*a*). The $\mathbf{L_1}$ layer is a dioctahedral layer formed by edge-sharing SiO_6 octahedra (Fig. 39*b*), whereas the $\mathbf{L_2}$ layer (Fig. 39*c*) is formed by dimers of face-sharing AlO_6 octahedra (Fig. 39*d*) and dimers of face-sharing AlO_4 tetrahedra (Fig. 39*e*). The face-sharing octahedra are fully occupied and strongly distorted due to the $Al^{3+}\cdots Al^{3+}$ repulsion, whereas the face-sharing AlO_4 tetrahedra are half-occupied only, due to the extremely short $^{IV}Al\cdots{}^{IV}Al$ distance. Zagamiite, $CaAl_2Si_{3.5}O_{11}$, is the Si-rich analogue of donwilhelmsite discovered by Ma and Tschauner (2017) and briefly described by Ma et al. (2019b) in basaltic shergottites Zagami and NWA856, where the mineral formed as a result of a shock metamorphism. Donwilhemsite and zagamiite crystallize in the same structure type and differ in the occupancies of the cation sites only.

Whereas both donwilhelmsite and zagamiite contain partially or mixed occupied sites, it seems that all other known quaternary phases in the Ca–Al–Si–O system are fully ordered. The crystal structure of the high-pressure compound $CaAl_{12}Si_4O_{27}$ was determined by Grey et al. (2000) and was described as consisting of a dense framework formed by AlO_6 and SiO_6 octahedra and SiO_4 tetrahedra (Fig. 40*a*). It can be considered as formed by layers of two types, $\mathbf{L_1}$ and $\mathbf{L_2}$. The $\mathbf{L_1}$ layer (Fig. 40*c*) is formed by two identical $\mathbf{L_1'}$ sublayers shown in Fig. 40*b*. The latter are built from SiO_6 octahedra sharing edges with trimers of edge-sharing AlO_6 octahedra. The $\mathbf{L_2}$ layer contains Lindquist-type $[Al_6O_{19}]$ hexamers interlinked by SiO_4 tetrahedra by sharing common corners.

Two other structurally characterized Ca-Al-Si-O phases belong to the group of defect perovskite structures and have been prepared during the investigation of incorporation of Al into $CaSiO_3$ perovskite. Fitz Gerald and Ringwood (1991), following early observations of Liu (1978b), reported the formation of the $Ca_2AlSiO_{5.5}$ phase with rhombohedral symmetry and fivefold perovskite superstructure, but structure details have never been reported in full (see also: Kojitani et al., 2009). The system was further investigated by Bläß et al. (2004, 2007), who discovered the $CaAl_{0.5}Si_{0.5}O_{2.75}$ (= $Ca_4Al_2Si_2O_{11}$) and $CaAl_{0.4}Si_{0.6}O_{2.8}$ (= $Ca_5Al_2Si_3O_{14}$) phases, along with the Fe analogue of the latter. The crystal-structure solution for these phases was done by Kanzaki et al. (2017) and Kanzaki (2020). Both structures (Fig. 41) can be viewed as belonging to the same polysomatic series and consist of perovskite slabs of corner-sharing

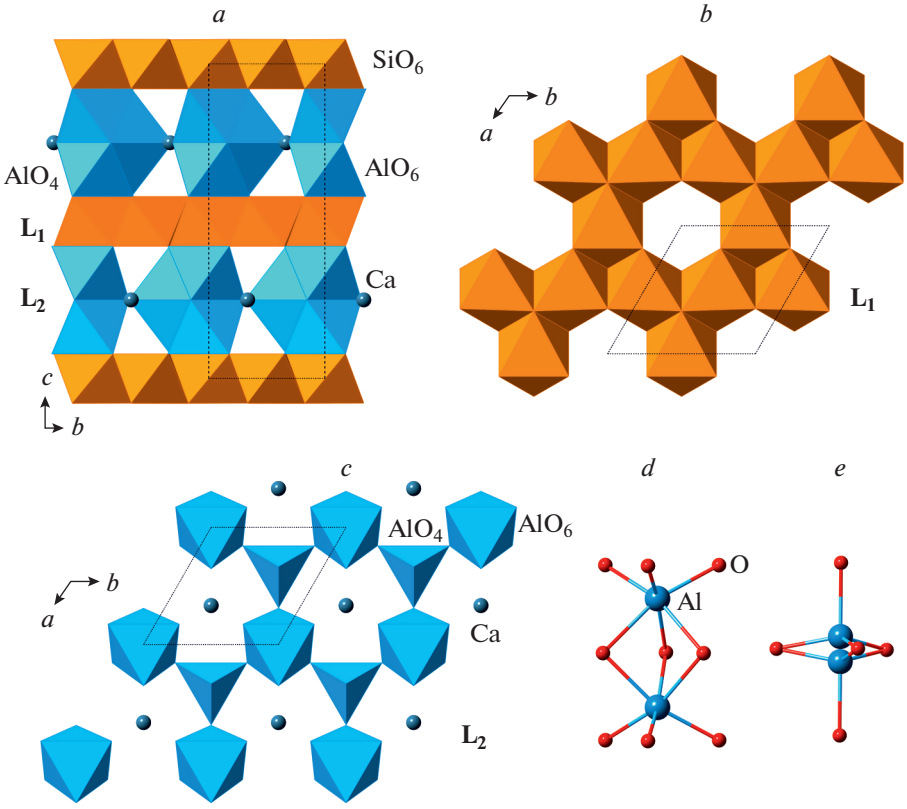

Fig. 39. The crystal structure of donwilhelmsite projected along the *a* axis (*a*) and the projections of the $\mathbf{L_1}$ (*b*) and $\mathbf{L_2}$ (*c*) layers along [001]. The $\mathbf{L_2}$ layer is based upon corner-sharing dimers of fully occupied AlO_6 octahedra (*d*) and dimers of face-sharing half-occupied AlO_4 tetrahedra (*e*).

Рис. 39. Кристаллическая структура донвилхемсита в проекции вдоль оси *a* (*a*) и проекции составляющих ее слоев $\mathbf{L_1}$ (*b*) и $\mathbf{L_2}$ (*c*) вдоль направления [001]. Слой $\mathbf{L_2}$ образован вершинным объединением димеров из гранно-связанных полностью заселенных октаэдров AlO_6 (*d*) и димеров из гранно-связанных полузаселенных тетраэдров AlO_4 (*e*).

octahedra incrustated on both sides by SiO_4 tetrahedra. In $CaAl_{0.5}Si_{0.5}O_{2.75}$ (= $Ca_4Al_2Si_2O_{11}$), the octahedra are occupied by Al and slabs are two octahedra thick, whereas, in $CaAl_{0.4}Si_{0.6}O_{2.8}$ (= $Ca_5Al_2Si_3O_{14}$), the slabs are three octahedra thick and contain both AlO_6 and SiO_6 octahedra. Thus, the crystal-chemical formulae of the first and the second compounds should be written as $Ca_4[^{VI}Al_2O_3(^{IV}SiO_4)_2]$ and $Ca_5[^{VI}Al_2{}^{VI}SiO_6(^{IV}SiO_4)_2]$, respectively. Considering the polysomatic series consisting of perovskite slabs, one may notice that merwinite, $Ca_3Mg(SiO_4)_2$, can be counted as the first phase in the family containing octahedral slabs one octahedron thick (Moore, Araki, 1972; Kim et al., 2017; Dewangan et al., 2019). Moore and Araki (1972) described the crystal structure of merwinite as distorted close packing formed by Ca and O atoms. However, the arrangement is quite far from being close-packed, despite the fact that it contains some closely packed layers. Moriyama et al. (1992) noted that merwinite is stable at least up to 16 GPa and 2300 K, whereas Zedgenizov et al. (2014) reported on the occurrence of merwinite in diamond inclusions along with breyite and olivine.

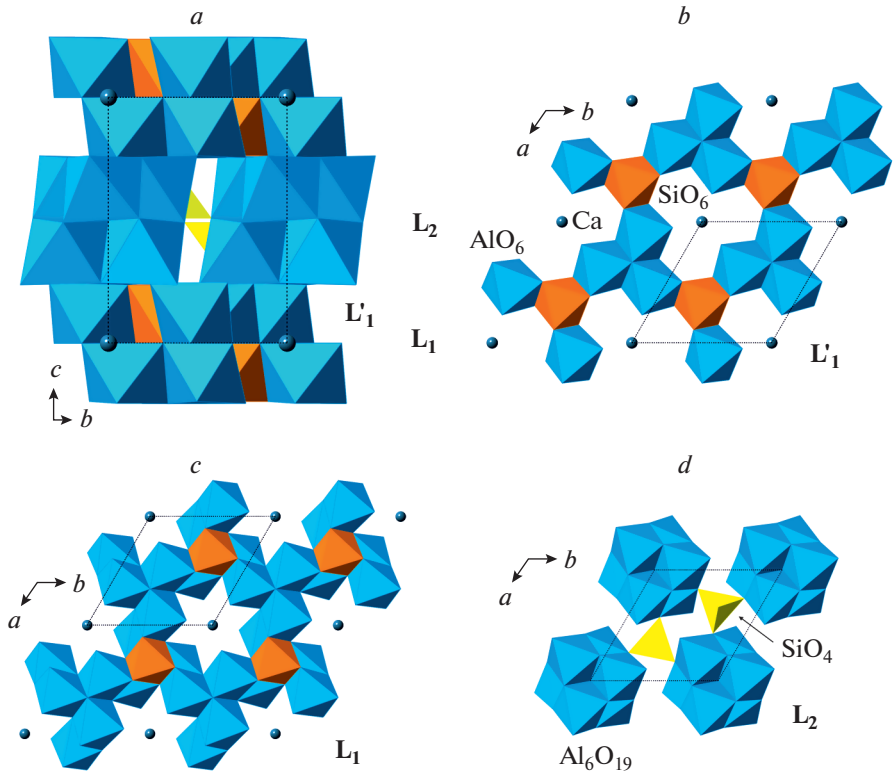

Fig. 40. The crystal structure of $CaAl_{12}Si_4O_{27}$ projected along the *a* axis (*a*) and the projections of the $\mathbf{L'_1}$ sublayer (*b*), and $\mathbf{L_1}$ (*c*) and $\mathbf{L_2}$ (*d*) layers along [001].

Рис. 40. Кристаллическая структура $CaAl_{12}Si_4O_{27}$ в проекции вдоль оси *a* (*a*) и проекции субслоя $\mathbf{L'_1}$ (*b*) и слоев $\mathbf{L_1}$ (*c*) и $\mathbf{L_2}$ (*d*) вдоль [001].

Tissintite, $(Ca,Na,\square)AlSi_2O_6$, is a Ca,Na aluminosilicate found in shock melt pockets in the Martian meteorite Tissint (Ma et al., 2015; Rucks et al., 2018) and found later in shock-lithifed lunar regolith (Zhang et al., 2021). It has a high-pressure *C*2/*c* clinopyroxene crystal structure with Si in tetrahedral coordination.

11. ALKALI METAL HP SILICATES AND ALUMINOSILICATES

Alkali metal high-pressure silicates and aluminosilicates have already been mentioned in this review (e.g., HP feldspar polymorphs and phase X). Herein we provide an overview on Na and K HP silicates with Si in octahedral coordination.

The alkali metal HP silicates with octahedral-tetrahedral structures (i.e. those based upon units of linked SiO_6 octahedra and SiO_4 tetrahedra) have been reviewed by Finger and Hazen (2000). Surprisingly enough, not much new information on these phases appeared in the literature over the past 20 years. The crystallographic data and relevant references are provided in Table 12.

The crystal structure of $Na_2{}^{VI}Si({}^{IV}Si_2O_7)$ is based upon 3D framework formed by corner linkage of SiO_6 octahedra and Si_2O_7 groups (Fig. 42*a*). Krivovichev (2005) noticed that the

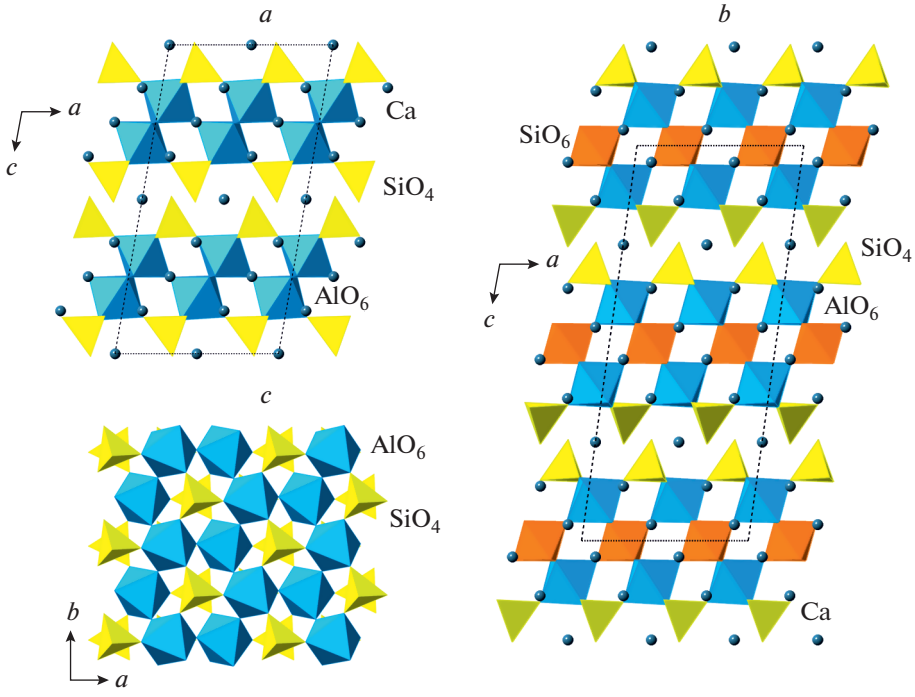

Fig. 41. Ca–Al–Si defect perovskites: the crystal structures of $CaAl_{0.5}Si_{0.5}O_{2.75}$ (= $Ca_4Al_2Si_2O_{11}$) (*a*) and $CaAl_{0.4}Si_{0.6}O_{2.8}$ (= $Ca_5Al_2Si_3O_{14}$) (*b*) projected along their *b* axes.

Рис. 41. Ca–Al–Si дефектные перовскиты: кристаллические структуры $CaAl_{0.5}Si_{0.5}O_{2.75}$ (= $Ca_4Al_2Si_2O_{11}$) (*a*) и $CaAl_{0.4}Si_{0.6}O_{2.8}$ (= $Ca_5Al_2Si_3O_{14}$) (*b*) в проекциях вдоль осей *b*.

structure topology of this compound corresponds to the **fsh** keldyshite-parakeldyshite type, which is also typical for khibinskite and several synthetic materials (see: Kabanova et al., 2020, and references therein). The crystal structure of $Na_8{}^{VI}Si(^{IV}Si_6O_{18})$ belongs to the lovozerite structure type and is the simplest archetype in the family of lovozerite-like structures (Pekov et al., 2009; Krivovichev, 2015). It represents a framework of six-membered silicate rings with a chair conformation linked via SiO_6 octahedra (Fig. 42*b*). The crystal structure of $Na_6{}^{VI}Si_3(^{IV}Si_9O_{27})$ has no natural or synthetic analogues and consists of nine-membered tetrahedral silicate rings arranged within the (010) plane and interlinked by SiO_6 octahedra into a 3D framework (Fig. 43). The crystal structure of $Na_{1.8}Ca_{1.1}{}^{VI}Si(^{IV}Si_5O_{14})$ belongs to the $Ca_3(Ga_2Ge)Ge_3O_{14}$ structure type (Belokoneva et al., 1980). Among minerals, this structure type is possessed by dugganite, $Pb_3Zn_3Te^{6+}As_2O_{14}$ (Lam et al., 1998), and its phosphate analogue kuksite, $Pb_3Zn_3Te^{6+}P_2O_{14}$ (Mills et al., 2010). The crystal structure (Fig. 44*a*, *b*) is based upon the $[Si_5O_{14}]$ layers of corner-sharing SiO_4 tetrahedra consisting of the nine-membered $[Si_9O_{27}]$ rings similar to those observed in $Na_6{}^{VI}Si_3(^{IV}Si_9O_{27})$ (Fig. 44*c, d*). In dugganite and kuksite, the layers are built up by condensation of ZnO_4 and TO_4 (T = P, As) tetrahedra. The crystal structure of $K_2{}^{VI}Si(^{IV}Si_3O_9)$ (Fig. 45) is of the wadeite, $K_2{}^{VI}Zr(^{IV}Si_3O_9)$, structure type (Krivovichev, 2005) and contains three-membered silicate tetrahedral rings interlinked by SiO_6 tetrahedra (Fig. 45). The wadeite framework topology is different from those of benitoite and trigonal $BaGe(Ge_3O_9)$ that had

Table 12. Crystallographic data for high-pressure alkali metal silicates and aluminosilicates
Таблица 12. Кристаллографические данные для высокобарических силикатов и алюмосиликатов щелочных металлов

Chemical formula	Structure topology	SG	*a* [Å]/α [°]	*b* [Å]/β [°]	*c* [Å]/γ [°]	*V*, Å^3	CN(Si)	Reference
$Na_2{}^{VI}Si(^{IV}Si_2O_7)$	Keldyshite	*C*2/*c*	8.922/90	4.849/102.6	11.567/90	488.3	4, 6	1
$Na_8{}^{VI}Si(^{IV}Si_6O_{18})$	Lovozerite	$R\bar{3}$	7.180/87.3	= *a*/α	= *a*/α	368.9	4, 6	2
$Na_6{}^{VI}Si_3(^{IV}Si_9O_{27})$	–	$P2_1/n$	10.875/90	9.326 /90.2	19.224/90	1949.7	4, 6	3
$Na_{1.8}Ca_{1.1}{}^{VI}Si(^{IV}Si_5O_{14})$	$Ca_3(Ga_2Ge)Ge_3O_{14}$	*P*321	7.889/90	= *a*/α	4.595/120	248.3	4, 6	4
$K_2{}^{VI}Si(^{IV}Si_3O_9)$	Wadeite	$P6_3/m$	6.612/90	= *a*/α	9.510/120	360.1	4, 6	5
$NaAlSiO_4$	$CaFe_2O_4$	*Pbnm*	10.155/90	8.664/90	2.739/90	240.9	6	6
$(K,Na)_{0.9}(Mg,Fe)_2(Mg,Fe,Al,Si)_6O_{12}$	$BaCa_2In_6O_{12}$	$P6_3/m$	8.830/90	= *a*/α	2.779/120	187.7	6	7
$KMg_2Al_{4.80}Si_{1.15}O_{12}$	$BaCa_2In_6O_{12}$	$P6_3/m$	8.817/90	= *a*/α	2.768/120	186.4	6	8
$Na_{1.04}Mg_{1.88}Al_{4.64}Si_{1.32}O_{12}$	$BaCa_2In_6O_{12}$	$P6_3/m$	8.727/90	= *a*/α	2.766/120	182.5	6	8

References: (1) Fleet, Hederson, 1995; (2) Fleet, 1998; (3) Fleet, 1996; (4) Gasparik et al., 1995; (5) Swanson, Prewitt, 1983; (6) Yamada et al., 1983; (7) Gasparik et al., 2000; (8) Kojitani et al., 2011.

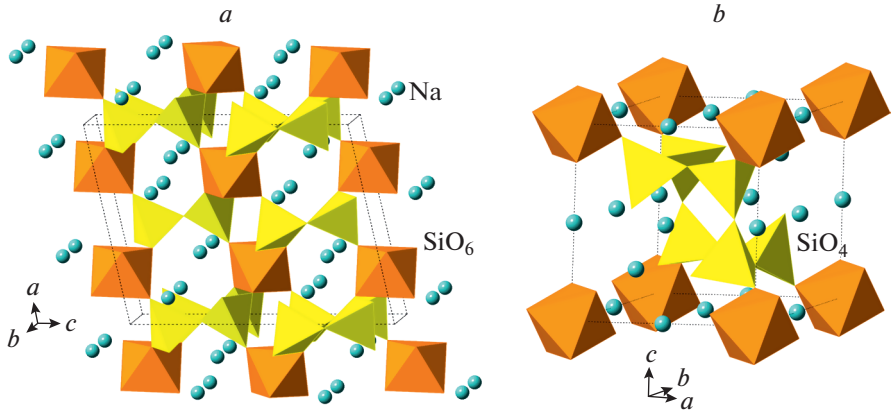

Fig. 42. The crystal structures of $Na_2{}^{VI}Si(^{IV}Si_2O_7)$ (*a*) and $Na_8{}^{VI}Si(^{IV}Si_6O_{18})$ (*b*).

Рис. 42. Кристаллические структуры $Na_2{}^{VI}Si(^{IV}Si_2O_7)$ (*a*) и $Na_8{}^{VI}Si(^{IV}Si_6O_{18})$ (*b*).

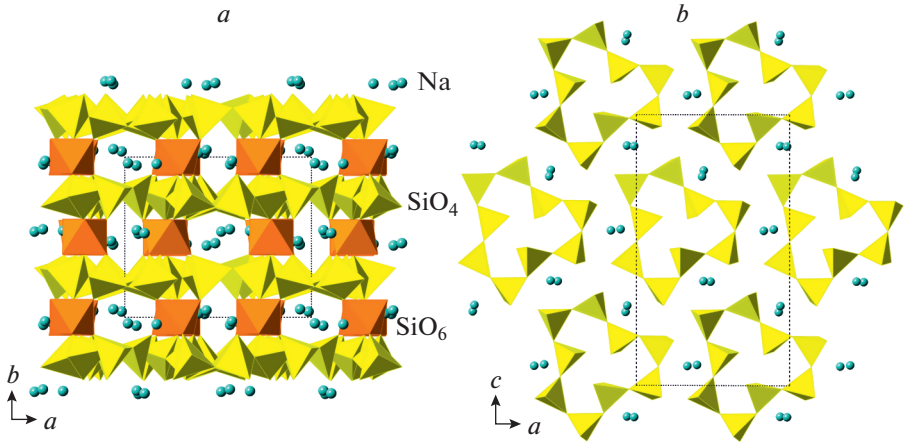

Fig. 43. The crystal structure of $Na_6{}^{VI}Si_3(^{IV}Si_9O_{27})$ (*a*) and the projection of the layer of nine-membered silicate rings parallel to (010) (*b*).

Рис. 43. Кристаллическая структура $Na_6{}^{VI}Si_3(^{IV}Si_9O_{27})$ (*a*) и проекция слоя из девятичленных колец, параллельного плоскости (010) (*b*).

been observed for isochemical $[^{VI}Si(^{IV}Si_3O_9)]$ frameworks in the $BaSi_4O_9$ polymorphs (see above). No crystal-structure information exists for the HP phases with sixfold coordination of Si in Rb- and Cs-bearing silicate systems, which represents an interesting avenue for the chemical explorative studies.

Except for the HP polymorphs of albite and microcline (Pakhomova et al., 2020; Krivovichev, 2020), the alkali metal HP aluminosilicates are remarkable in the fact that they possess exclusively octahedral coordination. In addition to the hollandite-type lingunite, $NaAlSi_3O_8$, and

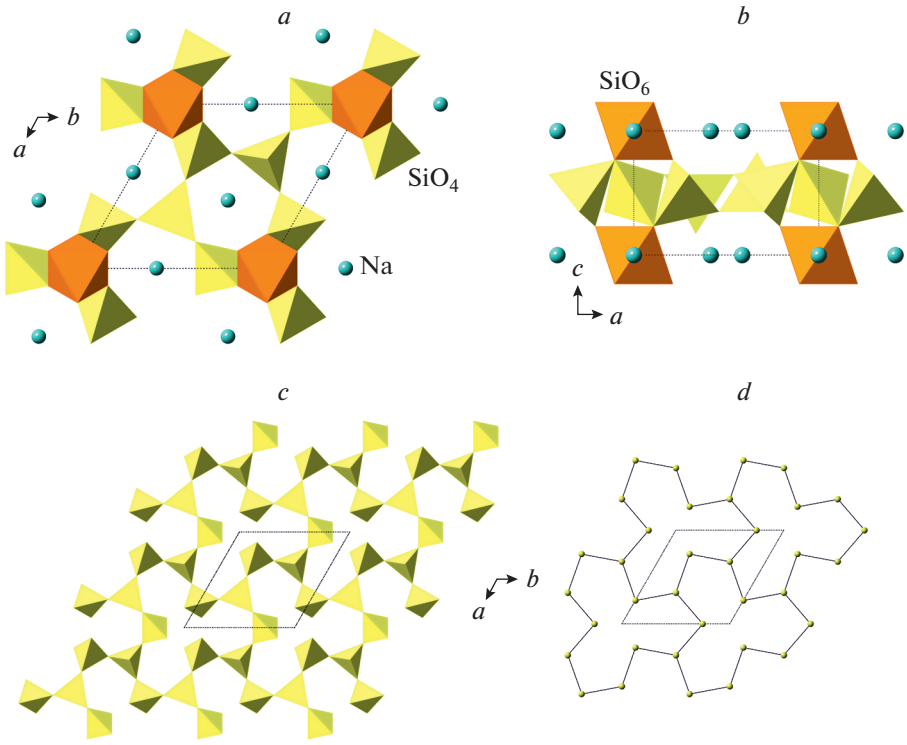

Fig. 44. The crystal structure of $Na_{1.8}Ca_{1.1}{}^{VI}Si(^{IV}Si_5O_{14})$ in projections along the *c* (a) and *b* (*b*) axes, the silicate layer (*c*) and its graph (*d*).

Рис. 44. Кристаллическая структура $Na_{1.8}Ca_{1.1}{}^{VI}Si(^{IV}Si_5O_{14})$ в проекциях вдоль осей *c* (*a*) и *b* (*b*), силикатный слой (*c*) и его граф (*d*).

liebermannite, $KAlSi_3O_8$ (see: Krivovichev, 2020), there are two structure types consisting of frameworks with tunnels outlined by double chains of edge-sharing MO_6 octahedra (M = Si, Al). The chemical analogue of trinepheline, $NaAlSiO_4$, with the $CaFe_2O_4$ (CF) structure type, was first reported by Liu (1977) and structurally characterized by Yamada et al. (1980). Its structure is based upon a 3D framework formed by lateral condensation of double octahedral chains that creates tunnels occupied by Na^+ cations (Fig. 46*a*). The NAL phase (new Al-rich phase) first prepared by Irifune and Ringwood (1993) has a complex crystal chemistry and is based upon a 3D framework also formed by double octahedral chains. However, the framework topology is different from that adopted by CF-$NaAlSiO_4$ and contains channels of two types (Fig. 46*b*). The channels with trigonal cross-section accommodate smaller cations (such as Mg^{2+}), whereas channels with hexagonal cross-section are large enough to host large cations such as K^+. In all known chemical variations of the NAL phase (Table 12), Al is the dominant octahedral cation, whereas Si is a subordinate component. Neither CF- nor NAL-type phases are known in nature, though their existence in inclusions in diamonds was suggested on the basis of the chemical studies (Walter et al., 2011; Kaminsky, 2017).

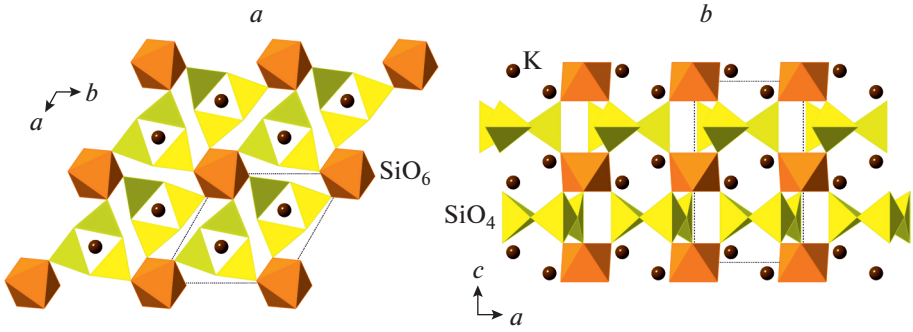

Fig. 45. The crystal structure of $K_2{}^{VI}Si(^{IV}Si_3O_9)$ projected along the *a* (*a*) and *b* (*b*) axes.

Рис. 45. Кристаллическая структура $K_2{}^{VI}Si(^{IV}Si_3O_9)$ в проекциях вдоль осей *a* (*a*) и *b* (*b*).

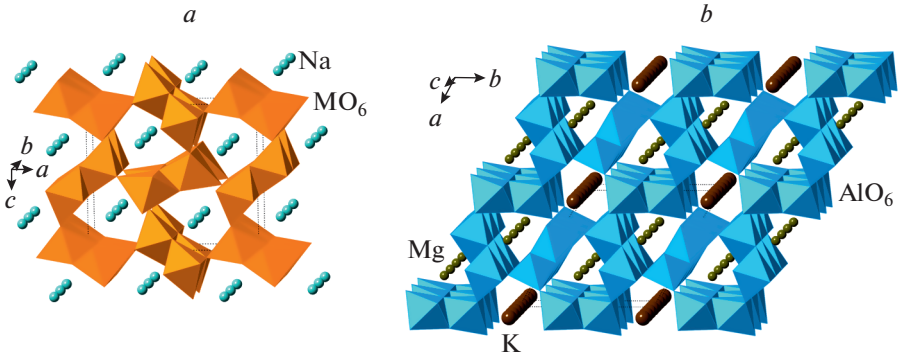

Fig. 46. The crystal structures of CF-$NaAlSiO_4$ (*a*) and the NAL phase (*b*).

Рис. 46. Кристаллическая структура CF-$NaAlSiO_4$ (*a*) и фазы NAL (*b*).

12. MISCELLANEOUS

12.1. Silicate pyrochlores and related structures

Silicate pyrochlores with Si in octahedral coordination have been first reported by Shannon and Sleight (1968). Reid et al. (1977) provided crystal-structure data for $Sc_2Si_2O_7$ and $In_2Si_2O_7$ (Table 13), whereas Xu et al. (2011) and Zhai et al. (2013) investigated structure and properties of $MgZrSi_2O_7$. All three mentioned compounds belong to the cubic pyrochlore structure type (Fig. 47) based upon three-dimensional framework consisting of corner-sharing SiO_6 octahedra. The framework has the $[^{VI}SiO_3]$ composition and the crystal-chemical formula of the compounds should be written as $A_2O[^{VI}Si_2O_6]$ (A = Sc, In, Mg, Zr). Bindi et al. (2017a) described the high-pressure synthesis and crystal structure of $MgTiSi_2O_7$, which is remarkably different from that of $MgZrSi_2O_7$ and belongs to the weberite structure type (Fig. 47*b*). The topological relations between the pyrochlore and weberite structure types is shown in Fig. 48 in terms of the nodal representation (Krivovichev, 2005). Both structures can be described as based upon kagomé-type layers of corner-sharing Si-centered octahedra with topology shown in Fig. 48*a*. However, the stacking sequence of the layers and their linkage is different (Figs. 48*b*–*e*).

Table 13. Crystallographic data for silicate pyrochlores and related phases
Таблица 13. Кристаллографические данные для силикатных пирохлоров и родственных фаз

Chemical formula	SG	*a*, Å	*c*, Å	*V*, Å^3	CN(Si)	Reference
$In_2O[Si_2O_6]$	$Fd\bar{3}m$	9.413	= *a*	834.0	6	1
$Sc_2O[Si_2O_6]$	$Fd\bar{3}m$	9.287	= *a*	801.0	6	1
$MgZrSi_2O_7$	$Fd\bar{3}m$	9.288	= *a*	801.3	6	2
$MgTiSi_2O_7$	$P3_121$	6.335	16.325	567.4	6	3

References: (1) Reid et al., 1977; (2) Xu et al., 2011; (3) Bindi et al., 2017a.

In both structures, the layers are linked by additional octahedra located in the interlayer space. In the pyrochlore structure type (Fig. 48*f*), the additional octahedron is six-connected and connects two triangular units from the adjacent layers, whereas, in the weberite structure type (Fig. 48*g*), the additional octahedron (centered by the Si1 site) is only four-connected, i.e. the $Si1O_6$ octahedron has pending Si–O bonds to non-shared O atoms. As a consequence, the silicate framework no longer has the Si : O ratio of 1 : 3 as in pyrochlore, but 2 : 7, i.e. the framework has the composition $[Si_2O_7]$. Thus the Zr ↔ Ti substitution has considerable influence upon the structural topology of the silicate octahedral framework.

12.2. HP behavior of the layered silicates of the gadolinite supergroup

The crystal structures of the gadolinite-supergroup minerals are based upon tetrahedral sheets of corner-sharing SiO_4 and TO_4 tetrahedra (T = B, Be) shown in Fig. 49*a*. The sheet is composed from four- and eight-membered tetrahedral rings. Gorelova et al. (2018) investigated the high-pressure behavior of datolite, $CaBSiO_4(OH)$, and found out that, in between

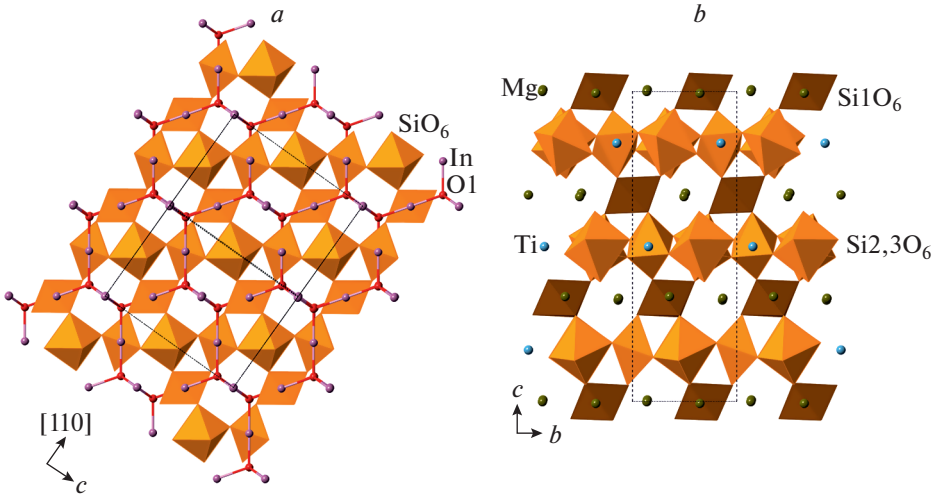

Fig. 47. The crystal structure of silicate pyrochlore $In_2O[Si_2O_6]$ in projection along [$\bar{1}$10] (*a*) and the crystal structure of the weberite-type $MgTi[Si_2O_7]$ projected along the *a* axis (*b*).

Рис. 47. Кристаллическая структура силикатного пирохлора $In_2O[Si_2O_6]$ в проекции вдоль направления [$\bar{1}$10] (*a*) и кристаллическая структура соединения $MgTi[Si_2O_7]$ со структурным типом веберита в проекции вдоль оси *a* (*b*).

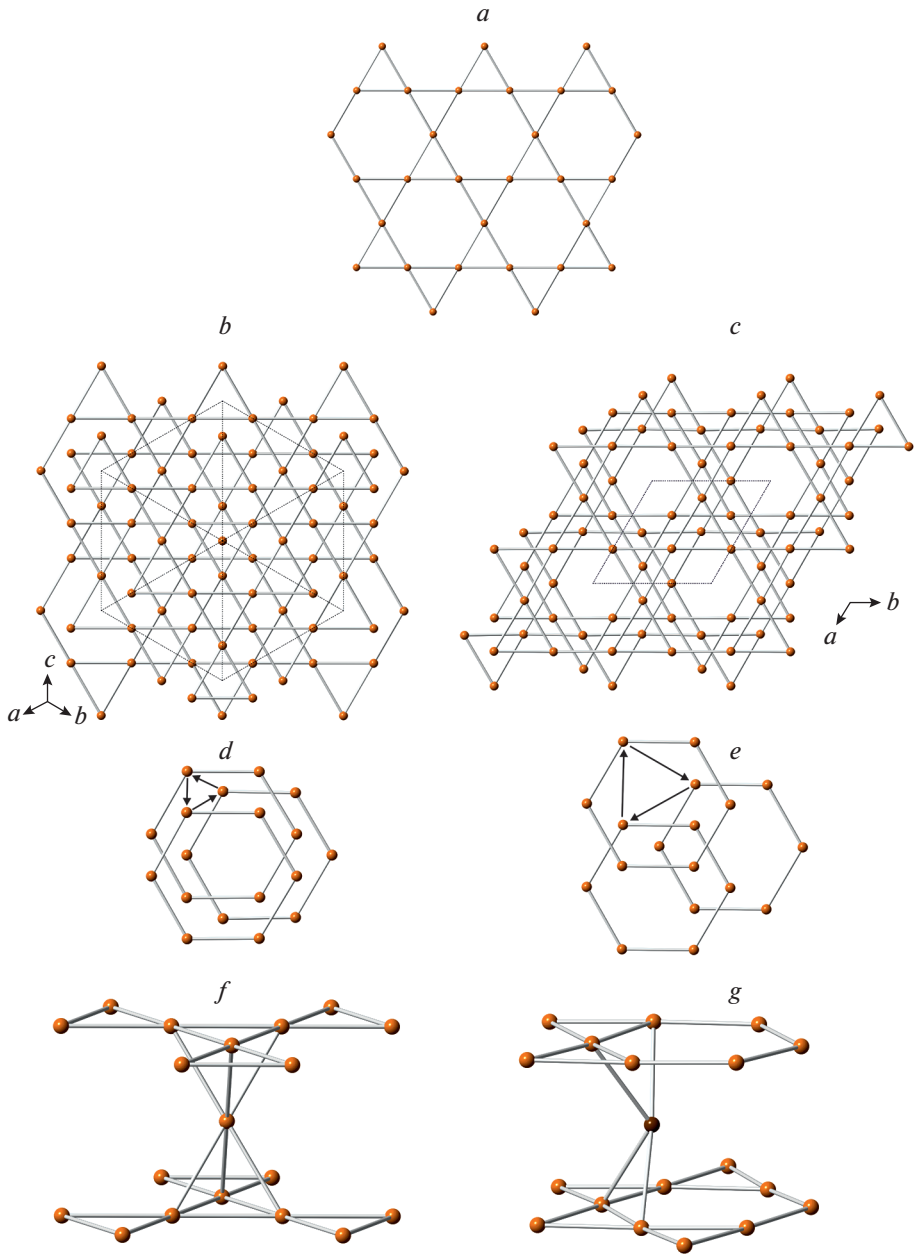

Fig. 48. Relations between topologies of octahedral frameworks in the pyrochlore and weberite structure types: both frameworks are based upon the same kagome-type layers (*a*), but with different stacking modes (*b*: pyrochlore; *c*: weberite) that can be described in terms of the arrangement of six-membered rings (*d*: pyrochlore; *e*: weberite; arrows indicate the stacking direction from bottom to top). The layers are linked by six-connected Si node in pyrochlore (*f*) and four-connected Si node in weberite (*g*).

Рис. 48. Сравнение топологии октаэдрических каркасов в структурных типах пирохлора и веберита: оба каркаса основаны на одинаковых сетках кагомэ (*a*) с различной укладкой (*b*: пирохлор; *c*: веберит), которая может быть описана в терминах укладки шестичленных колец (*d*: пирохлор; *e*: веберит; стрелки указывают направление укладки снизу вверх). Сетки кагомэ соединены шестисвязными Si-узлами в пирохлоре (*f*) и четырехсвязными Si-узлами в веберите (*g*).

Table 14. Crystallographic data for miscellaneous HP silicates
Таблица 14. Кристаллографические данные для разнообразных высокобарических силикатов

Mineral/phase name	Chemical formula	SG	*a* [Å]/α [°]	*b* [Å]/β [°]	*c* [Å]/γ [°]	*V*, Å^3	CN(Si)	Reference
Datolite (0.0001 GPa)	$CaBSiO_4(OH)$	$P2_1/c$	4.835/90	7.608/90.2	9.629/90	354.2	4	1
Datolite II (37.6 GPa)	$CaBSiO_4(OH)$	$P2_1/c$	4.479/90	6.717/90.6	9.242/90	278.0	5	1
Jeffbenite	$Mg_3Al_2Si_3O_{12}$	$I\bar{4}2d$	6.523/90	= *a*/α	18.176/90	773.4	4	2
Reidite	$ZrSiO_4$	$I4_1/a$	4.738/90	= *a*/α	10.506/90	235.8	4	3
“Scheelite-$USiO_4$”	$USiO_4$	$I4_1/a$	4.768/90	= *a*/α	10.988/90	249.8	4	4
Cordierite (0.0001 GPa)	$Mg_2Al_3(AlSi_5O_{18})(H_2O)$	*Cccm*	17.051/90	9.713/90	9.336/90	1546.1	4	5
Cordierite II (7.5 GPa)	$Mg_2Al_3(AlSi_5O_{18})(H_2O)$	*P*1	15.567/90.0	9.624/86.3	9.066/91.0	1355.1	4, 5	5
Cordierite III (15.2 GPa)	$Mg_2Al_3(AlSi_5O_{18})(H_2O)$	*P*1	8.519/85.7	8.245/86.0	9.163/70.8	605.5	4, 5, 6	5
“Beryl II”	$Cs(Be_2Li)Al_2Si_6O_{18}$	*R*3*c*	15.658/90	= *a*/α	27.166/120	5768.0	4	6
“Dravite II”	$NaMg_3Al_6(Si_6O_{18})(BO_3)_3(OH)_4$	*R*3	15.449/90	= *a*/α	6.695/120	1383.8	4	7

References: (1) Gorelova et al., 2018; (2) Nestola et al., 2016; (3) Glass et al., 2002; (4) Bauer et al., 2014; (5) Finkelstein et al., 2015b; (6) Ende et al., 2021; (7) O’Bannon et al., 2018.

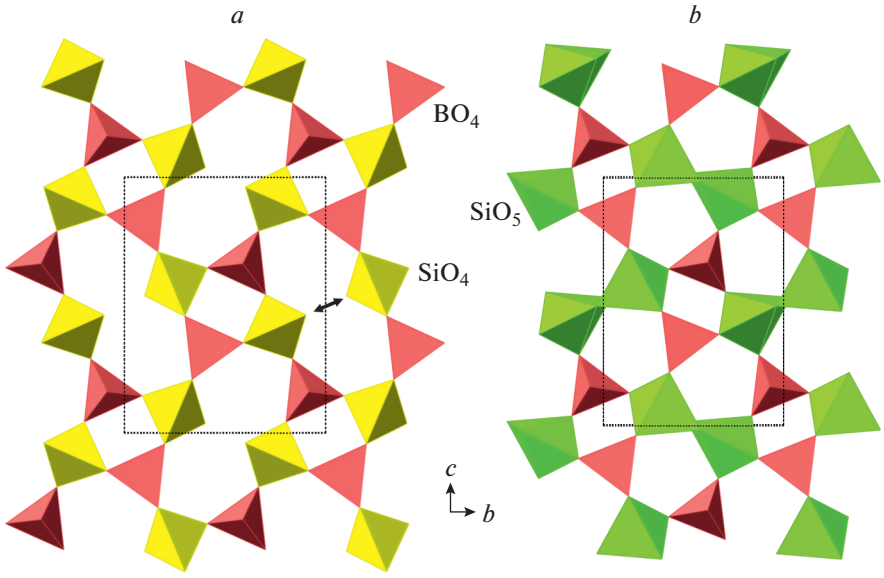

Fig. 49. The [$BSiO_4(OH)$] borosilicate layer in datolite (*a*) and its high-pressure polymorph datolite II (*b*).

Рис. 49. Боросиликатный слой [$BSiO_4(OH)$] в датолите (*a*) и его высокобарическом полиморфе датолите II (*b*).

27 and 33 GPa, the mineral isosymmetrically transforms into its HP polymorph datolite II. The phase transition is associated with the collapse of the eight-membered rings and the formation of dimers of edge-sharing SiO_5 trigonal bipyramids (Fig. 49*b*). The resulting sheet topology does not contain eight-membered rings, which transform into pairs of five-membered rings. It is of interest that another member of the gadolinite supergroup, hingganite-(Y), $YBeSiO_4(OH)$, does not show similar phase transitions, though there is a strong tendency of two SiO_4 tetrahedra across the ring to approach each other (Gorelova et al., 2020). After danburite II (Pakhomova et al., 2017a), datolite-II is the second example of an inorganic silicate that contains Si in exclusively fivefold coordination.

12.3. Jeffbenite

Jeffbenite, $Mg_3Al_2Si_3O_{12}$, was originally described by Harris et al. (1997) in an inclusion in a lower-mantle diamond and was identified as a "tetragonal almandine-pyrope phase" (TAPP). Nestola et al. (2016) established its status as a separate mineral species and discussed its origin (see also: Kaminsky, 2012, 2020; Zedgenizov et al., 2020). The crystal structure of jeffbenite represents a framework of Mg, Al and Si coordination polyhedra (Fig. 50*a*). The aluminosilicate subframework is formed by AlO_6 octahedra and SiO_4 tetrahedra as strongest structural subunits. It is remarkable that each AlO_6 octahedron shares an edge with the adjacent SiO_4 tetrahedron. The resulting units are linked by corner sharing into kröhnkite-type chains (Fig. 50*b*) that run parallel to the *a* and *c* axes on different *z* levels, thus forming a trellis-like arrangement. The adjacent chains are interlinked by additional SiO_4 tetrahedra into a 3D framework. Mg atoms are located in the cavities of the aluminosilicate framework.

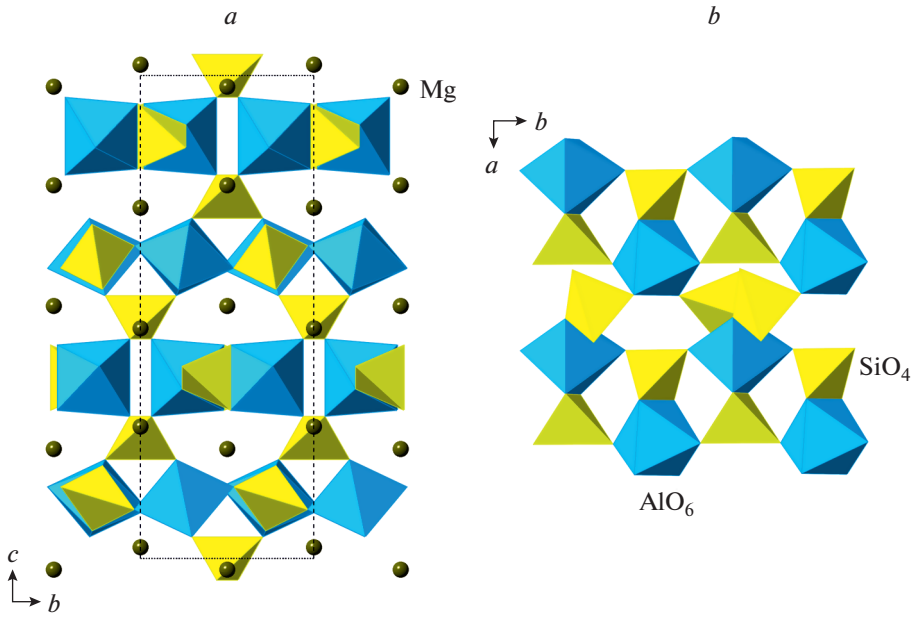

Fig. 50. The crystal structure of jeffbenite projected along the *a* axis (*a*) and the projection of the layer of kröhnkite-type chains (*b*).
Рис. 50. Кристаллическая структура джеффбенита в проекции вдоль оси *a* (*a*) и проекция слоя и крёнкитоподобных цепочек (*b*).

12.4. Reidite

Reidite is a high-pressure scheelite-type polymorph of zircon, $ZrSiO_4$, that was first obtained experimentally by Reid and Ringwood (1969). Glass and Liu (2001) found reidite in natural shock-metamorphized zircons, which allowed Glass et al. (2002) to establish it as a separate mineral species. Figure 51 compares the crystal structures of zircon and reidite (the latter is inferred from the scheelite structure model). Both minerals are based upon dense frameworks of ZrO_8 polyhedra and SiO_4 tetrahedra. However, the framework topologies are different. In zircon, the ZrO_8 and SiO_4 polyhedra share edges to produce chains parallel to [001], whereas, in reidite, only corner-linkage between the ZrO_8 and SiO_4 polyhedra is observed. The same type of zircon → scheelite pressure induced phase transition is also known for coffinite, $USiO_4$ (Bauer et al., 2014).

12.4. HP polymorphs of ring silicates

Finkelstein et al. (2015b) investigated high-pressure phase transitions in cordierite under ambient temperature and observed the formation of two new high-pressure polymorphs, cordierite II and III. Figure 52 provides a comparison of the three known polymorphs of cordierite. The ambient-pressure structure (Fig. 52*a*) possesses hexagonal channels occupied by H_2O molecules and outlined by hexagonal rings formed by (Si_2O_7) tetrahedral dimers and AlO_4 tetrahedra. During the phase transition from cordierite I to cordierite II, the channels collapse and some of the Si and Al atoms become pentacoordinated (Fig. 52*b*). Further compression results in the transformation of cordierite II into cordierite III that contains Si in four-, five- and sixfold coordination at the same time (Fig. 52*c*). From the viewpoint of sili-

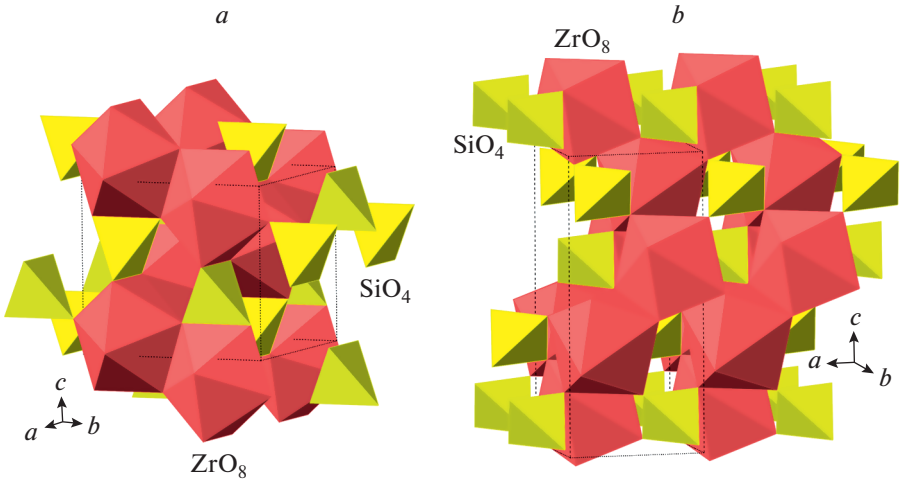

Fig. 51. Comparison of the crystal structures of zircon (*a*) and its high-pressure polymorph reidite (*b*).

Рис. 51. Сравнение кристаллических структур циркона (*a*) и его высокобарического полиморфа рейдита (*b*).

cate connectivity, the phase transitions result in the increasing degree of condensation of Si polyhedra. In cordierite I, only silicate dimers $^{IV}Si–^{IV}Si$ and isolated ^{IV}Si tetrahedra are present. In cordierite II, with the increasing of coordination number of Si sites, these two units are transformed into a single oligomer $^{IV}Si–^{IV}Si–^{V}Si$ that involves SiO_5 trigonal bipyramids. The formation of cordierite III results in the branched oligomeric unit shown in Fig. 52*d* and consisting of four SiO_6 octahedra, three dimers of edge-sharing SiO_5 trigonal bipyramids and five SiO_4 tetrahedra that exist as branches to the backbone formed by Si in five- and sixfold coordination.

Ende et al. (2021) and O'Bannon et al. (2018) studied the high-pressure transformations of beryl-type $Cs(Be_2Li)Al_2Si_6O_{18}$ and dravite, $NaMg_3Al_6(Si_6O_{18})(BO_3)_3(OH)_4$, respectively. In both cases, high-pressure-induced phase transitions have been observed associated with the symmetry reduction without remarkable coordination changes.

12.5. HP behavior and polymorphism in zeolites and other open-framework silicates

During last two decades, the HP polymorphism of zeolites and open-framework silicates was a subject of a number of studies, and several new pressure-induced polymorphic transitions were observed as partly reviewed by Gatta et al. (2018). In most cases, the observed phase transitions are displacive in character and are accompanied by the symmetry reduction (Gatta et al., 2006; Lotti et al., 2015, 2018; Thibaud et al., 2017; Seryotkin et al., 2017; Seryotkin, 2019; Comboni et al., 2019, etc.) associated with the increase in structural complexity and respective decrease in configurational entropy (Krivovichev, 2016). The detailed analysis of these phenomena will be described elsewhere. In all the case mentioned above, the coordination of Si atoms remains tetrahedral in the studied pressure ranges.

13. CONCLUSIONS

Finger and Hazen (1991) first reviewed the field of high-pressure silicates and listed twelve different structure types with octahedrally coordinated Si atoms. In 2000, the same authors provided a review of twenty-four such structure types, i.e. the number has doubled over one

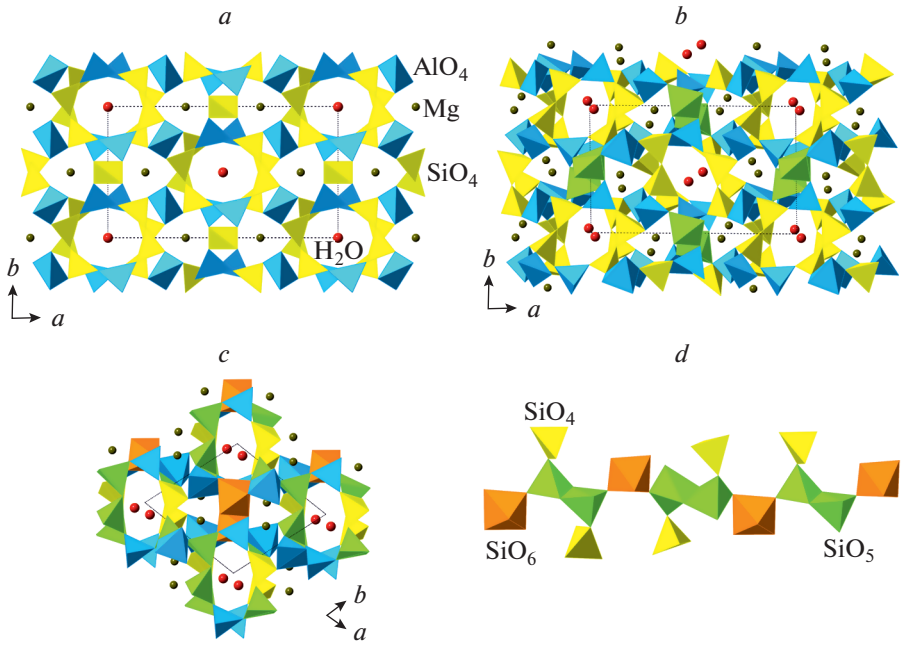

Fig. 52. The crystal structures of cordierite (*a*), cordierite II (*b*), and cordierite III (*c*), an oligomeric unit formed by Si-centered polyhedra in cordierite III (*d*).
Рис. 52. Кристаллическая структура кордиерита (*a*), кордиерита II (*b*), кордиерита III (*c*) и олигомер из пятнадцати Si-центрированных полиэдров в кордиерите III (*d*).

decade (Finger, Hazen, 2000). In this paper, more than seventy-six structure types with ^{VI}Si are considered, i.e. their number has tripled since 2000. The field was also extended due to the new discoveries of structures with pentacoordinated Si: in 2000, only such structure was known, whereas herein we provided description of at least twelve structures possessing this unique structural feature. Only thirteen structures containing both ^{IV}Si and ^{VI}Si were known in 2000 (Hazen et al., 1996; Finger, Hazen, 2000), whereas more than thirty have been described above.

Finger and Hazen (2000) classified all high-pressure silicates with ^{VI}Si into three major structural groups: octahedral structures, octahedral-tetrahedral frameworks and other structures containing both ^{IV}Si and ^{VI}Si. In 2021, this classification should be complemented by the structures containing ^{V}Si, and it should be noted that there exist structures containing exclusively ^{V}Si, and containing both ^{V}Si and ^{VI}Si, ^{IV}Si and ^{V}Si, and all three known types of Si coordination polyhedra, SiO_4, SiO_5 and SiO_6 groups. Thus, the systematics by Finger and Hazen (2000) should be extended by addition of four new structural groups according to the different combinations of Si coordination numbers in the same crystal structure. In the whole crystal chemistry of inorganic silicates, now seven groups can be recognized with CN(Si) = 4; 4 + 5; 4 + 5 + 6; 4 + 6; 5; 5 + 6; 6. We note that there many high-pressure inorganic silicates that contain Si in exclusively fourfold coordination, and only some are considered in this review.

The tendency of oxide crystal structures to form close-packed arrangements of anions under increasing pressure has been widely recognized (Prewitt, Downs, 1998). However, from over 160 HP silicates considered in this work less than half (~45%) are based upon closest packing of atoms, mostly oxygen, but also including mixed-ion closest packings based upon

O^{2-} and large M^{2+} cations (M = Ca, Sr, Ba). It is remarkable that the hypothetically most common Earth's mineral bridmanite, $MgSiO_3$, has an atomic arrangement that is quite far from the eutactic (close-packed) one. Pushcharovsky (1986) noted that, under compression, the $^{IV}Si \rightarrow {}^{VI}Si$ transition occurs more easily for silicates containing cations with higher eletronegativity.

Liebau (1985) formulated the rules of topology for silicate anions based upon SiO_4 tetrahedra with two major rules that "...[SiO_4] tetrahedra are linked to other [SiO_4] tetrahedra via corners rather than edges or faces" and that "...one oxygen atom can belong to no more than two [SiO_4] tetrahedra" (Liebau, 1985). The recent research on HP crystal chemistry of silicates complement the first rule by the additional experimental data on silicates containing SiO_5 and SiO_6 polyhedra. In particular, it was shown that SiO_5 polyhedra may share edges, whereas SiO_6 octahedra may share faces. It seems that the second rule has to be expressed as following: "one oxygen atom can belong to no more than three Si-centered oxygen polyhedra". The only one structure with fourfold coordination of O by Si atoms reported so far is the silica polymorph "IP-phase" (see above), which has been studied by the combination of experimental and theoretical methods so that the structure model is rather hypothetical than solidly proved.

The generalization of the existing data on crystal chemistry of silicates based on the new results allows for the formulation of general rules concerning their coordination features, topology, atomic arrangements, etc. A detailed analytical account of the HP crystal chemistry of silicates will be published elsewhere.

The oustanding progress in the HP crystal chemistry of silicates during recent two decades has been marked by the unique mineralogical discoveries. In particular, at least sixteen HP silicates have been established since 2000 as separate mineral species: ahrensite, asimowite, breyite, bridgmanite, downwilhelmsite, hemleyite, hiroseite, jeffbenite, liebermannite, lingunite, poirerite, reidite, seifertite, stöfflerite, tissintite, zagamiite (see references above). The number of potential new minerals discovered in shocked meteorites, mineral inclusions in diamonds, and other high-pressure environments is still high and there are no doubts that there will be interesting advances in the field of descriptive HP mineralogy in the nearest future.

I am grateful to Acad. D.Yu. Pushcharovsky for the useful comments on the first version of this paper.

The reported study was funded by RFBR, project number 20-15-50193.

Исследование выполнено при финансовой поддержке РФФИ в рамках научного проекта № 20-15-50193.

REFERENCES

Adams D.J., Oganov A.R. Ab initio molecular dynamics study of $CaSiO_3$ perovskite at $P-T$ conditions of Earth's lower mantle. *Phys. Rev. B*. **2006**. Vol. 73. P. 184106.

Ahmed-Zaïd I., Madon M. A high-pressure form of Al_2SiO_5 as a possible host of aluminum in the lower mantle. *Nature*. **1991**. Vol. 353. P. 426–428.

Ahmed-Zaïd I., Madon M. Electron microscopy of high-pressure phases synthesized from natural garnets in a diamond anvil cell: Implications for the mineralogy of the lower mantle. *Earth Planet. Sci. Lett.* **1995**. Vol. 129. P. 233–247.

Akaogi M., Haraguchi M., Nakanishi K., Ajiro H., Kojitani H. High-pressure phase relations in the system $CaAl_4Si_2O_{11}$–$NaAl_3Si_3O_{11}$ with implication for Na-rich CAS phase in shocked Martian meteorites. *Earth Planet. Sci. Lett*. **2010**. Vol. 289. P. 503–508.

Akber-Knutson S., Bukowinski M.S.T., Matas J. On the structure and compressibility of $CaSiO_3$ perovskite. *Geophys. Res. Lett*. **2002**. Vol. 29. P. 1034.

Akimoto S., Sato Y. High-pressure transformations in Co_2SiO_4 olivine and some geohysical implications. *Phys. Earth Planet. Inter*. **1968**. Vol. 1. P. 498–504.

Akins J.A., Ahrens T.J. Dynamic compression of SiO_2: A new interpretation. *Geophys. Res. Lett*. **2002**. Vol. 29. P. 31-1–31-4.

Al'tshuler L.V., Podurets M.A., Simakov G.V., Trunin R.F. High-density forms of fluorite and rutile. *Sov. Phys. Solid State*. **1973**. Vol. 15. P. 969–971.

Andrault D., Fiquet G., Guyot F., Hanfland M. Pressure-induced Landau-type transition in stishovite. *Science*. **1998**. Vol. 282. P. 720–724.

Andrault D., Angel R.J., Mosenfelder J.L., Le Bihan T. Equation of state of stishovite to lower mantle pressures. *Amer. Miner*. **2003**. Vol. 88. P. 301–307.

Angel R. J. High-pressure structure of anorthite. *Amer. Miner.* **1988.** Vol. 73. P. 1114–1119.

Angel R.J. Transformation of fivefold-coordinated silicon to octahedral silicon in calcium silicate, $CaSi_2O_5$. *Amer. Miner.* **1997**. Vol. 82. P. 836–839.

Angel R.J., Gasparik T., Ross N.L., Finger L.W., Prewitt C.T., Hazen R.M. A silica-rich sodium pyroxene phase with six-coordinated silicon. *Nature*. **1988**. Vol. 335. P. 156–158.

Angel R.J., Finger L.W., Hazen R.M., Kanzaki M., Weidner D.J., Liebermann R.C., Veblen D.R. Structure and twinning of single-crystal $MgSiO_3$ garnet synthesized at 17 GPa and 1800 °C. *Amer. Miner*. **1989**. Vol. 74. P. 509–512.

Angel R.J., Ross N.L., Seifert F., Fliervoet T.E. Structural characterization of pentacoordinate silicon in a calcium silicate. *Nature*. **1996**. Vol. 384. P. 441–444.

Angel R.J., Mosenfelder J.L., Shaw C.S.J. Anomalous compression and equation of state of coesite. *Phys. Earth Planet. Inter*. **2001a**. Vol. 124. P. 71–79.

Angel R.J., Frost D.J., Ross N.L., Hemley R. Stabilities and equations of state of dense hydrous magnesium silicates. *Phys. Earth Planet. Inter*. **2001b**. Vol. 127. P. 181–196.

Angel R.J., Shaw C.S.J., Gibbs G.V. Compression mechanisms of coesite. *Phys. Chem. Miner*. **2003**. Vol. 30. P. 167–176.

Anzolini C., Angel R.J., Merlini M., Derzsi M., Tokár K., Milani S., Krebs M.Y., Brenke F.E., Nestola F., Harris J.W. Depth of formation of $CaSiO_3$-walstromite included in super-deep diamonds. *Lithos*. **2006**. Vol. 265. P. 138–147.

Araki T., Zoltai T. Refinement of a coesite structure. *Z. Kristallogr*. **1969**. Bd. 129. S. 381–387.

Arlt T., Armbruster T., Ulmer P., Peters T. $MnSi_2O_5$ with the titanite structure: A new high-pressure phase in the $MnO–SiO_2$ binary. *Amer. Miner*. **1998**. Vol. 83. P. 657–660.

Ballaran T.B., Frost D.J., Miyajima N., Heidelblbach F. The structure of a super-aluminous version of the dense hydrous-magnesium silicate phase D. *Amer. Miner*. **2010**. Vol. 95. P. 1113–1116.

Bauer J.D., Labs S., Weiss S., Bayarjargal L., Morgenroth W., Milman V., Perlov A., Curtius H., Bosbach D., Zänker H., Winkler B. High-pressure phase transition of coffinite, $USiO_4$. *J. Phys. Chem. C*. **2014**. Vol. 118. P. 25141–25149.

Beck P., Gillet P., Gautron L., Daniel I., El Goresy A. A new natural high-pressure (Na,Ca)-hexaluminosilicate $[(Ca_xNa_{1-x})Al_x^{3+}Si_{3-x}O_{11}]$ in shocked Martian meteorites. *Earth Planet. Sci. Lett*. **2004**. Vol. 219. P. 1–12.

Belokoneva E.L., Simonov M.A., Batushin A.V., Mill B.V., Belov N.V. The crystal structure of Ca-gallogermanate $Ca_3Ga_2Ge_4O_{14}$ = $Ca_3Ge((Ga_2Ge)Ge_2O_{14})$ and its analog $Ba_3Fe_2Ge_4O_{14}$ = = $Ba_3Fe((FeGe_2)Ge_2O_{14})$. *Dokl. Acad. Sci. SSSR*. **1980**. Vol. 255. P. 1099–1104.

Bindi L., Bobrov A., Litvin Y.A. Incorporation of Fe^{3+} in phase-X, $A_{2-x}M_2Si_2O_7H_x$, a potential high- pressure K- rich hydrous silicate in the mantle. *Miner. Mag*. **2007**. Vol. 71. P. 265–272.

Bindi L., Dymshits A.M., Bobrov A.V., Litasov K.D., Shatskiy A.F., Ohtani E., Litvin Y.A. Crystal chemistry of sodium in the Earth's interior: The structure of $Na_2MgSi_5O_{12}$ synthesized at 17.5 GPa and 1700 °C. *Amer. Miner*. **2011**. Vol. 96. P. 447–450.

Bindi L., Nishi M., Tsuchiya J., Irifune T. Crystal chemistry of dense hydrous magnesium silicates: the structure of phase H, $MgSiH_2O_4$, synthesized at 45 GPa and 1000 °C. *Amer. Miner.* **2014**. Vol. 99. P. 1802–1805.

Bindi L., Sirotkina E.A., Bobrov A.V., Irifune T. Structural and chemical characterization of $Mg[(Cr,Mg)(Si,Mg)]O_4$, a new post-spinel phase with sixfold-coordinated silicon. *Amer. Miner*. **2015a**. Vol. 100. P. 1633–1636.

Bindi L., Nishi M., Irifune T. Partition of Al between Phase D and Phase H at high pressure: Results from a simultaneous structure refinement of the two phases coexisting in a unique grain. *Amer. Miner*. **2015b**. Vol. 100. P. 1637–1640.

Bindi L., Sirotkina E.A., Bobrov A.V., Pushcharovsky D., Irifune T. Discovery of $MgTiSi_2O_7$: a new high-pressure silicate with the weberite structure synthesized at transition-zone conditions. *Phys. Chem. Miner*. **2017a**. Vol. 44. P. 419–424.

Bindi L., Chen M., Xie X. Discovery of the Fe-analogue of akimotoite in the shocked Suizhou L6 chondrite. *Sci. Rep*. **2017b**. Vol. 7. P. 42674.

Bindi L., Brenker F.E., Nestola F., Koch T.E., Prior D.J., Lilly K., Krot A.N., Bizzarro M., Xie X. Discovery of asimowite, the Fe-analog of wadsleyite, in shock-melted silicate droplets of the Suizhou L6 and the Quebrada Chimborazo 001 CB3.0 chondrites. *Amer. Miner*. **2019**. Vol. 104. P. 775–778.

Bindi L., Bendeliani A., Bobrov A., Matrosova E., Irifune T. Incorporation of Mg in phase Egg, $AlSiO_3OH$: Toward a new polymorph of phase H, $MgSiH_2O_4$, a carrier of water in the deep mantle. *Amer. Miner*. **2020a**. Vol. 105. P. 132–135.

Bindi L., Shim S-H., Sharp T.G., Xie X. Evidence for the charge disproportionation of iron in extraterrestrial bridgmanite. *Sci. Adv*. **2020b**. Vol. 6. P. eaay7893.

Bindi L., Welch M.D., Bendeliani A.A., Bobrov A.V. Si-rich Mg-sursassite $Mg_4Al_5Si_7O_{23}(OH)_5$ with octahedrally coordinated Si: A new ultrahigh-pressure hydrous phase. *Amer. Miner.* **2020c**. Vol. 105. P. 1432–1435.

Binns R.A., Davis R.J., Reed S.J.B. Ringwoodite, natural $(Mg,Fe)_2SiO_4$ spinel in the Tenham meteorite. *Nature*. **1969**. Vol. 221. P. 943–944.

Bläß U.W., Langenhorst F., Boffa-Ballaran T., Seifert F., Frost D.J., McCammon C.A. A new oxygen-deficient perovskite phase $Ca(Fe_{0.4}Si_{0.6})O_{2.8}$ and phase relations along the join $CaSiO_3$–$CaFeO_{2.5}$ at transition zone conditions. *Phys. Chem. Miner.* **2004**. Vol. 31. P. 52–65.

Bläß U.W., Langenhorst F., Frost D.J., Seifert F. Oxygen deficient perovskites in the system $CaSiO_3$–$CaAlO_{2.5}$ and implications for the Earth's interior. *Phys. Chem. Miner.* **2007**. Vol. 34. P. 363–376.

Brenker F.E., Vincze L., Vekemans B., Nasdala L., Stachel T., Vollmer C., Kersten M., Somogyi A., Adams F., Joswig W., Harris J.W. Detection of a Ca-rich lithology in the earth's deep (>300 km) convecting mantle. *Earth Planet. Sci. Lett.* **2005**. Vol. 236. P. 579–587.

Brenker F.E., Nestola F., Brenker L., Peruzzo L., Harris J.W. Origin, properties, and structure of breyite: The second most abundant mineral inclusion in super-deep diamonds. *Amer. Miner.* **2021**. Vol. 106. P. 38–43.

Bykova E.A., Bobrov A.V., Sirotkina E.A., Bindi L., Ovsyannikov S.V., Dubrovinsky L.S., Litvin Y.A. X-ray single-crystal and Raman study of knorringite, $Mg_3(Cr_{1.58}Mg_{0.21}Si_{0.21})Si_3O_{12}$, synthesized at 16 GPa and 1600 °C. *Phys. Chem. Miner.* **2014**. Vol. 41. P. 267–272.

Bykova E., Bykov M., Černok A., Tidholm J., Simak S.I., Hellman O., Belov M.P., Abrikosov I.A., Liermann H.-P., Hanfland M., Prakapenka V.B., Prescher C., Dubrovinskaia N., Dubrovinsky L. Metastable silica high pressure polymorphs as structural proxies of deep Earth silicate melts. *Nature Comm.* **2018**. Vol. 9. P. 4789.

Cai N., Inoue T., Fujino K., Ohfuji H., Yurimoto H. A possible new Al-bearing hydrous Mg silicate (23 Å phase) in the deep upper mantle. *Amer. Miner.* **2015**. Vol. 100. P. 2330–2335.

Caracas R., Wentzcovitch R. Theoretical determination of the structures of $CaSiO_3$ perovskites. *Acta Crystallogr.* **2006**. Vol. B62. P. 1025–1030.

Caracas R., Wentzcovitch R., Price G.D., Brodholt J. $CaSiO_3$ perovskite at lower mantle pressures. *Geophys. Res. Lett.* **2005**. Vol. 32. P. L06306.

Carl E.-R., Mansfeld U., Liermann H.-P., Danilewsky A., Langenhorst F., Ehm L., Trullenque G., Kenkmann T. High-pressure phase transitions of α-quartz under nonhydrostatic dynamic conditions: A reconnaissance study at PETRA III. *Meteor. Planet. Sci.* **2017**. Vol. 52. P. 1465–1474.

Černok A., Bykova E., Boffa-Ballaran T., Liermann H.-P., Hanfland M., Dubrovinsky L. High-pressure crystal chemistry of coesite-I and its transition to coesite-II. *Z. Kristallogr.* **2014a**. Vol. 229. P. 761–773.

Černok A., Ballaran T.B., Caracas R., Miyajima N., Bykova E., Prakapenka V., Liermann H.-P., Dubrovinsky L.S. Pressure-induced phase transitions in coesite. *Amer. Miner.* **2014b**. Vol. 99. P. 755–763.

Černok A., Marquardt K., Caracas R., Bykova E., Habler G., Liermann H.-P., Hanfland M., Mezouar M., Bobocioiu E., Dubrovinsky L. Compressional pathways of α-cristobalite, structure of cristobalite X-I, and towards the understanding of seifertite formation. *Nature Comm.* **2017**. Vol. 8. P. 15647.

Chao E.C.T., Shoemaker E.M., Madsen B.M. First natural occurrence of coesite. *Science*. **1960**. Vol. 132. P. 220–223.

Chao E.C.T., Fahey J.J., Littler J., Milton E.J. Stishovite, a very high pressure new mineral from Meteor Crater, AZ. *J. Geophys. Res.* **1962**. Vol. 67. P. 419–421.

Chen H., Shim S.-H., Leinenweber K., Prakapenka V., Meng Y., Prescher C. Crystal structure of $CaSiO_3$ perovskite at 28–62 GPa and 300 K under quasi-hydrostatic stress conditions. *Amer. Miner.* **2018**. Vol. 103. P. 462–468.

Chopin C. Coesite and pure pyrope in high-grade blueschists of the Western Alps: A first record and some consequences. *Contrib. Miner. Petrol.* **1984**. Vol. 86. P. 107–118.

Choudhury N., Chaplot S.L. Ab initio studies of phonon softening and high-pressure phase transitions of α-quartz SiO_2. *Phys. Rev. B.* **2006**. Vol. 73. P. 094304.

Churakov S., Wunder B. Ab-initio calculations of the proton location in topaz-OH, $Al_2SiO_4(OH)_2$. *Phys. Chem. Miner.* **2004**. Vol. 31. P. 131–141.

Coes L. A new dense crystalline silica. *Science.* **1953**. Vol. 118. P. 131–132.

Coes L., Jr. Synthesis of minerals at high pressures. In: Wentorf R. (Ed.): *Modern Very High Pressure Techniques.* London: Butterworths, **1962**. P. 137–150.

Cohen R.E. Bonding and elasticity of stishovite SiO_2 at high pressure: linearized augmented plane wave calculations. *Amer. Miner.* **1991**. Vol. 76. P. 733–742.

Cohen R.E., Lin Y. Prediction of a potential high-pressure structure of $FeSiO_3$. *Phys. Rev. B.* **2014**. Vol. 90. P. 140102.

Comboni D., Lotti P., Gatta G.D., Lacalamita M., Mesto E., Merlini M., Hanfland M. Armstrongite at non-ambient conditions: An in-situ high-pressure single-crystal X-ray diffraction study. *Micropor. Mesopor. Mater.* **2019**. Vol. 274. P. 171–175.

Comodi P., Fumagalli P., Nazzareni S., Zanazzi P.F. The 10-Å phase: crystal structure from X-ray single-crystal data. *Amer. Miner.* **2005**. Vol. 90. P. 1012–1016.

Daniels P., Wunder B. $Al_3Si_2O_7(OH)_3$, phase Pi (formerly piezotite): Crystal structure of a synthetic high-pressure silicate rediscovered. *Eur. J. Miner.* **1996**. Vol. 8. P. 1283–1292.

Das P.K., Mohn C.E., Brodholt J.P., Trønnes R.G. High-pressure silica phase transitions: Implications for deep mantle dynamics and silica crystallization in the protocore. *Amer. Miner.* **2020**. Vol. 105. P. 1014–1020.

Dera P., Prewitt C.T., Boctor N.Z., Hemley R.J. Characterization of a high-pressure phase of silica from the Martian meteorite Shergotty. *Amer. Miner.* **2002**. Vol. 87. P. 1018–1023.

Dera P., Lazarz J.D., Prakapenka V.B., Barkley M., Downs R.T. New insights into the high-pressure polymorphism of SiO_2 cristobalite. *Phys. Chem. Miner.* **2011**. Vol. 38. P. 517–529.

Dera P., Finkelstein G.J., Duffy T.S., Downs R.T., Meng Y., Prakapenka V., Tkachev S. Metastable high-pressure transformations of orthoferrosilite Fs_{82}. *Phys. Earth Planet. Inter.* **2013**. Vol. 221. P. 15–21.

Dewangan P., Bisen D.P., Brahme N., Sharma S. Structural characterization and luminescence properties of Dy^{3+} doped $Ca_3MgSi_2O_8$ phosphors. *J. Alloys Compds.* **2019**. Vol. 777. P. 423–433.

Dobson D.P., Jacobsen S.D. The flux growth of magnesium silicate perovskite single crystals. *Amer. Miner.* **2004**. Vol. 89. P. 807–811.

Dove M., Craig M., Keen D., Marshall W., Redfern S., Trachenko K., Tucker M. Crystal structure of the high-pressure monoclinic phase-II of cristobalite, SiO_2. *Miner. Mag.* **2000**. Vol. 64. P. 569-576.

Downs R.T., Hazen R.M., Finger L.W., Gasparik T. Crystal chemistry of lead aluminosilicate hollandite: A new high-pressure synthetic phase with octahedral Si. *Amer. Miner.* **1995**. Vol. 80. P. 937–940.

Dubrovinsky L.S., Belonoshko A.B. Pressure-induced phase transition and structural changes under deviatoric stress of stishovite to $CaCl_2$-like structure. *Geochim. Cosmochim. Acta.* **1996**. Vol. 60. P. 3657–3663.

Dubrovinsky L.S., Saxena S.K., Lazor P., Ahuja R., Eriksson O., Wills J.M., Johansson B. Experimental and theoretical identification of a new high-pressure phase of silica. *Nature.* **1997**. Vol. 388. P. 362–365.

Dubrovinsky L.S., Dubrovinskaia N.A., Saxena S.K., Tutti F., Rekhi S., Le Bihan T., Shen G., Hu J. Pressure-induced transformations of cristobalite. *Chem. Phys. Lett.* **2001**. Vol. 333. P. 264–270.

Eggleton R.A., Boland J.N., Ringwood A.E. High pressure synthesis of a new aluminium silicate: $Al_5Si_5O_{17}(OH)$. *Geochem. J.* **1978**. Vol. 12. P. 191–194.

El Goresy A., Dubrovinsky L., Sharp T.G., Saxena S.K., Chen M. A monoclinic post-stishovite polymorph of silica in the Shergotty meteorite. *Science.* **2000a**. Vol. 288. P. 1632–1634.

El Goresy A., Chen M., Gillet P., Dubrovinsky L. S. Shock-induced high-pressure phase-transition of labradorite to hollandite "(Na_{47}–Ca_{51}–K_2)" in Zagami and the assemblage hollandite "(Na_{80}–Ca_{12}–K_8)" + jadeite in L chondrites: constraints to peak-shock pressures. *Meteor. Planet. Sci.* **2000b**. Vol. 35. Suppl. P. A51.

El Goresy A., Dubrovinsky L., Sharp T.G., Chen M. Stishovite and post-stishovite polymorphs of silica in the shergotty meteorite: their nature, petrographic settings versus theoretical predictions and relevance to Earth's mantle. *J. Phys. Chem. Solids.* **2004**. Vol. 65. P. 1597–1608.

El Goresy A., Dera P., Sharp T.G., Prewitt C.T., Chen M., Dubrovinsky L., Wopenka B., Boctor N.Z., Hemley R.J. Seifertite, a dense orthorhombic polymorph of silica from the Martian meteorites Shergotty and Zagami. *Eur. J. Miner.* **2008**. Vol. 20. P. 523–528.

El Goresy A., Gillet P., Miyahara M., Ohtani E., Ozawa S., Beck P., Montagnac G. Shock-induced deformation of Shergottites: Shock-pressures and perturbations of magmatic ages on Mars. *Geochim. Cosmochim. Acta.* **2013**. Vol. 101. P. 233–262.

Ende M., Gatta G.D., Lotti P., Grandtner A., Miletich R. $Cs(Be_2Li)Al_2Si_6O_{18}$, a cesium-stuffed host-guest structure, and its structure-property variations with temperature and pressure. *J. Solid State Chem.* **2021**. Vol. 293. Paper 121841.

Ferroir T., Onozawa T., Yagi T., Merkel S., Miyajima N., Nishiyama N., Irifune T., Kikegawa T. Equation of state and phase transition in $KAlSi_3O_8$ hollandite at high pressure. *Amer. Miner.* **2006**. Vol. 91. P. 327–332.

Ferroir T., Beck P., Van de Moortèle B., Bohn M., Reynard B., Simionovici A., El Goresy A., Gillet P. Akimotoite in the Tenham meteorite: Crystal chemistry and high-pressure transformation mechanisms. *Earth Planet. Sci. Lett.* **2008**. Vol. 275. P. 26–31.

Finger L.W., Hazen R.M. Crystal chemistry of six-coordinated silicon: a key to understanding the Earth's deep interior. *Acta Crystallogr.* **1991**. Vol. B47. P. 561–580.

Finger L.W., Hazen R.M. Systematics of high-pressure silicate structures. *Rev. Miner. Geochem.* **2000**. Vol. 41. P. 123–155.

Finger L.W., Ko J., Hazen R.M., Gasparik T., Hemley R.J., Prewitt C.T., Weidner D.J. Crystal chemistry of phase B and an anhydrous analogue: implications for water storage in the upper mantle. *Nature.* **1989**. Vol. 341. P. 140–142.

Finger L.W., Hazen R.M., Prewitt C.T. Crystal structures of $Mg_{12}Si_4O_{19}(OH)_2$ (phase B) and $Mg_{14}Si_5O_{24}$ (phase AnhB). *Amer. Miner.* **1991**. Vol. 76. P. 1–7.

Finger L.W., Hazen R.M., Fursenko B.A. Refinement of the crystal structure of $BaSi_4O_9$ in the benitoite form. *J. Phys. Chem. Solids.* **1995**. Vol. 56. P. 1389–1393.

Finkelstein G.J., Dera P.K., Jahn S., Oganov A.R., Holl C.M., Meng Y., Duffy T.S. Phase transitions and equation of state of forsterite to 90 GPa from single-crystal X-ray diffraction and molecular modeling. *Amer. Miner.* **2014**. Vol. 99. P. 35–43.

Finkelstein G.J., Dera P.K., Duffy T.S. Phase transitions in orthopyroxene (En_{90}) to 49GPa from single-crystal X-ray diffraction. *Phys. Earth Planet. Inter.* **2015a**. Vol. 244. P. 78–86.

Finkelstein G.J., Dera P.K., Duffy T.S. High-pressure phases of cordierite from single-crystal X-ray diffraction to 15 GPa. *Amer. Miner.* **2015b**. Vol. 100. P. 1821–1833.

Fitz Gerald J.D., Ringwood A.E. High pressure rhombohedral perovskite phase $Ca_2AlSiO_{5.5}$. *Phys. Chem. Miner.* **1991**. Vol. 18. P. 40–46.

Fleet M.E. Sodium tetrasilicate: A complex high-pressure framework silicate ($Na_6Si_3[Si_9O_{27}]$). *Amer. Miner.* **1996**. Vol. 81. P. 1105–1110.

Fleet M.E. Sodium heptasilicate: a high-pressure silicate with six-membered rings of tetrahedra interconnected by SiO_6 octahedra: ($Na_8Si[Si_6O_{18}]$). *Amer. Miner.* **1998**. Vol. 83. P. 618–624.

Fleet M.E., Henderson G.S. Sodium trisilicate: A new high-pressure silicate structure ($Na_2Si[Si_2O_7]$). *Phys. Chem. Miner.* **1995**. Vol. 22. P. 383–386.

Fritz J., Greshake A., Klementova M., Wirth R., Palatinus L., Trønnes R.G., Assis Fernandes V., Böttger U., Ferrière L. Donwilhelmsite, $[CaAl_4Si_2O_{11}]$, a new lunar high-pressure Ca-Al-silicate with relevance for subducted terrestrial sediments. *Amer. Miner.* **2020**. Vol. 105. P. 1704–1711.

Frost D.J. The stability of dense hydrous magnesium silicates in Earth's transition zone and lower mantle. In: Fei Y., Bertka C.M., Mysen B.O. (Eds.). *Mantle petrology: Field observations and high pressure experimentation: A tribute to Francis R. (Joe) Boyd*. The Geochemical Society Special Publication No. 6, Houston, TX, **1999**. P. 283– 296.

Frost D.J. The upper mantle and transition zone. *Elements*. **2008**. Vol. 4. P. 171–176.

Fujino K., Momoi H., Sawamoto H., Kumazawa M. Crystal structure and chemistry of $MnSiO_3$ tetragonal garnet. *Amer. Miner.* **1986**. Vol. 71. P. 781–785.

Fukuyama K., Ohtani E., Shibazaki Y., Kagi H., Suzuki A. Stability field of phase Egg, $AlSiO_3OH$ at high pressure and high temperature: possible water reservoir in mantle transition zone. *J. Miner. Petrol. Sci*. **2017**. Vol. 112. P. 31–35.

Fumagalli P., Sixtrude L., Poli S., Snyder D. The 10Å phase: a high-pressure expandable sheet silicate stable during subduction of hydrated lithosphere. *Earth Planet. Sci. Lett*. **2001**. Vol. 186. P. 125–141.

Fumagalli P., Poli S., Fischer J., Merlini M., Gemmi M. The high-pressure stability of chlorite and other hydrates in subduction mélanges: experiments in the system Cr_2O_3–MgO–Al_2O_3–SiO_2–H_2O. *Contrib. Miner. Petrol*. **2014**. Vol. 167. P. 979.

Gasparik T. Phase relations in the transition zone. *J. Geophys. Res*. **1990**. Vol. 95. P. 15751–15769.

Gasparik T., Litvin Y.A. Stability of $Na_2Si_2O_7$ and melting relations on the forsterite-jadeite join at pressure up to 22 GPa. *Eur. J. Miner*. **1997**. Vol. 9. P. 311–326.

Gasparik T., Parise J.B., Eiben B.A., Hreljac J.A. Stability and structure of a new high-pressure silicate, $Na_{1.8}Ca_{1.1}Si_6O_{14}$. *Amer. Miner*. **1995**. Vol. 80. P. 1269–1276.

Gasparik T., Tripathi A., Parise J.B. Structure of a new Al-rich phase, $[K,Na]_{0.9}[Mg,Fe]_2[Mg,Fe,Al,Si]_6O_{12}$, synthesized at 24 GPa. *Amer. Miner*. **2000**. Vol. 85. P. 613–618.

Gatta G.D., Nestola F., Ballaran T.B. Elastic behavior, phase transition, and pressure induced structural evolution of analcime. *Amer. Miner.* **2006**. Vol. 91. P. 568–578.

Gatta G.D., Lotti P., Tabacchi G. The effect of pressure on open-framework silicates: elastic behaviour and crystal–fluid interaction. *Phys. Chem. Miner*. **2018**. Vol. 45. P. 115–138.

Gautron L., Angel R.J., Miletich R. Structural characterisation of the high-pressure phase $CaAl_4Si_2O_{11}$. *Phys. Chem. Miner*. **1999**. Vol. 27. P. 47–51.

Gemmi M., Fischer J.K., Merlini M., Poli S., Fumagalli P., Mugnaioli E., Kolbe U. A new hydrous Al-bearing pyroxene as a water carrier in subduction zones. *Earth Planet. Sci. Lett*. **2011**. Vol. 310. P. 422–428.

Gemmi M., Merlini M., Palatinus L., Fumagalli P., Hanfland M. Electron diffraction determination of 11.5 Å and HySo structures: candidate water carriers to the upper mantle. *Amer. Miner*. **2016**. Vol. 101. P. 2645–2654.

German V.N., Podurets R.F., Trunin R.F. Synthesis of a high density phase of silicon dioxide in shock waves. *JETP*. **1973**. Vol. 37. P. 107.

Gibbs G.V., Pltewitt C.T., Baldwin K.J. A study of the structural chemistry of coesite. *Z. Kristallogr*. **1977**. Bd. 145. S. 108–123.

Gillet P., Chen M., Dubrovinsky L., El Goresy A. Natural $NaAlSi_3O_8$-hollandite in the shocked Sixiangkou meteorite. *Science*. **2000**. Vol. 287. P. 1633–1636.

Glass B.P., Liu S. Discovery of high-pressure $ZrSiO_4$ polymorph in naturally occurring shock-metamorphosed zircons. *Geology*. **2001**. Vol. 29. P. 371–373.

Glass B.P., Liu S., Leavens P.B. Reidite: An impact-produced high-pressure polymorph of zircon found in marine sediments. *Amer. Miner*. **2002**. Vol. 87. P. 562–565.

Gorelova L.A., Pakhomova A.S., Aprilis G., Dubrovinsky L.S., Krivovichev S.V. Pentacoordinated silicon in the high-pressure modification of datolite, $CaBSiO_4(OH)$. *Inorg. Chem. Front*. **2018**. Vol. 5. P. 1653–1660.

Gorelova L.A., Pakhomova A.S., Krivovichev S.V., Dubrovinsky L.S., Kasatkin A.V. High pressure phase transitions of paracelsian $BaAl_2Si_2O_8$. *Sci. Rep*. **2019**. Vol. 9. Paper 12652.

Gorelova L.A., Pakhomova A.S., Krzhizhanovskaya M.G., Winkler B., Krivovichev S.V., Dubrovinsky L.S. Pressure-induced phase transitions in danburite-type borosilicates. *J. Phys. Chem. C*. **2020a**. Vol. 124. P. 26048–26061.

Gorelova L.A., Pakhomova A.S., Krivovichev S.V., Kasatkin A.V., Dubrovinsky L.S. Compressibility of hingganite-(Y): high-pressure single crystal X-ray diffraction study. *Phys. Chem. Miner*. **2020b**. Vol. 47. Paper 22.

Gorelova L.A., Pakhomova A.S., Krzhizhanovskaya M.G., Pankin D.V., Krivovichev S.V., Dubrovinsky L.S., Kasatkin A.V. Crystal structure evolution of slawsonite $SrAl_2Si_2O_8$ and paracelsian $BaAl_2Si_2O_8$ upon compression and decompression. *J. Phys. Chem. C*. **2021a**. Vol. 125. P. 13014–13023.

Gorelova L.A., Pakhomova A.S., Aprilis G., Krivovichev S.V., Dubrovinsky L.S. Edge-sharing BO_4 tetrahedra in the high-pressure modification of the feldspar-related borosilicate reedmergnerite $NaBSi_3O_8$. *J. Phys. Chem. C*. **2021b**. Submitted.

Gottschalk M., Fockenberg T., Grevel K.D., Wunder B., Wirth R., Schreyer W., Maresch W.V. Crystal structure of the high-pressure phase $Mg_4(MgAl)Al_4[Si_6O_{21}/(OH)_7]$: an analogue of sursassite. *Eur. J. Miner*. **2000**. Vol. 12. P. 935–945.

Greenberg E., Dubrovinsky L.S., McCammon C., Rouquette J., Kantor I., Prakapenka V., Rozenberg G.K., Pasternak M.P. Pressure-induced structural phase transition of the iron end-member of ringwoodite (γ-Fe_2SiO_4) investigated by X-ray diffraction and Mössbauer spectroscopy. *Amer. Miner*. **2011**. Vol. 96. P. 833–840.

Grey I.E., Madsen I.C., O'Neill H.S.C., Kesson S.E., Hibberson W.O. Rietveld refinement of high-pressure $CaAl_4Si_2O_{11}$ with the R-type ferrite structure. *N. Jb. Miner. Mh*. **1999**. Bd. 1999. S. 104–112.

Grey I.E., Madsen I.C., Hibberson W.O., O'Neill H.St.C. $CaAl_{12}Si_4O_{27}$, a new high-pressure phase containing Al_6O_{19} clusters. *J. Solid State Chem*. **2000**. Vol. 153. P. 391–397.

Haines J., Leǵer J.M., Gorelli F., Hanfland M. Crystalline post-quartz phase in silica at high-pressure. *Phys. Rev. Lett*. **2001**. Vol. 87. P. 155503.

Harris J., Hutchison M.T., Hursthouse M., Light M., Harte B. A new tetragonal silicate mineral occurring as inclusions in lower-mantle diamonds. *Nature*. **1997**. Vol. 387. P. 486–488.

Hazen R.M., Downs R.T., Conrad P.G., Finger L.W., Gasparik T. Comparative compressibilities of majorite-type garnets. *Phys. Chem. Miner*. **1994a**. Vol. 21. P. 344–349.

Hazen R.M., Downs R.T., Finger L.W., Conrad P.G., Gasparik T. Crystal chemistry of Ca-bearing majorite. *Amer. Miner*. **1994b**. Vol. 79. P. 581–584.

Hazen R.M., Downs R.T., Finger L.W. High-pressure framework silicates. *Science*. **1996**. Vol. 272. P. 1769–1771.

Hazen R.M., Yang H., Prewitt C.T., Gasparik T. Crystal chemistry of superfluorous phase B ($Mg_{10}Si_3O_{14}F_4$): implications for the role of fluorine in the mantle. *Amer. Miner*. **1997**. Vol. 82. P. 647–650.

Hazen R.M., Yang H., Finger L.W., Fursenko B.A. Crystal chemistry of high-pressure $BaSi_4O_9$ in the trigonal (*P*3) barium tetragermanate structure. *Amer. Miner*. **1999**. Vol. 84. P. 987–989.

Hazen R.M., Weinberger M.B., Yang H., Prewitt C.T. Comparative high-pressure crystal chemistry of wadsleyite, β-$(Mg_{1-x}Fe_x)_2SiO_4$, with $x = 0$ and 0.25. *Amer. Miner*. **2000a**. Vol. 85. P. 770–777.

Hazen R.M., Yang H., Prewitt C.T. High-pressure crystal chemistry of Fe^{3+}-wadsleyite, β-$Fe_{2.33}Si_{0.67}O4$. *Amer. Miner*. **2000b**. Vol. 85. P. 778–783.

Heinemann S., Sharp T.G., Seifert F., Rubie D.C. The cubic-tetragonal phase transition in the system majorite ($Mg_4Si_4O_{12}$)–pyrope ($Mg_3Al_2Si_3O_{12}$) and garnet symmetry in the earth's transition zone. *Phys. Chem. Miner*. **1997**. Vol. 24. P. 206–221.

Hemley R.J., Prewitt C.T., Kingma K.J. High pressure behaviour of silica. *Rev. Miner*. **1996**. Vol. 29. P. 41–81.

Hill R.J., Newton M.D., Gibbs G.V. A crystal chemical study of stishovite. *J. Solid State Chem*. **1983**. Vol. 47. P. 185–200.

Hirose K. Deep Earth mineralogy revealed by ultrahigh-pressure experiments. *Miner. Mag*. **2014**. Vol. 78. P. 437–446.

Hirose K., Takafuji N., Sata N., Ohishi Y. Phase transition and density of subducted MORB crust in the lower mantle. *Earth Planet. Sci. Lett*. **2005**. Vol. 237. P. 239–251.

Hirose K., Brodholt J., Lay T., Yuen D.A., eds. Post-Perovskite: The Last Mantle Phase Transition, Post-Perovskite: The Last Mantle Phase Transition. Geophysical Monograph 174. Washington D.C., American Geophysical Union, **2013**. 287 p.

Hirose K., Sinmyo R., Hernlund J. Perovskite in Earth's deep interior. *Science*. **2017**. Vol. 358. P. 734–738.

Hofmeister A., Giesting P., Wopenka B., Gwanmesia G., Jolliff B. Vibrational spectroscopy of pyrope-majorite garnets: structural implications. *Amer. Miner*. **2004**. Vol. 89. P. 132–146.

Holl C., Smyth J., Manghnani M., Amulele G., Sekar M., Frost D., Prakapenka V., Shen G. Crystal structure and compression of an iron-bearing phase A to 33 GPa. *Phys. Chem. Miner*. **2006**. Vol. 33. P. 192–199.

Holl C.M., Smyth J.R., Jacobsen S.D., Frost D.J. Effects of hydration on the structure and compressibility of wadsleyite, β-(Mg_2SiO_4). *Amer. Miner.* **2008**. Vol. 93. P. 598–607.

Horioka K., Takahashi K.I., Morimoto N., Horiuchi H., Akaogi M., Akimoto S.I. Structure of nickel aluminosilicate (phase IV): a high pressure phase related to spinel. *Acta Crystallogr.* **1981a**. Vol. B37. P. 635–638.

Horioka K., Nishiguchi M., Morimoto N., Horiuchi H., Wkaogi M., Akimoto S.I. Structure of nickel aluminosilicate (phase V): a high-pressure phase related to spinel. *Acta Crystallogr.* **1981b**. Vol. B37. P. 638–640.

Horiuchi H., Morimoto N., Yamamoto K., Akimoto S.I. Crystal structure of $Mg_2SiO_4 \cdot 3Mg(OH)_2$, a new high-pressure structure type. *Amer. Miner.* **1979**. Vol. 64. P. 593–598.

Horiuchi H., Horioka K., Morimoto N. Spinelloid: A systematics of spinel-related structures obtained under high-pressure conditions. *J. Miner. Soc. Japan*. **1980**. Vol. 14. P. 253–264.

Horiuchi H., Hirano M., Ito E., Matsui Y. $MgSiO_3$ (ilmenite-type): single crystal X-ray diffraction study. *Amer. Miner.* **1982**. Vol. 67. P. 788–793.

Horiuchi H., Ito E., Weidner D.J. Perovskite-type $MgSiO_3$: single-crystal x-ray diffraction study. *Amer. Miner.* **1987**. Vol. 72. P. 357–360.

Hu Q.Y., Shu J.-F., Cadien A., Meng Y., Yang W.G., Sheng H.W., Mao H.-K. Polymorphic phase transition mechanism of compressed coesite. *Nature Comm*. **2015a**. Vol. 6. P. 6630.

Hu Y., Dera P., Zhuravlev K. Single-crystal diffraction and Raman spectroscopy of hedenbergite up to 33 GPa. *Phys. Chem. Miner.* **2015b**. Vol. 42. P. 595–608.

Hu Q.Y., Shu J.-F., Yang W.G., Park C., Chen M.W., Fujita T., Mao H.-K., Sheng H.W. Stability limits and transformation pathways of αα-quartz under high pressure. *Phys. Rev. B.* **2017a**. Vol. 95. P. 104 112.

Hu Y., Kiefer B., Bina C.R., Zhang D., Dera P.K. High-pressure γ-$CaMgSi_2O_6$: does penta-coordinated silicon exist in the Earth's mantle? *Geophys. Res. Lett.* **2017b**. Vol. 44. P. 11340–11348.

Hummer D.R., Fei Y. Synthesis and crystal chemistry of Fe^{3+}-bearing $(Mg,Fe^{3+})(Si,Fe^{3+})O_3$ perovskite. *Amer. Miner.* **2012**. Vol. 97. P. 1915–1921.

Hyde B.G., White T.J., O'Keeffe M., Johnson A.W.S. Structures related to those of spinel and the β-phase, and a possible mechanism for the transformation olivine ↔ spinel. *Z. Kristallogr.* **1982**. Vol. 160. P. 53–62.

Irifune T., Ringwood A.E. Phase transformations in subducted oceanic crust and buoyancy relationships at depths of 600–800 km in the mantle. *Earth Planet. Sci. Lett.* **1993**. Vol. 117. P. 101–110.

Irifune T., Ringwood A.E., Hibberson W.O. Subduction of continental crust and terrigenous and pelagic sediments: an experimental study. *Earth Planet. Sci. Lett.* **1994**. Vol. 126. P. 351–368.

Ismailova L., Bobrov A., Bykov M., Bykova E., Cerantola V., Kantor I., Kupenko I., McCammon C., Dyadkin V., Chernyshov D., Pascarelli S., Chumakov A., Dubrovinskaia N., Dubrovinsky L. High-pressure synthesis of skiagite-majorite garnet and investigation of its crystal structure. *Amer. Miner.* **2015**. Vol. 100. P. 2650–2654.

Ito E., Matsui Y. Synthesis and crystal-chemical characterization of $MgSiO_3$ perovskite. *Earth Planet. Sci. Lett.* **1978**. Vol. 38. P. 443–450.

Joswig W., Stachel T., Harris J.W., Baur W.H., Brey G.P. New Ca-silicate inclusions in diamonds — tracers from the lower mantle. *Earth Planet. Sci. Lett.* **1999**. Vol. 173. P. 1–6.

Joswig W., Paulus E.F., Winkler B., Milman V. The crystal structure of $CaSiO_3$-walstromite, a special isomorph of wollastonite-II. *Z. Kristallogr.* **2003**. Vol. 218. P. 811–818.

Jung D.Y., Oganov A.R. Ab initio study of the high-pressure behavior of CaSiO3 perovskite. *Phys. Chem. Miner.* **2005**. Vol. 32. P. 146–153.

Kabanova N.A., Panikorovskii T.L., Shilovskikh V.V., Vlasenko N.S., Yakovenchuk V.N., Aksenov S.M., Bocharov V.N., Krivovichev S.V. The $Na_{2-n}H_n[Zr(Si_2O_7)] \cdot mH_2O$ minerals and related compounds (n = 0–0.5; m = 0.1): Structure refinement, framework topology, and possible Na+-ion migration paths. *Crystals*. **2020**. Vol. 10. Paper 1016.

Kagi H., Parise J.B., Cho H., Rossman G.R., Loveday J.S. Hydrogen bonding interactions in phase A $[Mg_7Si_2O_8(OH)_6]$ at ambient and high pressure. *Phys. Chem. Miner.* **2000**. Vol. 27. P. 225–233.

Kaminsky F. Mineralogy of the lower mantle: A review of "super-deep" mineral inclusions in diamond. *Earth-Sci. Rev.* **2012**. Vol. 110. P. 127–147.

Kaminsky F.V. The Earth's Low Mantle. Composition and Structure. Cham, Switzerland: Springer, **2017**.

Kaminsky F.V. Basic problems concerning the composition of the Earth's lower mantle. *Lithos*. **2020**. Vol. 364–365. Paper 105515.

Kanzaki M. Crystal structure of a new high-pressure polymorph of topaz-OH. *Amer. Miner.* **2010**. Vol. 95. P. 1349–1352.

Kanzaki M. Crystal structure of $Ca(Fe_{0.4}Si_{0.6})O_{2.8}$ oxygen-deficient perovskite. *J. Ceram. Soc. Japan*. **2020**. Vol. 128. P. 843–846.

Kanzaki M., Stebbins J.F., Xue X. Characterization of quenched high pressure phases in $CaSiO_3$ system by XRD and ^{29}Si NMR. *Geophys. Res. Lett.* **1991**. Vol. 18. P. 463–466.

Kanzaki M., Xue X., Wu Y., Nie S. Crystal structures of two oxygen-deficient perovskite phases in the $CaSiO_3$–$CaAlO_{2.5}$ join. *Phys. Chem. Miner.* **2017**. Vol. 44. P. 717–733.

Kawai N., Tachimori M., Ito E. A high-pressure hexagonal form of $MgSiO_3$. *Proc. Japan Acad.* **1974**. Vol. 50. P. 378–380.

Khisina N.R., Wirth R. Nanoinclusions of high-pressure hydrous silicate, $Mg_3Si_4O_{10}(OH)_2{\cdot}nH_2O$ (10Å-phase), in mantle olivine: Mechanisms of formation and transformation. *Geochem. Intern.* **2008**. Vol. 46. P. 319–327.

Kim D., Lim D., Ryu H., Lee J., Ahn S.I., Son B.S., Kim S.-J., Kim C.H., Park J.-C. Highly luminous and thermally stable Mg-substituted $Ca_{2-x}Mg_xSiO_4$: Ce ($0 \le x \le 1$) phosphor for NUV-LEDs. *Inorg. Chem.* **2017**. Vol. 56. P. 12116–12128.

Kim D., Tracy S.J., Smith R.F., Gleason A.E., Bolme C.A., Prakapenka V.B., Appel K., Speziale S., Wicks J.K., Berryman E.J., Han S.K., Schoelmerich M.O., Lee H.J., Nagler B., Cunningham E.F., Akin M.C., Asimow P.D., Eggert J.H., Duffy T.S. Femtosecond X-Ray Diffraction of Laser-Shocked Forsterite (Mg_2SiO_4) to 122 GPa. *J. Geophys. Res. Solid Earth*. **2021**. Vol. 126. Paper e2020JB020337.

Kingma K.J., Meade C., Hemley R.J., Mao H., Veblen D.R. Microstructural observations of α-quartz amorphization. *Science*. **1993a**. Vol. 259. P. 666–669.

Kingma K.J., Hemley R.J., Mao H., Veblen D.R. New high-pressure transformation in α-quartz. *Phys. Rev. Lett.* **1993b**. Vol. 70. P. 3927–3930.

Kingma K.J., Cohen R.E., Hemley R.J., Mao H.-K. Transformation of stishovite to a denser phase at lower-mantle pressures. *Nature*. **1995**. Vol. 374. P. 243–245.

Koch-Müller M., Dera P., Fei Y., Hellwig H., Liu Z., Orman J.V., Wirth R. Polymorphic phase transition in superhydrous phase B. *Phys. Chem. Miner.* **2005**. Vol. 32. P. 349–361.

Kojitani H., Kido M., Akaogi M. Rietveld analysis of a new high-pressure strontium silicate $SrSi_2O_5$. *Phys. Chem. Miner.* **2005**. Vol. 32. P. 290–294.

Kojitani H., Wakabayashi Y., Tejima Y., Kato C., Haraguchi M., Akaogi M. High-pressure phase relations in $Ca_2AlSiO_{5.5}$ and energetics of perovskite-related compounds with oxygen defects in the $Ca_2Si_2O_6$–$Ca_2Al_2O_5$ join. *Phys. Earth Planet. Inter.* **2009**. Vol. 173. P. 349–353.

Kojitani H., Iwabuchi T., Kobayashi M., Miura H., Akaogi M. Structure refinement of high-pressure hexagonal aluminous phases $K_{1.00}Mg_{2.00}Al_{4.80}Si_{1.15}O_{12}$ and $Na_{1.04}Mg_{1.88}Al_{4.64}Si_{1.32}O_{12}$. *Amer. Miner.* **2011**. Vol. 96. P. 1248–1253.

Komabayashi T., Hirose K., Sata N., Ohishi Y., Dubrovinsky L.S. Phase transition in $CaSiO_3$ perovskite. *Earth Planet. Sci. Lett.* **2007**. Vol. 260. P. 564–569.

Kono Y., Shu Y., Kenney-Benso C., Wang Y., Shen G. Structural Evolution of SiO_2 Glass with Si Coordination Number Greater than 6. *Phys. Rev. Lett.* **2020**. Vol. 125. P. 205701.

Krivovichev S.V. Topology of microporous structures. *Rev. Miner. Geochem.* **2005**. Vol. 57. P. 17–68.

Krivovichev S.V. Minerals with antiperovskite structure: a review. *Z. Kristallogr.* **2008**. Vol. 223. P. 109–113.

Krivovichev S.V. Structural complexity of minerals: information storage and processing in the mineral world. *Miner. Mag.* **2013**. Vol. 77. N 3. P. 275—326.

Krivovichev S.V. Local approach and the theory of lovozerite structures. *Proc. Steklov Inst. Math.* **2015**. Vol. 288. P. 105–116.

Krivovichev S. V. Structural complexity and configurational entropy of crystalline solids. *Acta Crystallogr.* **2016**. Vol. B72. P. 274–276.

Krivovichev S.V. Feldspar polymorphs: diversity, complexity, stability. *Zapiski RMO* (*Proc. Russian Miner. Soc*). **2020**. Vol. 149(4). P. 16–66.

Kroll H., Ribbe P. H. Determining (Al,Si) distribution and strain in alkali feldspars using lattice parameters and diffraction-peak positions: a review. *Am. Miner.* **1987**. Vol. 72. P. 491–506.

Kudoh Y. Structural relation of hydrous ringwoodite to hydrous wadsleyite. *Phys. Chem. Miner.* **2001**. Vol. 28. P. 523–530.

Kudoh Y., Kanzaki M. Crystal chemical characteristics of α-$CaSi_2O_5$, a new high pressure calcium silicate with five-coordinated silicon synthesized at 1500 °C and 10 GPa. *Phys. Chem. Miner.* **1998**. Vol. 25. P. 429–433.

Kudoh Y., Ito E., Takeda H. Effect of pressure on the crystal structure of perovskite-type $MgSiO_3$. *Phys. Chem. Miner.* **1987**. Vol. 14. P. 350–354.

Kudoh Y., Finger L., Hazen R.M., Prewitt C., Kanzaki M., Veblen D. Phase E: A high pressure hydrous silicate with unique crystal chemistry. *Phys. Chem. Miner.* **1993**. Vol. 19. P. 357–360.

Kudoh Y., Inoue T., Arashi H. Structure and crystal chemistry of hydrous wadsleyite, $Mg_{1.75}SiH_{0.504}$: possible hydrous magnesium silicate in the mantle transition zone. *Phys. Chem. Miner.* **1996**. Vol. 23. P. 461–469.

Kudoh Y., Nagase T., Mizohata H., Ohtani E., Sasaki S., Tanaka M. Structure and crystal chemistry of phase G, a new hydrous magnesium silicate synthesized at 22 GPa and 1050 °C. *Geophys. Res. Lett.* **1997**. Vol. 24. P. 1051–1054.

Kurashina T., Hirose K., Ono S., Sata N., Ohishi Y. Phase transition in Al-bearing $CaSiO_3$ perovskite: Implications for seismic discontinuities in the lower mantle. *Phys. Earth Planet. Inter.* **2004**. Vol. 145. P. 67–74.

Kuribayashi T., Kudoh Y., Kagi H. Compressibility of phase A, $Mg_7Si_2H_6O_{14}$ up to 11.2 GPa. *J. Miner. Petrol. Sci*. **2003**. Vol. 98. P. 215–234.

Kuwayama Y., Hirose K., Sata N., Ohishi Y. The pyrite-type high-pressure form of silica. *Science*. **2005**. Vol. 309. P. 923–925.

Kuwayama Y., Hirose K., Sata N., Ohishi Y. Pressure-induced structural evolution of pyrite-type SiO_2. *Phys. Chem. Miner*. **2011**. Vol. 38. P. 591–597.

Lam A.E., Groat L.A., Ercit T.S. The crystal structure of dugganite, $Pb_3Zn_3Te^{6+}As_2O_{14}$. *Canad. Miner*. **1998**. Vol. 36. P. 823–830.

Langenhorst F., Poirier J.P. Anatomy of black veins in Zagami: Clues to the formation of high-pressure phases. *Earth Planet. Sci. Lett*. **2000**. Vol. 184. P. 37–55.

Lazarz J.D., Dera P., Hu Y., Meng Y., Bina C.R., Jacobsen S.D. High-pressure phase transitions of clinoenstatite. *Amer. Miner*. **2019**. Vol. 104. P. 897–904.

Li B., Rigden S.M., Liebermann R.C. Elasticity of stishovite at high pressure. *Phys. Earth Planet. Inter*. **1996**. Vol. 96. P. 113–127.

Liebau F. Structural Chemistry of Silicates. Structure, Bonding and Classification. Berlin–Heidelberg–New York–Tokyo: Springer, **1985**.

Liu L.G. Silicate perovskite from phase transformations of pyrope-garnet at high pressure and temperature. *Geophys. Res. Lett*. **1974**. Vol. 1. P. 277–280.

Liu L.G. Post-oxide phases of olivine and pyroxene and mineralogy of the mantle. *Nature*. **1975**. Vol. 258. P. 510–512

Liu L.G. The high-pressure phases of $MgSiO_3$. *Earth Planet. Sci. Lett*. **1976**. Vol. 31. P. 200–208.

Liu L.-G. High pressure $NaAlSiO_4$: The first silicate calcium ferrite isotype. *Geophys. Res. Lett*. **1977**. Vol. 4. P. 183–186.

Liu L.G. High pressure Ca_2SiO_4, the silicate K_2NiF_4-isotype with crystal chemical and geophysical implications. *Phys. Chem. Miner*. **1978a**. Vol. 3. P. 291–299.

Liu L.G. A new high-pressure phase of $Ca_2Al_2SiO_7$ and implications for the Earth's interior. *Earth Planet. Sci. Lett*. **1978b**. Vol. 40. P. 401–406.

Liu L.-G. Effects of H_2O on the phase behaviour of the forsterite–enstatite system at high pressures and temperatures and implications for the Earth. *Phys. Earth Planet. Inter.* **1987**. Vol. 49. P. 142–167.

Liu L.G., El Goresy A. High-pressure phase transitions of the feldspars, and further characterization of lingunite. *Intern. Geol. Rev*. **2007**. Vol. 49. P. 854–860.

Liu L.G., Ringwood A.E. Synthesis of a perovskite-type polymorph of $CaSiO_3$. *Earth Planet. Sci. Lett*. **1975**. Vol. 28. P. 209–211.

Liu L.G., Bassett W.A., Sharry J. New high-pressure modifications of GeO_2 and SiO_2. *J. Geophys. Res*. **1978**. Vol. 83. P. 2301–2305.

Liu W., Wu X., Liang Y., Liu C., Miranda C.R., Scandolo S. Multiple pathways in pressure-induced phase transition of coesite. *Proc. Natl. Acad. Sci. USA*. **2017a**. Vol. 114. P. 12894–12899.

Liu Z., Du W., Shinmei T., Gréaux S., Zhou C., Arimoto T., Kunimoto T., Irifune T. Garnets in the majorite–pyrope system: symmetry, lattice microstrain, and order–disorder of cations. *Phys. Chem. Miner*. **2017b**. Vol. 44. P. 237–245.

Liu Z., Dubrovinsky L., McCammon C., Qysyannikov S.V., Koemets I., Chen L., Cui Q., Su N., Cheng J., Cui T., Liu B., Katsura T. A new $(Mg_{0.5}Fe^{3+}_{0.5})(Si_{0.5}Al^{3+}_{0.5})O_3$ $LiNbO_3$-type phase synthesized at lower mantle conditions. *Amer. Miner*. **2019**. Vol. 104. P. 1213–1216.

Liu C., Shi J., Gao H., Wang J., Han Y., Lu X., Wang H.-T., Xing D., Sun J. Mixed coordination silica at megabar pressure. *Phys. Rev. Lett*. **2021**. Vol. 126. P. 035701.

Lotti P., Gatta G.D., Merlini M., Liermann H.-P. High-pressure behavior of synthetic mordenite-Na: an in situ single-crystal synchrotron X-ray diffraction study. *Z. Kristallogr*. **2015**. Vol. 230. P. 201–211.

Lotti P., Comboni D., Merlini M., Hanfland M. High-pressure behavior of intermediate scapolite: compressibility, structure deformation and phase transition. *Phys. Chem. Miner*. **2018**. Vol. 45. P. 945–962.

Luo S.-N., Tschauner O., Asimow P.D., Ahrens T.J. A new dense silica polymorph: A possible link between tetrahedrally and octahedrally coordinated silica. *Amer. Miner.* **2004**. Vol. 89. P. 455–461.

Luth R.W. Experimental study of the system phlogopite-diopside from 3.5 to 17 GPa. *Amer. Miner.* **1997**. Vol. 82. P. 1198–1209.

Lyle M.J., Pickard C.J., Needs R.J. Prediction of 10-fold coordinated TiO_2 and SiO_2 structures at multimegabar pressures. *Proc. Natl. Acad. Sci. U.S.A*. **2015**. Vol. 112. P. 6898–6901.

Ma C., Tillmanns E. Nickel alumosilicate, phase II. *Acta Crystallogr*. **1975**. Vol. 31. P. 2139–2141.

Ma C., Sahl K., Tillmanns E. Nickel alumosilicate, phase I. *Acta Crystallogr*. **1975**. Vol. B31. P. 2137–2139.

Ma C., Tschauner O. Zagamiite, IMA 2015-022a. CNMNC Newsletter No. 36, April 2017, page 409. *Miner. Mag*. **2017**. Vol. 81. P. 403–409.

Ma C., Tschauner O., Beckett J.R., Liu Y., Rossman G.R., Zhuravlev K., Prakapenka V., Dera P., Taylor L.A. Tissintite, (Ca,Na,¨)$AlSi_2O_6$, a highly-defective, shock-induced, high-pressure clinopyroxene in the Tissint martian meteorite. *Earth Planet. Sci. Lett*. **2015**. Vol. 422. P. 194–205.

Ma C., Tschauner O., Beckett J.R., Liu Y., Rossman G.R., Sinogeikin S.V., Smith J.S., Taylor L.A. Ahrensite, γ-Fe_2SiO_4, a new shock-metamorphic mineral from the Tissint meteorite: Implications for the Tissint shock event on Mars. *Geochim. Cosmochim. Acta*. **2016**. Vol. 184. P. 240–256.

Ma C., Tschauner O., Beckett J.R., Rossman G.R., Prescher C., Prakapenka V.B., Bechtel H.A., MacDowell A. Liebermannite, $KAlSi_3O_8$, a new shock-metamorphic, high-pressure mineral from the Zagami Martian meteorite. *Meteor. Planet. Sci*. **2018**. Vol. 53. P. 50–61.

Ma C., Tschauner O., Bindi L., Beckett J.R., Xie X. A vacancy-rich, partially inverted spinelloid silicate, $(Mg,Fe,Si)_2(Si,\square)O_4$, as a major matrix phase in shock melt veins of the Tenham and Suizhou L6 chondrites. *Meteorit. Planet. Sci*. **2019a**. Vol. 54. P. 1907–1918.

Ma C., Tschauner O., Beckett J.R. A closer look at Martian meteorites: discovery of the new mineral zagamiite, $CaAl_2Si_{3.5}O_{11}$, a shock-metamorphic, high-pressure, calcium aluminosilicate. *Proc. Ninth International Conference on Mars*, 22–25 July **2019b**. Pasadena, California. LPI Contribution No. 2089.

Machida K.-I., Adachi G.-Y., Shiokawa J., Shimada M., Koizumi M. Structure and high-pressure polymorphism of strontium metasilicate. *Acta Crystallogr*. **1982a**. Vol. B38. P. 386–389.

Machida K., Adachi G., Shiokawa J., Shimada M., Koizumi M., Suito K., Onodera A. High-pressure synthesis, crystal structures, and luminescence properties of europium(II) metasilicate and europium(II)-activated calcium and strontium metasilicates. *Inorg. Chem*. **1982b**. Vol. 21. P. 1512–1519.

Madon M., Poirier J.P. Transmission electron microscope observation of α, β and γ $(Mg,Fe)_2SiO_4$in shocked meteorites: planar defects and polymorphic transitions. *Phys. Earth Planet. Inter.* **1983**. Vol. 33. P. 31–44.

Mancini F., Harlow G., Chaill C. Crystal structure of potassium dimagnesium disilicate hydroxide, $K_{1.3}(Mg_{0.95}Al_{0.03}Cr_{0.02})_2Si_2O_{6.4}(OH)_{0.6}$. *Z. Kristallogr. NCS*. **2001**. Vol. 216. P. 189– 190.

Mancini F., Harlow G., Chaill C. The crystal structure and cation ordering of Phase-X- $(K_{1-x-n})_2(Mg_{1-n}[Al,Cr]_n)_2Si_2O_7H_{2x}$: a potential K- and H- bearing phase in the mantle. *Amer. Miner*. **2002**. Vol. 87. P. 302–306.

Mao H.K., Chen L.C., Hemley R.J., Jephcoat A.P., Wu Y., Bassett W.A. Stability and equation of state of $CaSiO_3$-perovskite to 134 GPa. *J. Geophys. Res*. **1989**. Vol. 94. P. 17889–17894.

Marsh R.E., Herbstein F.H. Some additional changes in space groups of published crystal structures. *Acta Crystallogr*. **1983**. Vol. B39. P. 280–287.

Matsuzaki T., Hagiya K., Shatskiy A., Katsura T., Matsui M. Crystal structure of anhydrous phase X, $K_{1.93}(Mg_{2.02}Cr_{0.02})Si_{2.00}O_7$. *J. Miner. Petrol. Sci*. **2010**. Vol. 105. P. 303–308.

McNeil L.E., Grimsditch M. Pressure-amorphized SiO_2 α-quartz: An anisotropic amorphous solid. *Phys. Rev. Lett*. **1992**. Vol. 68. P. 83–85.

Milani S., Comboni D., Lotti P., Fumagalli P., Ziberna L., Maurice J., Hanfland M., Merlini M. Crystal structure evolution of $CaSiO_3$ polymorphs at Earth's mantle pressures. *Minerals*. **2021**. Vol. 11. P. 652.

Mills S.J., Kampf A.R., Kolitsch U., Housley R.M., Raudsepp M. The crystal chemistry and crystal structure of kuksite, $Pb_3Zn_3Te^{6+}P_2O_{14}$, and a note on the crystal structure of yafsoanite, $(Ca,Pb)_3Zn(TeO_6)_2$. *Amer. Miner*. **2010**. Vol. 95. P. 933–938.

Miyahara M., Kaneko S., Ohtani E., Sakai T., Nagase T., Kayama M., Nishido H., Hirao N. Discovery of seifertite in a shocked lunar meteorite. *Nat. Comm*. **2013**. Vol. 4. P. 1737.

Mookherjee M., Tsuchiya J., Hariharan A. Crystal structure, equation of state, and elasticity of hydrous aluminosilicate phase, topaz-OH $(Al_2SiO_4(OH)_2)$ at high pressures. *Phys. Earth Planet. Inter.* **2016**. Vol. 251. P. 24–35.

Moore P.B., Araki T. Atomic arrangement of merwinite, $Ca_3Mg[SiO_4]_2$, an unusual dense-packed structure of geophysical interest. *Amer. Miner*. **1972**. Vol. 57. P. 1355–1374.

Moore P.B., Smith J.V. Crystal structure of β-Mg_2SiO_4: crystal-chemical and geophysical implications. *Phys. Earth Planet. Inter*. **1970**. Vol. 3. P. 166–177.

Mori H. Hollandite type $NaAlSi_3O_8$ in shocked meteorites. *31st High Pressure Conf Japan Soc. High Press. Sci. Technol.*, Osaka, Japan, **1990**. P. 134–135.

Mori H. Shock-induced phase transformations of the Earth and planetary materials. *J. Miner. Soc. Japan*. **1994**. Vol. 23. P. 171–178.

Moriyama J., Kawabe I., Fujino K., Ohtani E. Experimental study of ele- ment partitioning between majorite, olivine, merwinite, diopside and silicate melts at 16 GPa and 2000 °C. *Geochem. J*. **1992**. Vol. 26. P. 357–382.

Murakami M., Hirose K., Kawamura K., Sata N., Ohish Y. Post-perovskite phase transition in $MgSiO_3$. *Science*. **2004**. Vol. 304. P. 855–858.

Nakatsuka A., Yoshiasa A., Yamanaka T., Ohtaka O., Katsura T., Ito E. Symmetry change of majorite solid-solution in the system $Mg_3Al_2Si_3O_{12}$–$MgSiO_3$. *Amer. Miner*. **1999**a. Vol. 84. P. 1135–1143.

Nakatsuka A., Yoshiasa A., Yamanaka T., Ito E. Structure of a birefringent Cr-bearing majorite $Mg_3(Mg_{0.34}Si_{0.34}Al_{0.18}Cr_{0.14})_2(SiO_4)_3$. *Amer. Miner*. **1999**b. Vol. 84. P. 199–202.

Náray-Szabó S., Taylor W.H., Jackson W.W. VIII. The structure of cyanite. *Z. Kristallogr*. **1929**. Bd. 71. S. 117–130.

Németh P., Leinenweber K., Ohfuji H., Groy T., Domanik K.J., Kovács I.J., Kovács J.S., Buseck P.R. Water-bearing, high-pressure Ca-silicates. *Earth Planet. Sci. Lett*. **2017**. Vol. 469. P. 148–155.

Nestola F., Burnham A.D., Peruzzo L., Tauro L., Alvaro M., Walter M.J., Gunter M., Anzolini C., Kohn S.C. Tetragonal Almandine-Pyrope Phase, TAPP: Finally a name for it, the new mineral jeffbenite. *Miner. Mag.* **2016**. Vol. 80. P. 1219–1232.

Nestola F., Korolev N., Kopylova M., Rotiroti N., Pearson D.G., Pamato M.G., Alvaro M., Peruzzo L., Gurney J.J., Moore A.E., Davidson J. $CaSiO_3$ perovskite in diamond indicates the recycling of oceanic crust into the lower mantle. *Nature*. **2018**. Vol. 555. P. 237–241.

Nishi M., Irifune T., Tsuchiya J., Tange Y., Nishihara Y., Fujino K., Higo Y. Stability of hydrous silicate at high pressures and water transport to the deep lower mantle. *Nat. Geosci*. **2014**. Vol. 7. P. 224–227.

O'Bannon III E., Beavers C.M., Kunz M., Williams Q. High-pressure study of dravite tourmaline: Insights into the accommodating nature of the tourmaline structure. *Amer. Miner.* **2018**. Vol. 103. P. 1622–1633.

Oganov A.R., Brodholt J.P. High-pressure phases in the Al_2SiO_5 system and the problem of aluminous phase in the Earth's lower mantle: ab initio calculations. *Phys. Chem. Miner.* **2000**. Vol. 27. P. 430–439.

Oganov A.R., Ono S. Theoretical and experimental evidence for a post-perovskite phase of $MgSiO_3$ in Earth's D" layer. *Nature*. **2004**. Vol. 430. P. 445–448.

Ohtani E., Mizobata H., Yurimoto H. Stability of dense hydrous magnesium silicate phases in the systems Mg_2SiO_4–H_2O and $MgSiO_3$–H_2O at pressures up to 27 GPa. *Phys. Chem. Miner*. **2000**. Vol. 27. P. 533–544.

Ohtani E., Toma M., Litasov K., Kubo T., Suzuki A. Stability of dense hydrous magnesium silicate phases and water storage capacity in the transition zone and lower mantle. *Phys. Earth Planet. Inter.* **2001**. Vol. 124. P. 105–117.

Ohtani E., Litasov K., Hosoya T., Kubo T., Kondo T. Water transport into the deep mantle and formation of a hydrous transition zone. *Phys. Earth Planet. Inter*. **2004**. Vol. 143–144. P. 255–269.

O'Keeffe M., Hyde B.G., Bovin J.-O. Contribution to the crystal chemistry of orthorhombic perovskites: $MgSiO_3$ and $NaMgF_3$. *Phys. Chem. Miner*. **1979**. Vol. 4. P. 299–305.

Ono S., Hirose K., Murakami M., Isshiki M. Post-stishovite phase boundary in SiO2 determined by in situ X-ray observations. *Earth Planet. Sci. Lett*. **2002**. Vol. 197. P. 187–192.

Ono S., Iizuka T., Kikegawa T. Compressibility of the calcium aluminosilicate, CAS, phase to 44 GPa. *Phys. Earth Planet. Inter*. **2005**. Vol. 150. P. 331–338.

Pacalo R.E.G., Parise J.B. Crystal structure of superhydrous B, a hydrous magnesium silicate synthesized at 1400 °C and 20 GPa. *Amer. Miner*. **1992**. Vol. 77. P. 681–684.

Pakhomova A., Bykova E., Bykov M., Glazyrin K., Gasharova B., Liermann H.-P., Mezouar M., Gorelova L., Krivovichev S., Dubrovinsky L. A closer look into close packing: pentacoordinated silicon in a high-pressure polymorph of danburite. *IUCrJ*. **2017a**. Vol. 4. P. 671–677.

Pakhomova A., Ismailova L., Bykova E., Bykov M., Ballaran T.B., Dubrovinsky L. A new high-pressure phase transition in clinoferrosilite: In situ single-crystal X-ray diffraction study. *Amer. Miner.* **2017b**. Vol. 102. P. 666–673.

Pakhomova A., Simonova D., Koemets I., Koemets E., Aprilis G., Bykov M., Gorelova L., Fedotenko T., Prakapenka V., Dubrovinsky L. Polymorphism of feldspars above 10 GPa. *Nat. Comm*. **2020**. Vol. 11. P. 2721.

Panero W.R, Benedetti L.R., Raymond J. Equation of state of stishovite and interpretation of SiO_2 shock-compression data. *J. Geophys. Res*. **2003**. Vol. 108(B1). P. 1–5.

Parise J.B., Wang Y., Gwanmesia G.D., Zhang J., Sinelnikov Y., Chmielowski J., Weidner D.J., Liebermann R.C. The symmetry of garnets on the pyrope ($Mg_3Al_2Si_3O_{12}$)–majorite ($MgSiO_3$) join. *Geophys. Res. Lett*. **1996**. Vol. 23. P. 3799–3802

Park K.T., Terakura K., Matsui Y. Theoretical evidence for a new ultra-high-pressure phase of SiO_2. *Nature*. **1988**. Vol. 336. P. 670–672.

Pautov L.A., Agakhanov A.A., Sokolova E., Hawthorne F.C. Maleevite, $BaB_2Si_2O_8$, and pekovite, $SrB_2Si_2O_8$, new mineral species from the Dara-I-Pioz Alkaline Massif, northern Tajikistan: description and crystal structure. *Canad. Miner*. **2004**. Vol. 42. P. 107–119.

Pearson D.G., Brenker F.E., Nestola F., McNeill J., Nasdala L., Hutchison M.T., Matveev S., Mather K., Silversmit G., Schmitz S., Vekemans B., Vincze L. Hydrous mantle transition zone indicated by ringwoodite included within diamond. *Nature*. **2014**. Vol. 507. P. 221–224.

Pekov I.V., Krivovichev S.V., Zolotarev A.A., Yakovenchuk V.N., Armbruster T., Pakhomovsky Y.A. Crystal chemistry and nomenclature of the lovozerite group. *Eur. J. Miner*. **2009**. Vol. 21. P. 1061–1071.

Phillips M. W., Gibbs G. V., Ribbe P.H. The crystal structure of danburite: A comparison with anorthite, albite, reedmergnerite. *Amer. Miner*. **1974**. Vol. 59. P. 79–85.

Plonka A.M., Dera P., Irmen P., Rivers M.L., Ehm L., Parise J.B. β-diopside, a new ultrahigh-pressure polymorph of $CaMgSi_2O_6$ with six-coordinated silicon. *Geophys. Res. Lett*. **2012**. Vol. 39. P. L24307.

Posner E.S., Konzett J., Frost D.J., Downs R.T., Yang H. High-pressure synthetic $(Na_{0.97}Mg_{0.03})(Mg_{0.43}Fe^{3+}_{0.17}Si_{0.40})Si_2O_6$, with six-coordinated silicon, isostructural with *P*2/*n* omphacite. *Acta Crystallogr. E.* **2012**. Vol. 68. P. i18.

Prakapenka V.P., Shen G., Dubrovinsky L.S., Rivers M.L., Sutton S.R. High pressure induced phase transformation of SiO_2 and GeO_2: difference and similarity. *J. Phys. Chem. Solids*. **2004**. Vol. 65. P. 1537–1545.

Preisinger A. Struktur des Stishovits, Höchstdruck-SiO_2. *Naturwiss*. **1962**. Bd. 49. S. 345.

Prescher C., Prakapenka V.B., Stefanski J., Jahn S., Skinner L.B., Wang Y. Beyond sixfold coordinated Si in SiO_2 glass at ultrahigh pressures. *Proc. Natl. Acad. Sci. U.S.A*. **2017**. Vol. 114. P. 10041–10046.

Prewitt C.T., Downs R.T. High-pressure crystal chemistry. *Rev. Miner*. **1998**. Vol. 37. P. 284–318.

Price G.D., Putnis A., Agrell S.O., Smith D.G.W. Wadsleyite, natural ß-$(Mg,Fe)_2SiO_4$ from the Peace River meteorite. *Canad. Miner*. **1983**. Vol. 21. P. 29–35.

Prokopenko V.B., Dubrovinsky L.S., Dmitriev V., Weber H.-P. In situ characterization of phase transitions in cristobalite under high pressure by Raman spectroscopy and X-ray diffraction. *J. Alloys Compds*. **2001**. Vol. 327. P. 87–95.

Pushcharovsky D.Yu. Structural mineralogy of silicates and their synthetic analogues. Moscow: Nedra, **1986** (*in Russian*).

Pushcharovsky D.Yu. Minerals of the deep geospheres. *Phys.-Usp*. **2012**. Vol. 45. P. 439–444.

Pushcharovsky D.Yu. Mineralogical Crystallography. Moscow: GEOKART; GEOS, **2020**. 342 p.

Pushcharovsky D.Yu., Pushcharovsky Yu.M. The mineralogy and the origin of deep geospheres: A review. *Earth-Sci. Rev*. **2012**. Vol. 113. P. 94–109.

Pushcharovsky D.Yu., Pushcharovsky Yu.M. New Insight into the Composition and the Structure of the Deep Layers of the Terrestrial Planets. *Moscow Univ. Geol. Bull*. **2016**. Vol. 71. № 1. P. 1–7.

Reid A.F., Ringwood A.E. Newly observed high pressure transformations in Mn_3O_4, $CaAl_2O_4$, and $ZrSiO_4$. *Earth Planet. Sci. Lett*. **1969**. Vol. 6. P. 205–208.

Reid A.F., Li C., Ringwood A.E. High-pressure silicate pyrochlores, $Sc_2Si_2O_7$ and $In_2Si_2O_7$. *J. Solid State Chem*. **1977**. Vol. 20. P. 219–226.

Ringwood A.E. Mineralogical constitution of the deep mantle. *J. Geophys. Res*. **1962**. Vol. 67. P. 4005–4010.

Ringwood A.F., Major A. Synthesis of Mg_2SiO_4–Fe_2SiO_4 spinel solid solutions. *Earth Planet. Sci. Lett*. **1966**. Vol. 1. P. 241–245.

Ringwood A.E., Major A. Some high-pressure transformations of geophysical interest. *Earth Planet. Sci. Lett*. **1967a**. Vol. 2. P. 106–110.

Ringwood A.E., Major, A. High pressure reconnaissance investigations in the system Mg_2SiO_4–MgO–H_2O. *Earth Planet. Sci. Lett*. **1967b**. Vol. 2. P. 130–133.

Ringwood A.E., Reid A.F., Wadsley A.D. High-pressure $KAlSi_3O_8$, an aluminosilicate with sixfold coordination. *Acta Crystallogr*. **1967**. Vol. 23. P. 1093–1095.

Ross N.L., Hazen R.M. Single crystal X-ray diffraction study of $MgSiO_3$ perovskite from 77 to 400 K. *Phys. Chem. Miner*. **1989**. Vol. 16. P. 415–420.

Ross N.L., Hazen R.M. High-pressure crystal chemistry of $MgSiO_3$ perovskite. *Phys Chem Miner*. **1990**. Vol. 17. P. 228–237.

Ross N.L., Shu J.F., Hazen R.M., Gasparik T. High-pressure crystal chemistry of stishovite. *Amer. Miner*. **1990**. Vol. 75. P. 739–747.

Rucks M.J., Whitaker M.L., Glotch T.D., Parise J.B., Jaret S.J., Catalano T., Dyar M.D. Making tissintite: Mimicking meteorites in the multi-anvil. *Amer. Miner*. **2018**. Vol. 103. P. 1516–1519.

Sano-Furukawa A., Kuribayashi T., Komatsu K., Yagi T., Ohtani E. Investigation of hydrogen sites of wadsleyite: A neutron diffraction study. *Phys. Earth Planet. Inter*. **2011**. Vol. 189. P. 56–62.

Sasaki S., Prewitt C.T., Sato Y., Ito, E. Single-crystal X-ray study of γ-Mg_2SiO_4. *J. Geophys. Res*. **1982**. Vol. B87. P. 7829–7832.

Schmidt M., Finger L., Angel R., Dinnebier R. Synthesis, crystal structure, and phase relations of $AlSiO_3OH$, a high-pressure hydrous phase. *Amer. Miner*. **1998**. Vol. 83. P. 881–888.

Schulze K., Pamato M., Kurnosov A., Ballaran T., Glazyrin K., Pakhomova A., Marquardt H. High-pressure single-crystal structural analysis of $AlSiO_3OH$ phase egg. *Amer. Miner*. **2018**. Vol. 103. P. 1975–1980.

Sekine T., Akaishi M., Setaka N. Fe_2N-type SiO_2 from shocked quartz. *Geochim. Cosmochim. Acta*. **1987**. Vol. 51. P. 379–381.

Seryotkin Y.V. Evolution of the brewsterite structure at high pressure: A single-crystal X-ray diffraction study. *Micropor. Mesopor. Mater*. **2019**. Vol. 276. P. 167–172.

Seryotkin Yu.V., Bakakin V.V., Likhacheva A.Yu., Dementiev S.N., Rashchenko S.V. Structural behavior of Tl-exchanged natrolite at high pressure depending on the composition of pressure-transmitting medium. *Phys. Chem. Miner*. **2017**. Vol. 44. P. 615–626.

Shannon R.D., Sleight A.W. Synthesis of new high-pressure pyrochlore phases. *Inorg. Chem*. **1968**. Vol. 7. P. 1649–1651.

Sharp T.G., Lingemann C.M., Dupas C., Stöffler D. Natural occurrence of $MgSiO_3$-limenite and evidence for $MgSiO_3$-perovskite in a shocked L chondrite. *Science*. **1997**. Vol. 277. P. 352–355.

Sharp T.G., El Goresy A., Wopenka B., Chen M. A post-stishovite SiO_2 polymorph in the meteorite Shergotty: Implications for impact events. *Science*. **1999**. Vol. 284. P. 1511–1513.

Shelton H., Bi T., Zurek E., Smith J., Dera P. The ideal crystal structure of cristobalite X-I: a bridge in SiO_2 densification. *J. Phys. Chem. C.* **2018**. Vol. 122. P. 17437–17446.

Shieh S.R., Duffy T.S., Shen G. X-ray diffraction study of phase stability in SiO2 at deep mantle conditions. *Earth Planet. Sci. Lett.* **2005**. Vol. 235. P. 273–282.

Shim S.-H., Jeanloz R., Duffy T.S. Tetragonal structure of $CaSiO_3$ perovskite above 20 GPa. *Geophys. Res. Lett.* **2002**. Vol. 29. P. 2166.

Simakov G.V., Podurets M.A., Trunin R.F. New data on the compressibility of oxides and fluorides and the theory of homogeneous composition of the earth. *Dokl. Acad. Sci. USSR*. **1973**. Vol. 211. P. 1330–1332 (*in Russian*).

Sinclair W., Ringwood A.E. Single crystal analysis of the structure of stishovite. *Nature*. **1978**. Vol. 272. P. 714–715.

Sirotkina E.A., Bindi L., Bobrov A.V., Aksenov S.M., Irifune T. Synthesis and crystal structure of chromium-bearing anhydrous wadsleyite. *Phys. Chem. Miner.* **2018**. Vol. 45. P. 361–366.

Smith J.V. Further discussion of framework structures formed from parallel four-and eight-membered rings. *Miner. Mag.* **1968**. Vol. 33. P. 202–212.

Smith J.V. Feldspar Minerals. I. Crystal Structure and Physical Properties. Berlin: Springer-Verlag, **1974**. 627 p.

Smith J.V., Mason B. Pyroxene-garnet transformation in Coorara meteorite. *Science*. **1970**. Vol. 168. P. 832–833.

Smyth J.R., Hatton C.J. A coesite-sanidine grospydite from the Roberts Victor kimberlite. *Earth Planet. Sci. Lett.* **1977**. Vol. 77. P. 284–290.

Smyth J.R., Hazen R.M. The crystal structures of forsterite and hortonolite at several temperatures up to 900 °C. *Amer. Miner.* **1973**. Vol. 58. P. 588–593.

Smyth J.R., Kawamoto T. Wadsleyite II: a new high pressure hydrous phase in the peridotite-H_2O system. *Earth Planet. Sci. Lett.* **1997**. Vol. 146. P. 9–16.

Smyth J.R., Smith J.V., Artioli G., Kvick Å. Crystal structure of coesite, a high-pressure form of SiO_2, at 15 and 298 K from single-crystal neutron and x-ray diffraction data: Test of bonding models. *J. Phys. Chem*. **1987**. Vol. 91. P. 988–992.

Smyth J.R., Kawamoto T., Jacobsen S.D., Swope R.J., Hervig R.L., Holloway J.R. Crystal structure of monoclinic hydrous wadsleyite [β-$(Mg,Fe)_2SiO_4$]. *Amer. Miner.* **1997**. Vol. 82. P. 270–275.

Stishov S.M., Belov N.V. Crystal structure of a new dense modification of silica SiO_2. *Dokl. Acad. Sci. USSR*. **1962**. Vol. 143. P. 951–954.

Stishov S.M., Popova S.V. A new modification of silica. *Geochem*. **1961**. Vol. 10. P. 923–926 (*in Russian*).

Stixrude L., Cohen R.E., Rici Y., Krakauer H. Prediction of phase transition in $CaSiO_3$ perovskite and implications for lower mantle structure. *Amer. Miner.* **1996**. Vol. 81. P. 1293–1296.

Sugahara M., Yoshiasa A., Komatsu Y., Yamanaka T., Bolfan-Casanova N., Nakatsuka A., Sasaki S., Tanaka M. Reinvestigation of the $MgSiO_3$ perovskite structure at high pressure. *Amer. Miner.* **2006**. Vol. 91. P. 533–536.

Swamy V., Dubrovinsky L. Thermodynamic data for the phases in the $CaSiO_3$ system. *Geochim. Cosmochim. Acta*. **1997**. Vol. 61. P. 1181–1191.

Swanson D.K., Prewitt C.T. The crystal structure of $K_2Si^{VI}Si_3{}^{IV}O_9$. *Amer. Miner.* **1983**. Vol. 68. P. 581–585.

Teter D.M., Hemley R.J., Kresse G., Hafner J. High pressure polymorphism in silica. *Phys. Rev. Lett.* **1998**. Vol. 80. P. 2145–2148.

Thibaud J.-M., Rouquette J., Hermet P., Dziubek K., Gorelli F.A., Santoro M., Garbarino G., Alabarse F.G., Cambon O., Di Renzo F., van der Lee A., Haines J. High-pressure phase transition, pore collapse, and amorphization in the siliceous 1D zeolite, TON. *J. Phys. Chem. C.* **2017**. Vol. 121. P. 4283–4292.

Tomioka N., Miyahara M. High-pressure minerals in shocked meteorites. *Meteor. Planet. Sci*. **2017**. Vol. 52. P. 2017–2039.

Tomioka N., Okuchi T. A new high-pressure form of Mg_2SiO_4 highlighting diffusionless phase transitions of olivine. *Sci. Rep*. **2017**. Vol. 11. P. 17351.

Tomioka N., Fujino K. Natural $(Mg,Fe)SiO_3$-ilmenite and -perovskite in the Tenham meteorite. *Science*. **1997**. Vol. 277. P. 1084–1086.

Tomioka N., Fujino K. Akimotoite, $(Mg,Fe)SiO_3$, a new silicate mineral of the ilmenite group in the Tenham chondrite. *Amer. Miner.* **1999**. Vol. 84. P. 267–271.

Tomioka N., Miyahara M., Ito M. Discovery of natural $MgSiO_3$ tetragonal garnet in a shocked chondritic meteorite. *Sci. Adv*. **2016**. Vol. 2. P. e1501725.

Tomioka N., Bindi L., Okuchi T., Miyahara M., Iitaka T., Li Z., Kawatsu T., Xie X., Purevjav N., Tani R., Kodama Yu. Poirierite, a dense metastable polymorph of magnesium iron silicate in shocked meteorites. *Commun. Earth. Environ*. **2021**. Vol. 2. P. 16.

Tschauner O. High-pressure minerals. *Amer. Miner*. **2019**. Vol. 104. P. 1701–1731.

Tschauner O., Ma C., Beckett J.R., Prescher C., Prakapenka V.B., Rossman G.R. Discovery of bridgmanite, the most abundant mineral in Earth, in a shocked meteorite. *Science*. **2014**. Vol. 346. P. 1100–1102.

Tschauner O., Ma C., Prescher C., Prakapenka V.B. Structure analysis and conditions of formation of akimotoite in the Tenham chondrite. *Meteor. Planet. Sci.* **2018**. Vol. 53. P. 62–74.

Tschauner O., Ma C., Spray J.G., Greenberg E., Prakapenka V.B. Stöfflerite, $(Ca,Na)(Si,Al)_4O_8$ in the hollandite structure: A new high-pressure polymorph of anorthite from martian meteorite NWA 856. *Amer. Miner.* **2021**. Vol. 106. P. 650–655.

Tsuchida Y., Yagi T. A new, post-stishovite high-pressure polymorph of silica. *Nature*. **1989**. Vol. 340. P. 217–220.

Tsuchiya T., Tsuchiya J. Prediction of a hexagonal SiO_2 phase affecting stabilities of $MgSiO_3$ and $CaSiO_3$ at multimegabar pressures. *Proc. Natl. Acad. Sci. U.S.A.* **2011**. Vol. 108. P. 1252–1255.

Tsuneyuki S., Matsui Y., Aoki H., Tsukada M. New pressure-induced structural transformations in silica obtained by computer simulation. *Nature*. **1989**. Vol. 339. P. 209–211.

Uchida T., Wang Y., Nishiyama N., Funakoshi K.-i., Kaneko H., Nozawa A., von Dreele R.B., Rivers M.L., Sutton S.R., Yamada A., Kunimoto T., Irifune T., Inoue T., Li B. Non-cubic crystal symmetry of $CaSiO_3$ perovskite up to 18 GPa and 1600 K. *Earth Planet. Sci. Lett*. **2009**. Vol. 282. P. 268–274.

Urusov V.S., Oganov A.R., Eremin N.N. Computer simulation of the structure, properties and stability of the Al_2SiO_5 polymorphs: I. Ionic model. *Geochem. Int*. **1998**. Vol. 36. P. 397–414.

Van de Moortèle B., Reynard B., McMillan P.F., Wilson M., Beck P., Gillet P., Jahn S. Shock-induced transformation of olivine to a new metastable $(Mg,Fe)_2SiO_4$ polymorph in Martian meteorites. *Earth Planet. Sci. Lett*. **2007**. Vol. 261. P. 469–475.

Vanpeteghem C.B., Zhao J., Angel R.J., Ross N.L., Bolfan-Casanova N. Crystal structure and equation of state of $MgSiO_3$ perovskite. *Geophys. Res. Lett*. **2006**. Vol. 33. P. L03306.

Wainwright J.E., Starkey J. A refinement of the structure of anorthite. *Z. Kristallogr*. **1971**. Bd. 133. S. 75–84.

Walter M.J., Kohn S.C., Araujo D., Bulanova G.P., Smith C.B., Gaillou E., Wang J., Steele A., Shirey S.B. Deep mantle cycling of oceanic crust: Evidence from diamonds and their mineral inclusions. *Science*. **2011**. Vol. 334. P. 54–57.

Welch M.D., Wunder B. A single-crystal X-ray diffraction study of the 3.65 Å-phase $MgSi(OH)_6$, a high-pressure hydroxide perovskite. *Phys. Chem. Miner.* **2012**. Vol. 39. P. 693–697.

Welch M.D., Cámara F., Ventura G.D., Iezzi G. Non-ambient in situ studies of amphiboles. *Rev. Miner. Geochem*. **2007**. Vol. 67. P. 223–260.

Welch M.D., Konzett J., Bindi L., Kohn S.C., Frost D.J. New structural features of the high-pressure synthetic sheet-disilicate Phase-X, $K_{2-x}Mg_2Si_2O_7H_x$. *Amer. Miner*. **2012**. Vol. 97. P. 1849–1857.

Wicks J.K., Duffy T.S. Crystal structures of minerals in the lower mantle. In: *Deep Earth: Physics and Chemistry of the Lower Mantle and Core*. Geophysical Monograph 217. Terasaki H., Fischer R.A. (Eds.). Wiley: AGU, **2016**. P. 69–87.

Winter J.K., Ghose S. Thermal expansion and high temperature crystal chemistry of the Al_2SiO_5 polymorphs. *Amer. Miner*. **1979**. Vol. 64. P. 573–586.

Winter J.K., Okamura F.P., Ghose S. A high-temperature structural study of high albite, monalbite, and the analbite → monalbite phase transition. *Amer. Miner*. **1979**. Vol. 64. P. 409–423.

Woodland A.B., Girnis A.V., Bulatov V.K., Brey G.P., Höfer H.E. Breyite inclusions in diamond: Experimental evidence for possible dual origin. *Eur. J. Miner*. **2020**. Vol. 32. P. 171–185.

Wu S., Umemoto K., Ji M., Wang C.-Z., Ho K.-M., Wentzcovitch R.M. Identification of post-pyrite phase transitions in SiO_2 by a genetic algorithm. *Phys. Rev. B*. **2011**. Vol. 83. P. 184102.

Wu Y., Liu H., Huang H., Fei Y., Feng X., Redfern S.A.T. Pressure-induced structural modulations in coesite. *Phys. Rev*. **2018**. Vol. B98. P. 104016.

Wunder B., Rubie D., Ross C., Medenbach O., Seifert F., Schreyer W. Synthesis, stability, and properties of $Al_2SiO_4(OH)_2$ – a fully hydrated analog of topaz. *Amer. Miner*. **1993a**. Vol. 78. P. 285–297.

Wunder B., Medenbach O., Krause W., Schreyer W. Synthesis, properties and stability of $Al_3Si_2O_7(OH)_3$ (phase Pi), a hydrous high – pressure phase in the system Al_2O_3–SiO_2–H_2O (ASH). *Eur. J. Miner*. **1993b**. Vol. 5. P. 637–649.

Wunder B., Wirth R., Koch-Müller M. The 3.65 Å phase in the system MgO–SiO_2–H_2O: Synthesis, composition, and structure. *Amer. Miner*. **2011**. Vol. 96. P. 1207–1214.

Xiao W., Tan D., Zhou W., Liu J., Xu J. Cubic perovskite polymorph of strontium metasilicate at high pressures. *Amer. Miner*. **2013**. Vol. 98. P. 2096–2104.

Xu J., Ito E., Yamazaki D., Guo X., Wu X. Synthesis and crystal chemical characterization of the pyrochlore type $MgZrSi_2O_7$. *Mater. Chem. Phys*. **2011**. Vol. 128. P. 410–412.

Xu J., Fan D., Zhang D., Guo X., Zhou W., Dera P.K. Phase transition of enstatite-ferrosilite solid solutions at high pressure and high temperature: constraints on metastable orthopyroxene in cold subduction. *Geophys. Res. Lett*. **2020**. Vol. 47. P. e2020GL087363.

Xue X., Zhai S., Kanzaki M. Si–Al distribution in high-pressure $CaAl_4Si_2O_{11}$ phase: a ^{29}Si and ^{27}Al NMR study. *Amer. Miner*. **2009**. Vol. 94. P. 1739–1742.

Xue X., Kanzaki M., Fukui H. Unique crystal chemistry of two polymorphs of topaz-OH: A multinuclear NMR and Raman study. *Amer. Miner*. **2010**. Vol. 95. P. 1276–1293.

Yagi T., Mao H.K., Bell P.M. Structure and crystal chemistry of perovskite-type $MgSiO_3$. *Phys. Chem. Miner.* **1978**. Vol. 3. P. 97–110.

Yamada H., Matsui Y., Eiji I. Crystal–chemical characterization of $NaAlSiO_4$ with the $CaFe_2O_4$ structure. *Miner. Mag.* **1983**. Vol. 47. P. 177–181.

Yamada H., Matsui Y., Ito E. Crystal-chemical characterization of $KAlSi_3O_8$ with the hollandite structure. *Miner. J.* **1984**. Vol. 12. P. 29–34.

Yamakata M., Yagi T. New stishovite-like phase of silica formed by hydrostatic compression of cristobalite. *Proc. Japan Acad. Ser. B.* **1997**. Vol. 73. P. 85–88.

Yamamoto K., Akimoto S.I. The system $MgO–SiO_2–H_2O$ at high pressures and temperatures stability field hydroxyl-chondrodite, hydroxyl-clinohumite and 10 Å phase. *Amer. J. Sci.* **1977**. Vol. 277. P. 288–312.

Yamanaka T., Kyono A., Nakamoto Y., Kharlamova S., Struzhkin V.V., Gramsch S.A., Mao H.-K., Hemley R.J. New structure of high-pressure body-centered orthorhombic Fe_2SiO_4. *Amer. Miner.* **2015**. Vol. 100. P. 1736–1743.

Yang H., Konzett J. Crystal chemistry of a high-pressure *C*2/*c* clinopyroxene with six-coordinated silicon. *Amer. Miner.* **2005**. Vol. 90. P. 1223–1226.

Yang H., Prewitt C.T. Chain and layer silicates at high temperatures and pressures. *Rev. Miner. Geochem.* **2000**. Vol. 41. P. 211–255.

Yang H., Prewitt C.T., Frost D.J. Crystal structure of the dense hydrous magnesium silicate, phase D. *Amer. Miner.* **1997**. Vol. 82. P. 651–654.

Yang H., Konzett J., Prewitt C.T. Crystal structure of phase X, a high pressure alkali- rich hydrous silicate and its anhydrous equivalent. *Amer. Miner.* **2001**. Vol. 86. P. 1483–1488.

Yang H., Prewitt C.T., Liu Z. Crystal structures and infrared spectra of two Fe-bearing hydrous magnesium silicates synthesized at high temperature and pressure. *J. Miner. Petrol. Sci.* **2002**. Vol. 97. P. 137–143.

Yang H., Konzett J., Frost D.J., Downs R.T. X-ray diffraction and Raman spectroscopic study of clinopyroxenes with six coordinated Si in the $Na(Mg_{0.5}Si_{0.5})Si_2O_6–NaAlSi_2O_6$ system. *Amer. Miner.* **2009a**. Vol. 94. P. 942–949.

Yang H., Konzett J., Downs R.T., Frost D.J. Crystal structure and Raman spectrum of a high-pressure Li-rich majoritic garnet, $(Li_2Mg)Si_2(SiO_4)_3$. *Amer. Miner.* **2009b**. Vol. 94. P. 630–633.

Ye Y., Smyth J.R., Hushur A., Manghnani M.H., Lonappan D., Derara P., Frost D.J. Crystal structure of hydrous wadsleyite with 2.8% H_2O and compressibility to 60 GPa. *Amer. Miner.* **2010**. Vol. 95. P. 1765–1772.

Ye Y., Smyth J.R., Frost D.J. Structural study of the coherent dehydration of wadsleyite. *Amer. Miner.* **2011**. Vol. 96. P. 1760–1767.

Yong T., Bina C.R., Finkelstein G.J., Zhang D., Dera P. A new high-pressure phase transition in natural gedrite. *Crystals.* **2019a**. Vol. 9. P. 521.

Yong T., Dera P., Zhang D. Single-crystal X-ray diffraction of grunerite up to 25.6 GPa: a new high-pressure clinoamphibole polymorph. *Phys. Chem. Miner.* **2019b**. Vol. 46. P. 215–227.

Yusa H., Akaogi M., Sata N., Kojitani H., Kato Y., Ohishi Y. Unquenchable hexagonal perovskite in high-pressure polymorphs of strontium silicates. *Amer. Miner.* **2005**. Vol. 90. P. 1017–1020.

Yusa H., Sata N., Ohishi Y. Rhombohedral (9R) and hexagonal (6H) perovskites in barium silicates under high pressure. *Amer. Miner.* **2007**. Vol. 92. P. 648–654.

Zedgenizov D.A., Shatskiy A., Ragozin A.L., Kagi H., Shatsky V.S. Merwinite in diamond from São Luiz, Brazil: A new mineral of the Ca-rich mantle environment. *Amer. Miner.* **2014**. Vol. 99. P. 547–550.

Zedgenizov D., Kagi H., Ohtani E., Tsujimori T., Komatsu K. Retrograde phases of former bridgmanite inclusions in superdeep diamonds. *Lithos.* **2020**. Vol. 370–371. Paper 105659.

Zhai S., Shan S., Yamazak D., Funakoshi K.-I. Compressibility of pyrochlore-type $MgZrSi_2O_7$ determined by in situ X-ray diffraction in a large-volume high pressure apparatus. *High Press. Res.* **2013**. Vol. 33. P. 1–7.

Zhang J., Ko J., Hazen R.M., Prewitt C.T. High-pressure crystal chemistry of $KAlSi_3O_8$ hollandite. *Amer. Miner.* **1993**. Vol. 78. P. 493–499.

Zhang J., Li B., Utsumi W., Liebermann R.C. In situ X-ray observations of the coesite-stishovite transition: reversed phase boundary and kinetics. *Phys. Chem. Miner.* **1996**. Vol. 23. P. 1–10.

Zhang R.Y., Liou J.G., Shu J.F. Hydroxyl-rich topaz in high-pressure and ultrahigh-pressure kyanite quartzites, with retrograde woodhouseite, from the Sulu terrane, eastern China. *Amer. Miner.* **2002**. Vol. 87. P. 445–453.

Zhang J.S., Dera P., Bass J.D. A new high-pressure phase transition in natural Fe-bearing orthoenstatite. *Amer. Miner.* **2012**. Vol. 97. P. 1070–1074.

Zhang L., Meng Y., Yang W., Wang L., Mao W.L., Zeng Q.-S., Jeong J.S., Wagner A.J., Mkhoyan K.A., Liu W., Xu R., Mao H. Disproportionation of $(Mg,Fe)SiO_3$ perovskite in Earth's deep lower mantle. *Science.* **2014**. Vol. 344. P. 877–882.

Zhang L., Popov D., Meng Y., Wang J., Ji C., Li B., Mao H.-K. In-situ crystal structure determination of seifertite SiO_2 at 129 GPa: Studying a minor phase near Earth's core-mantle boundary. *Amer. Miner.* **2016**a. Vol. 101. P. 231–234.

Zhang L., Smyth J.R., Allaz J., Kawazoe T., Jacobsen S.D., Jin Z. Transition metals in the transition zone: Crystal chemistry of minor element substitution in wadsleyite. *Amer. Miner.* **2016b**. Vol. 101. P. 2322–2330.

Zhang A.-C., Jiang Q.-T., Tomioka N., Guo Y.-J., Chen J.-N., Li Y., Sakamoto N., Yurimoto H. Widespread tissintite in strongly shock-lithified lunar regolith breccias. *Geophys. Res. Lett.* **2021**. Vol. 48. P. e2020GL091554.

Zhou Y., Irifune T. Formation of hexagonal $NaAl_3Si_3O_{11}$ (NAS) phase, the Na end-member of hexagonal $CaAl_4Si_2O_{11}$ (CAS) phase, near 23 GPa above 2373 K in the compositions of $NaAl_3Si_3O_{11}$ and $NaAlSi_3O_8$. *Phys. Chem. Miner.* **2020**. 47. P. 37.

Zhou Y., Irifune T., Ohfuji H., Kuribayashi T. New high-pressure forms of Al_2SiO_5. *Geophys. Res. Lett.* **2018**. Vol. 45. P. 8167– 8172.

Zhou Y., Irifune T., Kuribayashi T. Phase relations of the Al_2O_3–SiO_2 system at 13–21 GPa and 2300–2800 K and a new high-pressure $Al_2Si_2O_7$ phase. *Phys. Chem. Miner.* **2021**. Vol. 48. P. 26.

Zoltai T., Buerger M.J. The crystal structure of coesite, the dense, high-pressure form of silica. *Z. Kristallogr.* **1959**. Bd. 111. S. 129–141.

СИЛИКАТЫ ВЫСОКИХ ДАВЛЕНИЙ: КРИСТАЛЛОХИМИЯ И СИСТЕМАТИКА

д. чл. С. В. Кривовичев[a, b, *]

[a] *Центр наноматериаловедения, Кольский научный центр РАН, ул. Ферсмана, 14, Апатиты, 184209 Россия*

[b] *Кафедра кристаллографии, Институт наук о Земле, Санкт-Петербургский государственный университет, Университетская наб., 7/9, Санкт-Петербург, 199034 Россия*

** e-mail: s.krivovichev@ksc.ru*

Поступила в редакцию 03.08.2021 г.
После доработки 09.08.2021 г.
Принята к публикации 15.08.2021 г.

Проведен обзор высокобарических силикатов с подробным анализом их структурной топологии и координации кремния. Высокобарические силикаты разделены на одиннадцать основных групп в согласии с их химическим составом: (i) полиморфы кремнезема; (ii) полиморфы полевых шпатов; (iii) полиморфы пироксенов и амфиболов; (iv) гранатоподобные фазы с октаэдрическим Si; (v) полиморфы $MSiO_3$ (M = = Mg, Fe); (vi) полиморфы M_2SiO_4 (M = Mg, Fe); (vii) плотные водные магнезиальные силикаты и родственные им структуры; (viii) силикаты систем Al_2O_3–SiO_2 и Al_2O_3–SiO_2–H_2O; (ix) силикаты и алюмосиликаты Ca, Sr и Ba; (x) силикаты и алюмосиликаты щелочных металлов; (xi) разнообразные высокобарические силикаты. Всего рассмотрено более 160 высокобарических силикатов, которые кристаллизуются в более чем 115 различных структурных типах. На основе последних достижений предложена общая систематика неорганических силикатов на основе координации кремния в отношении атомов кислорода. По координации кремния выделено семь структурных групп: 4; 4 + 5; 4 + 5 + 6; 4 + 6; 5; 5 + 6; 6. Структуры менее половины всех известных высокобарических силикатов образованы плотнейшими упаковками атомов. Топологические свойства объединения силикатных полиэдров включают объединение по вершинам (для всех координационных чисел (КЧ) кремния), по ребрам (для КЧ = 5 и 6) и граням (для КЧ = 6). Один атом кислорода может быть поделен не более чем между тремя координационными полиэдрами кремния.

Ключевые слова: высокие давления, силикаты, кристаллическая структура, кристаллохимия, шестикоординированный кремний, пятикоординированный кремний, минералогия высоких давлений, фазовые переходы, структурная сложность, структурная топология